1994

Density Functional Calculations Of F-Center Related Positron Annihilation In Alkali Halides.

Keunjoo Kim
University of Alabama at Birmingham

Order Number 9512262

Density functional calculations of F-center related positron annihilation in alkali halides

Kim, Keunjoo, Ph.D.

University of Alabama at Birmingham, 1994

U·M·I
300 N. Zeeb Rd.
Ann Arbor, MI 48106

DENSITY FUNCTIONAL CALCULATIONS OF F-CENTER RELATED POSITRON ANNIHILATION IN ALKALI HALIDES

by

KEUNJOO KIM

A DISSERTATION

Submitted in partial fulfillment of the requirements for the degree of
Doctor of Philosophy in the Department of Physics in
the Graduate School, The University of
Alabama at Birmingham

BIRMINGHAM, ALABAMA

1994

ABSTRACT OF DISSERTATION
GRADUATE SCHOOL, UNIVERSITY OF ALABAMA AT BIRMINGHAM

Degree Doctor of Philosophy Major Subject Physics

Name of Candidate Keunjoo Kim

Title Density Functional Calculations of F-Center Related Positron Annihilation in Alkali Halides

Positron annihilation is useful as a probe in the study of electronic structure in a wide range of condensed matter systems. Positron lifetimes oftenhold key information about the presence of defect electronic states. Although the experimental data may contain information about the presence of defects in solids, the analysis of that information in terms of local defect structure may be difficult. Many of these problems of data analysis could be resolved with theoretical calculations of the expected positron lifetimes for the bulk materials and associated defects. Until now, most of theoretical calculations of the positron lifetimes in defect crystals have been based on parameterized fits to experimental data. In systems such as these where the experimental characterization is incomplete or uncertain, parameter-free tools are essential. A first-principles method for the self-consistent calculation of the positron states in many electron systems has been developed, but some important features have not been fully implemented. In this work, density functional calculations are carried out for positron bound states by using the self-interaction corrected, local spin density approximation of density functional theory and by using the linear combinations of atomic Gaussian orbitals to the point cluster in the embedded-cluster method for crystals. Positron lifetimes are calculated for the

halide and alkali atomic systems ($H^-:e^+$, $F^-:e^+$, $Cl^-:e^+$, $Li:e^+$, and $Na:e^+$) for several bound states. These calculations provide the reference for the lifetime shift by including crystal field in alkali halides (LiF, NaF, LiCl, and NaCl). Finally, the well-documented crystal system can be applied into the positron bound states in defect centers ($F_c:e^+$) in the alkali halides listed above, and the local features of the positron bound states can be analyzed from relationships between the annihilation rates and the lattice constants for alkali fluorides [LiF, NaF] and the corresponding alkali chlorides (LiCl, NaCl).

Abstract Approved by: Committee Chairman Joseph D. Harrison

Program Director W. J. Shea

Date 8/24/94 Dean of Graduate School Grant T. Lodge

DEDICATION

To my glorious Lord & Ermernyee

ACKNOWLEDGEMENTS

I would like to express my sincere appreciation and great respect for my advisor, Dr. Joseph G. Harrison, for his philosophy, continuous guidance, advice, and encouragement throughout my graduate research and preparation of this work. I also wish to express my gratitude to Dr. David L. Shealy, chair of the Department of Physics and a member of my committee, whose thoughtful kindness and financial support with a teaching assistantship helped me complete this work.

Sincere thanks also go to Dr. John H. Young, the supervisor for the graduate program and a member of my committee, for his excellent teaching philosophy--that the right result should come from the right reason, which becomes my background knowledge for physical insight. I also thank Drs. Tiit H. Tohver, Ian W. Knowles, and Koop Lammertsma for serving on my committee.

The author wishes to thank Drs. Lester D. Hulett Jr. and Jun Xu, Oak Ridge National laboratory and Frank H. Hsu, Georgia State University. They gladly shared their information on experimental techiniques of the positron annihilation. I am glad to thank Dr. Eric G. Bradford for his computational guidance in ASNCRAY and Mr. Joseph F. Tombrello and Mr. John P. Robinson for their computer organization.

The kindness of faculties and staffs and the friendship with graduate peers made my graduate career very enjoyable and an experience I greatly appreciate. I gratefully appreciate Mr. David C. Patton, Mrs. Julia S. Austin, and V. Masi Masi for their careful proofreading and editing advice.

The author also deeply thanks Drs. Jung Hong Kim, Chunho Lee, Young-Jin Shin, Ki-Bang Lee, Seung Gon Kim, Hyung Jae Lee, Jin Seung Kim, Chaiho Rim, and Young-Hee Lee who are faculties in the Department of Physics, Jeonbuk National University in Korea. They encouraged me to complete this work with long range invisible love and best wishes. My special thanks go to professors Ik-Ju Kang, Southern Illinois University at Edwardsville, and Young-Suh Kim, University of Maryland. They cared and guided my life-style in America.

The author would also express his gratitude to professor On-Sik Kim, who bred a bee of the vermilion-Kim eye as the natural enemy against corn insects, Kongju National University in Korea. He gave me a chance to reach another milestone in my life by introducing me to Wonlan Park. I am grateful for the joys I shared with the Birmingham Korean community who gave me love and a homelike feeling.

Finally, my special gratitude goes to my brothers and sisters for their love served as a source for inspiration and my mother who prays for her son in my hometown, Duworli, Korea.

TABLE OF CONTENTS

TABLE OF CONTENTS (Continued)

LIST OF TABLES

LIST OF TABLE (Continued)

LIST OF FIGURES

LIST OF FIGURES (Continued)

CHAPTER I

INTRODUCTION

While positron annihilation (PA) is a widely-used tool in condensed matter systems, it presents a vexing theoretical problem because of its strong perturbation of the states it is intended to probe. Unlike other probes where final-state effects can often be neglected, in the case of PA the annihilation event can take place from a bound state which represents a significant perturbation of the original electronic states. The goal of first-principles theories is to adequately take into account for the perturbation of the electronic states, including electron-positron correlation effects which directly relate to the observed annihilation rates.[1, 2] In this work, we only consider the 2γ annihilation channel and determine our computed annihilation rates from the overlap of electron and positron densities.

Much experimental work has been carried out in connection with defect centers using thermalized positrons.[3-5] Recently, numerous experimental studies have yielded data on the positron annihilation rate for a trapped positron in defect centers of solids. Variable-energy positron beams[6-8] have also been used in the study of vacancy-defect structures such as an EL2 defect in the GaAs crystal. In formulating a computational approach to PA, in such systems, we begin with atomic systems. *Ab initio* calculations have been carried out at the Hartree-Fock (H-F) level[9-10] and for smaller atoms or ions, at the post-HF level in terms of configuration-interaction (CI)

and Hylleraas-type calculations.[11-13] Correlation effects are crucial for addressing the issue of bound states of positrons in neutral atoms. Therefore, another method is preferable for including correlation that is more tractable in larger systems.

In general, one can expect positron annihilation in condensed matter to occur via channels involving localized, as well as delocalized, electronic states. The full range of such states may be analyzed within density functional theory (DFT),[14, 15] which includes the energy functional correlational effects between electrons and between electrons and the positron. The well-documented problems of the local density a pproximation (LDA) of DFT in regard to localized states, viz. the self-interaction error,[16] may be dealt with in a number of ways such as ΔSCF,[17] GW approximation,[18, 19] or the self-interaction correction (SIC).[16, 20] In this work, we adopt the orbital SIC scheme and employ the Perdew-Zunger parametrization of the Ceperley-Alder[21] values of the electron-electron correlation energy.

The two-component DFT in the self-consistent formalism of Chakraborty,[22, 23] where densities of the electron and the positron are defined as basic variables of the functional, has proven to be useful in the study of positron states in metallic sytems.[24, 25] Expressions for the electron-positron correlation energy per unit volume E_V^{ep} based on calculations by Arponen and Pajanne[26] and Lantto[27] have been employed. Boronski and Nieminen[2] have devised an interpolation scheme to use these data to fill in values of E_V^{ep} throughout the (ρ_+, ρ_-) plane. Applications of the two-component DFT include an electron-hole plasma in semiconductors[28, 29] and electron-positron systems in metals.[1]

In order to include a self-interaction correction not only for the electrons but also for the positrons,[30] the proper theoretical framework is a three-component DFT formalism.[31] We attempt to improve our local approximation to the exact

three-component DFT by imposing the same fundamental requirement as the exact functional so that it is self-interaction free in the limit of a single orbital density.[16] The LDA energy functional retains a residual self interaction resulting from the local approximation for the exact exchange and correlation. The problem of the orbital SIC scheme associated with a lack of invariance to linear transformations among the orbitals can be remedied by solving the localization equations.[32] In this work, we do not adopt this extra computational step although its effect on calculated positron lifetimes should be explored. Bound state of positrons in negative ions have been dealt with in the context of the exchange-only (X-O) SIC-LSDA in a previous work.[31] Moreover, the delicate problem of positron bound states in neutral atoms[33, 34] has yet to be addressed and should provide a good test of the correlation functional to be employed.

Positron lifetimes often hold key information about the presence of defect electronic states. Although the experimental data may contain information about the presence of defects in solids, the analysis of that information in terms of local defect structure may be difficult. Many of these problems of data analysis could be resolved with theoretical calculations of the expected positron lifetimes for the bulk materials and associated defects. Until now, most of theoretical calculations of the positron lifetimes in defect crystals have been based on semiempirical models. In systems such as these where the experimental characterization is incomplete or uncertain, parameter-free tools are essential. The calculated positron lifetime in a system is directly related to the amount of overlap in the electron and positron densities. This could conceivably be described by a number of parameters in a semi-empirical theory,[35, 36] but without sufficient information from experimental measurement, a unique correlation between positron lifetimes and local electron structure would be

impossible. A first-principles method for the self-consistent calculation of the positron states in many electron systems has been developed,[31] but some important features have not been fully implemented.

In this work, based on a first-principles calculations of electronic structure for both the electron and positron, we calculate the positron lifetimes in the F-center of alkali halide crystals (LiF, NaF, LiCl, and NaCl). The electron and positron many body interactions are computed using the self-interaction corrected, local spin density approximation of density functional theory and using the linear combinations of Gaussian orbitals in the embedded-cluster method. The calculation of the positron lifetimes is carried out on the negative and neutral free atomic systems ($F^-:e^+$ and $Cl^-:e^+$). We also calculate positron lifetimes for those of pure alkali halide crystals, in which the positron interacts with electrons in periodic systems. These data are used as a reference for lifetime shifts which may result from the introduction of defects. Finally, we complete the calculation on the F-center ($F_c:e^+$) in the alkali halides listed above and analyze the local features of the positron bound states, annihilation rates of the positron from the various possible bound states, and relationships between the annihilation rate and the lattice constant for the alkali fluorides (LiF, NaF) and the corresponding alkali chlorides (LiCl, NaCl).

The rest of the text is organized as follows: Chapter II reviews the theoretical formalism for the many-body interactions in the context of the DFT. Chapter III takes up the issue of the positron annihilation phenomenon including positron properties. Chapter IV is devoted to the crystal field effect. The embedded cluster method as a computational technique is introduced in Chapter V. In Chapter VI, density functional calculations are carried out for positron annihilation lifetimes on free-atom systems such as negative and neutral atoms, the bulk states for the pure

alkali halide crystals, and F-centers as a point defect in those crystals. Finally, Chapter VII contains concluding remarks. Throughout this work unless otherwise noted, we use Hartree atomic units (a.u.) in which ($e^2 = h/2\pi = m = 1$).

CHAPTER II

DENSITY FUNCTIONAL THEORY

A. Many-body problems

An interesting question in the many-body problems is the maximum numbers of bodies for which we may find exact solutions. Historically in classical mechanics,[37] the three-body problem was not exactly solvable. With the advent of general relativity[38] and quantum mechanics,[39] we find that the two-body problem has no exact solution. In quantum electrodynamics,[40] one-body problems can not be solved exactly, and within modern quantum field theory,[41] the problem of zero bodies (vacuum) is not exactly solvable. So, if we are looking for exact solutions, no bodies at all is already too many.

Of course, we are not really interested in exact solutions, but instead we look for a better strategy to handle the many-body problem in which we want to describe the observed physical properties of the system in terms of the behavior of the particles composing it. In quantum mechanics, the exact solution of the motion of one particle is possible by solving the Schrödinger equation for the particle. A many-body system may be considered in zeroth order as many one-body problems. The real many-body system is more properly regarded as a system of particles which interact with one another. The particles no longer act independently, and the solution must take into account the enormously complicated influence that each particle has on the motion of

all the others. Many physical systems besides gases are of this type--molecules in a liquid, electrons in a solid, protons in a nucleus, and so on.

This leads to the fact that the many-body problem is the study of the effects of interactions between particles on the behavior of a many-particle system. These interactions decisively influence the physical properties of the system. In general, the many-body problem is extremely difficult because of the incredibly intricate motions of the particles in an interacting system. One of the most successful of the early methods of approaching the problem, and one which is still used extensively today, is the canonical transformation technique. This involves transforming the Schrödinger equation to a new set of coordinates in which the interaction term becomes small. The principal drawback with this technique is that it is not as systematic as one would like, sometimes making it difficult to apply.

The situation has changed radically with the methods of quantum field theory.[42-44] This theory is already famous for its success in elementary particle physics, providing a powerful, unified way of attacking the many-body problem. In rapid succession, the idea was applied to nuclei, superfluids, superconductors (even though there are still some problems), electrons in solids, phonons, ferromagnets, plasmas, atoms, and molecules. In the last several decades, many-body theory[45] has come of age, making possible increasing amounts of exciting and fundamental research into the nature of matter. Quantum field theory is also useful for understanding the inhomogeneous interacting electron system. This theory can provide many-body effect on the electron-electron quantum correlation which is an important ingredient in density functional theory.

It would be helpful to review several background methods to understand a many-body problem, such as the Born-Oppenheimer approximation,[46] Hartree-

Fock,[47, 48] and Thomas-Fermi-Dirac-Weizsäcker density approximations.[49-52] As to the electronic structure, the non-relativistic, time-independent Schrödinger equation for an inhomogeneous system of M nuclei and N electrons may be written as

$$\hat{H}\Psi(\boldsymbol{r}_1, \boldsymbol{r}_2, \ldots, \boldsymbol{r}_N; \boldsymbol{R}_1, \boldsymbol{R}_2, \ldots, \boldsymbol{R}_M) = E\Psi, \tag{2. 1}$$

where E is the total energy, Ψ represents the total wavefunction, and the Hamiltonian operator is written as

$$\hat{H} = \hat{T}_{el} + \hat{T}_{nu} + V(\boldsymbol{r}_1, \boldsymbol{r}_2, \ldots, \boldsymbol{r}_N; \boldsymbol{R}_1, \boldsymbol{R}_2, \ldots, \boldsymbol{R}_M) \tag{2. 2}$$

with

$$\hat{T}_{el} = \sum_{i=1}^{N} \frac{1}{2}\nabla_i^2, \tag{2. 3}$$

$$\hat{T}_{nu} = \sum_{\nu=1}^{M} \frac{1}{2M_\nu}\nabla_\nu^2, \tag{2. 4}$$

$$V = V_{ee} + V_{ne} + V_{nn}, \tag{2. 5}$$

and

$$V_{ee} = \frac{1}{2}\sum_{i=1}^{N}\sum_{j\neq i}^{N} \frac{1}{|\boldsymbol{r}_i - \boldsymbol{r}_j|}, \tag{2. 6}$$

$$V_{ne} = \sum_{i=1}^{N}\sum_{\nu=1}^{M} \frac{-Z_\nu}{|\boldsymbol{r}_i - \boldsymbol{R}_\nu|}, \tag{2. 7}$$

$$V_{nn} = \frac{1}{2}\sum_{\nu=1}^{M}\sum_{\mu\neq\nu}^{M} \frac{Z_\mu Z_\nu}{|\boldsymbol{R}_\mu - \boldsymbol{R}_\nu|}. \tag{2. 8}$$

Here $\boldsymbol{r}_i$ denotes the coordinates of the electrons, $\boldsymbol{R}_\nu$ the coordinates of the nuclei, and Z_ν, M_ν to the charge and the mass of the nucleus at $\boldsymbol{R}_\nu$, respectively. In this system, the length unit is the Bohr radius (0.529 Å); the energy unit is the Hartree (27.211 eV). A double counting can be avoided on the electron-electron and the nucleus-

nucleus interactions by multiplying one half and excluding the terms $i \neq j$ and $\mu \neq \nu$, respectively. The many-body system is a coupled system, consisting of two components, nuclei and electrons, which interact with themselves and with each other. To address the problem of Eq. (2.1) for such a many-body system, it is useful to approximate the system to be separable into the electronic and the nuclear motions.

The first approximation is justified with Born-Oppenheimer theorem,[46] which is valid only because electrons are so much lighter than nuclei and move so much faster ($M_\nu / m_e \approx 1839$). If the nuclei are assumed to be fixed on their positions, the only part of the total Hamiltonian to be considered is for electrons:

$$\hat{H}_e \Psi (\boldsymbol{r}_1, \boldsymbol{r}_2, \ldots, \boldsymbol{r}_N; \boldsymbol{R}_1, \boldsymbol{R}_2, \ldots, \boldsymbol{R}_M) = E_e \Psi , \tag{2. 9}$$

where

$$\hat{H}_e = \hat{T}_e + V_{ne} + V_{ee} . \tag{2. 10}$$

The substantial difficulty with Eq. (2.9) still comes from its many-body interaction. This makes the problem too complicated. In order to carry out the calculation, it is necessary to make further approximations. There are several possible alternatives to solve many-body systems with one-electron approximations.

Hartree[47] introduced a product of wavefunctions for the individual electrons just as for bosons which are symmetric under their exchange:

$$\Psi_S = \prod_i \phi_i (\boldsymbol{r}_i, \sigma_i) , \tag{2. 11}$$

where σ_i is spin coordinates of electron. Following the quantum-statistics, electrons are fermions which satisfy the Pauli exclusion principle. The wavefunction of electrons should be antisymmetric. In the Hartree and Fock method[47, 48] the antisymmetric wavefunction can be written as a Slater determinant:[53]

$$\Psi_A = \frac{1}{\sqrt{N!}} \begin{vmatrix} \phi_1(r_1, \sigma_1) \ldots \phi_1(r_N, \sigma_N) \\ \ldots\ldots\ldots\ldots\ldots\ldots \\ \phi_N(r_1, \sigma_1) \ldots \phi_N(r_N, \sigma_N) \end{vmatrix}. \tag{2. 12}$$

It can be readily seen that the interchange of two particle labels in Eq. (2.12) merely changes the sign of Ψ_A. If this determinantal wavefunction is used in the Hamiltonian H_e, the new additional exchange term is obtained as

$$E_x = \sum_{i,j=1}^{N} \delta(\sigma_i, \sigma_j) \iint \phi_i^*(r_1)\, \phi_j^*(r_2) \frac{1}{r_{12}} \phi_i(r_2)\, \phi_j(r_1)\, dr_1 dr_2 . \tag{2. 13}$$

The Hartree-Fock equation for i-th orbital is the following:

$$\hat{H}_0 \phi_i(r_1) - \sum_{j=1}^{N} \delta(\sigma_i, \sigma_j) \int \phi_j^*(r_2)\, \phi_i(r_2) \frac{1}{|r_1 - r_2|} \phi_j(r_1)\, dr_2 = \varepsilon_i \phi_i(r_1) , \tag{2. 14}$$

where

$$\hat{H}_0 = -\frac{1}{2}\nabla^2 - \sum_{\nu=1}^{M} \frac{Z_\nu}{|r - R_\nu|} + \sum_{j=1}^{N} \int \frac{|\phi_j(r_2)|^2}{r_{12}} dr_2 . \tag{2. 15}$$

The exchange energy term is in a non-local form of $\sum \int V(r, r')\, \phi(r')\, d^3 r'$, leading to complicated multi-center integrals. This non-locality implies that the H-F approach is not appropriat for large systems. Because the computation becomes so demanding with a large number of complicated multi-centered integrals, further severe approximations would be required to make it tractable. The local approximation of the exchange term may be useful to avoid this problem.

A review of the Thomas-Fermi density approximation[49-52] is useful before the local exchange approximation is introduced. The distribution of electrons can be assumed to be treated statistically in the inhomogeneous electron system. Electrons are modeled to be distributed uniformly in the six-dimensional phase space for the motion of an electron. The effective potential can be determined by the nuclear

charge and the distribution of electrons. In this Thomas-Fermi approximation, the kinetic energy in terms of the density $\rho(r)$ is derived for a non-interacting uniform electron gas. The energy functional of the Thomas-Fermi theory of atoms is given by

$$E_{TF}[\rho(r)] = C_F\int\rho^{5/3}(r)\,dr - Z\int\frac{\rho(r)}{r}dr + \frac{1}{2}\iint\frac{\rho(r_1)\,\rho(r_2)}{|r_1-r_2|}dr_1dr_2, \qquad (2.16)$$

where the kinetic coefficient is $C_F = \frac{3}{10}\left(3\pi^2\right)^{2/3}$.

For the ground state of an atom of interest, the electron density minimizes the energy functional under the constraint

$$N = \int\rho(r)\,dr, \qquad (2.17)$$

where N is the total number of electrons in the atom. This constraint may be incorporated by the method of Lagrange multipliers. Once an approximate total energy functional is specified, ground state energies and densities are obtained by solving the variational equation,

$$\delta\left\{E_{TF}[\rho] - \mu_{TF}\left(\int\rho(r)\,dr - N\right)\right\} = 0, \qquad (2.18)$$

which yields the Euler-Lagrange equation

$$\mu_{TF} = \frac{\delta E_{TF}[\rho]}{\delta\rho(r)} = \frac{5}{3}C_F\rho^{2/3}(r) - \Phi(r), \qquad (2.19)$$

where $\Phi(r)$ is the electrostatic potential at point r due to the nucleus and the entire electron distribution:

$$\Phi(r) = \frac{Z}{r} - \int\frac{\rho(r_2)}{|r-r_2|}dr_2. \qquad (2.20)$$

Countless modifications and improvements of the Thomas-Fermi theory have been made over several decades. The non-local Hartree-Fock exchange term is simplified by Dirac:[51]

$$E_{TFD}[\rho] = E_{TF}[\rho] - C_x \int \rho^{4/3}(r)\, dr, \tag{2. 21}$$

where the exchange coefficient is $C_x = \frac{3}{4}\left(\frac{3}{\pi}\right)^{1/3}$.

As an effort to take into account the effect of the inhomogeneous electron density, which is large in atoms and molecules, Weizsäcker[52] added the gradient correction to the non-interacting Thomas-Fermi kinetic energy functional to second order:

$$E_{TFDW}[\rho] = E_{TFD}[\rho] + \frac{\lambda}{8}\int \frac{|\nabla \rho(r)|^2}{\rho(r)} dr, \tag{2. 22}$$

where the coefficient is optimized within the range $1/9 \le \lambda \le 1$. In spite of the improvement with the gradient correction, the accuracy of the prediction for atoms is not as high as that with other methods. This means that the Thomas-Fermi approximation is classified as an oversimplified model which is not of much real importance for quantitative predictions in atomic, molecular, or solid-state electronic structures.

However, the situation changes with the systematic treatment of density as a basic variable of energy functional by Hohenberg and Kohn.[14] They provided the fundamental theorem showing that for ground states. The Thomas-Fermi model may be regarded as an approximation to an exact theory, the density functional theory. The existence of an exact energy functional $E[\rho]$ and also an exact variational principle is discussed in the next section.

B. Density functional formalism

From the quantum field theoretical viewpoint, ground state properties of a many-body system can be described in terms of the one-particle density by including the many-body effect of the quantum correlation as the density functional. The Green function techniques suggest that the ground state energy can be expressed

directly in terms of one- and two-particle Green functions. However, the determination of these quantities involves a set of differential equations coupling eventually all N-particle Green functions, with N being less than or equal to the number of particles. The refined Thomas-Fermi theory with the gradient correction expanded by power series for the non-interacting kinetic energy functional cannot describe the correlation effect. This implies that this early density functional model could not appropriately take into account the contribution of the many-body correlation effect. The correlation effect from quantum field theory has been used to develop the self-consistent one-electron formalism for the many body system.

The exact general formulation of the density functional theory (DFT) was realized by the Hohenberg-Kohn theorem. This implies that the many-body ground state of an electronic system is a unique functional of the true density of electron. This theorem can be readily proved by *reductio ad absurdum* as follows.

The electron density $\rho(\boldsymbol{r})$ is defined for the non-degenerate ground state of some N-electron system. For if there were two external potentials $V_{ext}(\boldsymbol{r})$ and $V'_{ext}(\boldsymbol{r})$ differing by more than a constant, each giving the same ρ for its ground state, there would be two Hamiltonians H and H' whose ground state densities would be the same although the normalized wavefunctions Ψ and Ψ' of the N-electron system would be different. Taking Ψ' as a trial function for the $\hat{H}$ problem, and using the variational principle for the ground state,

$$E = \langle\Psi|\hat{H}|\Psi\rangle < \langle\Psi'|\hat{H}|\Psi'\rangle \tag{2.23}$$

and

$$\langle\Psi'|\hat{H}|\Psi'\rangle = \langle\Psi'|\hat{H}'|\Psi'\rangle + \langle\Psi'|\hat{H} - \hat{H}'|\Psi'\rangle$$

$$= E' + \int\rho(\boldsymbol{r})\,[V_{ext}(\boldsymbol{r}) - V'_{ext}(\boldsymbol{r})]\,d\boldsymbol{r}, \tag{2.24}$$

where $\hat{H}, \hat{H}'$ and E, E' are the Hamiltonians and the ground-state energies for Ψ and Ψ', respectively. Likewise, after taking Ψ as a trial function for the $\hat{H}'$ problem,

$$E' = \langle \Psi' | \hat{H}' | \Psi' \rangle < \langle \Psi | \hat{H}' | \Psi \rangle \tag{2. 25}$$

and

$$\begin{aligned} \langle \Psi | \hat{H}' | \Psi \rangle &= \langle \Psi | \hat{H} | \Psi \rangle + \langle \Psi | \hat{H}' - \hat{H} | \Psi \rangle \\ &= E - \int \rho(\boldsymbol{r}) \, [V_{ext}(\boldsymbol{r}) - V'_{ext}(\boldsymbol{r})] \, d\boldsymbol{r} . \end{aligned} \tag{2. 26}$$

Adding Eq. (2.24) and Eq. (2.26), $E + E' < E + E'$ can be obtained as a contradiction. Therefore, there cannot be two different external potentials that give the same density for their ground states. This implies that the external potential is a unique functional of density and that the density determines the ground-state wavefunction Ψ and all other properties of the N-body system. The energy functional may be written with the explicit dependence on the external potentials V_{ext}:

$$E_v[\rho] = \int \rho(\boldsymbol{r}) \, V_{ext}(\boldsymbol{r}) \, d\boldsymbol{r} + F_{HK}[\rho] , \tag{2. 27}$$

where the Hohenberg and Kohn universal functional,

$$\begin{aligned} F_{HK}[\rho] &= \langle \Psi | T + V_{ee} | \Psi \rangle \\ &= T[\rho] + \langle V_{ee} \rangle . \end{aligned} \tag{2. 28}$$

The second Hohenberg-Kohn theorem provides an energy variational principle for a non-negative trial density $\rho'(\boldsymbol{r})$, such that $\int \rho'(\boldsymbol{r}) \, d\boldsymbol{r} = N$,

$$E_0 \leq E_v[\rho'] , \tag{2. 29}$$

where $E_v[\rho']$ is the energy functional of Eq. (2.27). This is analogous to the variational principle for wavefunctions. To prove this theorem, note that the

previous theorem assures that ρ' determines its own V'_{ext}, Hamiltonian $\hat{H}$, and wavefunction Ψ', which can be taken as a trial function for the problem of interest having external potential V_{ext}. Thus,

$$\langle \Psi' | \hat{H} | \Psi' \rangle = \int \rho'(\boldsymbol{r})\, V_{ext}(\boldsymbol{r})\, d\boldsymbol{r}' + F_{HK}[\rho']$$

$$= E_v[\rho'] \geq E_v[\rho] . \qquad (2.30)$$

Assuming the differentiability of $E_v[\rho]$, the variational principle of the Eq. (2.29) requires that the ground-state density satisfies the stationary principle

$$\delta \{ E_v[\rho] - \mu \left[\int \rho(\boldsymbol{r})\, d\boldsymbol{r} - N \right] \} = 0, \qquad (2.31)$$

which gives the Euler-Lagrange equation from the following constraint:

$$\mu = \frac{\delta E_v[\rho]}{\delta \rho(\boldsymbol{r})} = V_{ext}(\boldsymbol{r}) + \frac{\delta F_{HK}[\rho]}{\delta \rho(\boldsymbol{r})} . \qquad (2.32)$$

The usual method for determining the self-consistent ground state charge density ρ is due to the Kohn-Sham theorem.[15] It is supposed that a non-interacting electron system exists with the same ground state charge density as the interacting system. Indicating with $T_0[\rho]$ the kinetic energy of the non-interacting electron system

$$T_0[\rho] = \sum_i^N \langle \Psi_i | -\frac{1}{2} \nabla^2 | \Psi_i \rangle , \qquad (2.33)$$

the universal functional becomes

$$F_{HK}[\rho] = T_0[\rho] + U_C[\rho] + E_{xc}[\rho] , \qquad (2.34)$$

where $U_C[\rho]$ is the Coulomb potential energy and $E_{xc}[\rho]$ is introduced as the exchange-correlation functional defined by

$$E_{xc}[\rho] = T[\rho] - T_0[\rho] + \langle V_{ee} \rangle - U_C[\rho] . \qquad (2.35)$$

The N-electron charge density which makes Eq. (2.27) stationary is the solution of the equation:

$$\frac{\delta T_0}{\delta \rho} + \frac{\delta U_C}{\delta \rho} + \frac{\delta E_{xc}}{\delta \rho} + V_{ext} = \mu . \tag{2. 36}$$

Since the Eq. (2.36) is identical to the equation that would be obtained for a non-interacting system in an external effective potential given by

$$V_{eff}(r) = V_{ext}(r) + \frac{\delta U_C}{\delta \rho} + \frac{\delta E_{xc}}{\delta \rho}, \tag{2. 37}$$

the ground-state charge density can be obtained after solving Schrödinger-like equations

$$\left[-\frac{1}{2}\nabla^2 + V_{eff}(r) \right] \Psi_i(r) = \varepsilon_i \Psi_i(r) , \tag{2. 38}$$

and then by summing the square of the N lowest orbitals

$$\rho(r) = \sum_{i=1}^{N} \left| \Psi_i(r) \right|^2 . \tag{2. 39}$$

Now, these one-particle Kohn-Sham equations can systematically describe many body systems and can be applicable for self-consistent calculations of electronic structures. The remaining complexity is the determination of the universal functional for the exact exchange and correlation functional.

Although the search for an accurate $E_{xc}[\rho]$ has encountered a tremendous difficulty, the explicit form for the functional is essential to specify the Kohn-Sham equations and is the greatest challenge in the density functional theory (DFT). As the simplest approximation for the above one-component formalism of DFT, there is the local density approximation.[15]

As the concept of the uniform electron gas has been used locally to obtain the Thomas-Fermi functional for kinetic energy and the Dirac functional for the exchange energy, now the kinetic energy $T_0[\rho]$ is rigorously treated in the Kohn-Sham scheme. The local density approximation (LDA) for the exchange and correlation energy can be written as

$$E_{xc}^{LDA}[\rho] = \int \rho(r)\,\varepsilon_{xc}(\rho)\,dr\,, \tag{2.40}$$

where $\varepsilon_{xc}(\rho)$ indicates the exchange and correlation energy per particle of a uniform electron gas of density ρ. The corresponding exchange-correlation potential then becomes

$$V_{xc}^{LDA}(r) = \frac{\delta E_{xc}^{LDA}}{\delta \rho(r)} = \varepsilon_{xc}[\rho(r)] + \rho(r)\frac{\delta \varepsilon_{xc}(\rho)}{\delta \rho}, \tag{2.41}$$

and the Kohn-Sham orbital equations read

$$\left[-\frac{1}{2}\nabla^2 + V_{ext}(r) + \int \frac{\rho(r')}{|r-r'|}dr' + V_{xc}^{LDA}(r)\right]\Psi_i = \varepsilon_i \Psi_i\,. \tag{2.42}$$

This self-consistent solution defines the Kohn-Sham local density approximation. The function $\varepsilon_{xc}(\rho)$ can be divided into the exchange and the correlation contribution without losing the physics,

$$\varepsilon_{xc}(\rho) = \varepsilon_x(\rho) + \varepsilon_c(\rho)\,. \tag{2.43}$$

The exchange energy is already known from work by Dirac,[51] Slater,[54] and Kohn[15]:

$$\varepsilon_x(\rho) = -C_x \rho(r)^{1/3}, \tag{2.44}$$

where the exchange constant is given with several values such as $\frac{3}{4}(3/\pi)^{1/3}$ for the Dirac and the Kohn-Sham types and $\frac{9}{8}(3/\pi)^{1/3}$ for the Slater type.

The X_α method[55] may be regarded as a density functional scheme with neglect of correlation and with approximation to the exchange energy functional

$$E_x^{LDA}[\rho] = -\frac{3}{2}\alpha K_D[\rho] = -\frac{9}{8}\alpha\left(\frac{3}{\pi}\right)^{1/3}\int\rho(\boldsymbol{r})^{4/3}d\boldsymbol{r} \tag{2.45}$$

which gives the X_α potential upon the functional differentiation. Kohn and Sham[15] realized that the X_α equation[54,55] is equivalent to their local density approximation if the correlation in Eq. (2.43) is ignored. Namely, if one uses the Dirac exchange formula [Eq. (2.21)]

$$E_x^{LDA}[\rho] = -K_D[\rho] = -\frac{3}{4}\left(\frac{3}{\pi}\right)^{1/3}\int\rho(\boldsymbol{r})^{4/3}d\boldsymbol{r} \tag{2.46}$$

and

$$V_x^{LDA}(\boldsymbol{r}) = -\left[\frac{3}{\pi}\rho(\boldsymbol{r})\right]^{1/3}, \tag{2.47}$$

then the resulting Kohn-Sham equation is precisely the X_α equation with $\alpha = \frac{2}{3}$. The correlation functional is also available with accurate values from the quantum Monte Carlo calculations of Ceperley and Alder.[21] These values have been interpolated to provide an analytic form.[16]

The LDA is applicable to systems with slowly varying densities but cannot be formally justified for highly inhomogeneous systems such as atoms and molecules. The exchange-only LDA calculation[56] shows an error of about 10% from the unrestricted Hartree-Fock calculation. This is the major source of error in the LDA since correlation energy is a magnitude smaller than the exchange energy. This inexactedness of exchange energy can be improved by the introduction of spin-polarization in the density functional theory which is corresponding to the local spin density approximation (LSDA). The spin polarization effects in the effective potential for the spin polarized electron densities need to be taken into account; these

may not only cause changes between energies of spin ↑ and ↓ electrons, but may also significantly change the wavefunctions corresponding to the energy changes. This improves the accuracy of the density functional calculation and provides two component formalism of DFT for spin ↑ and ↓ electron densities as basic variables of energy functional.

The formal discussion on this extension of the LDA is available in the work of Von Barth and Hedin[57] and also Rajagopal and Callaway.[58] The formalism of LSDA is summarized with the following total energy and equations:

$$E^{LSDA}[\rho\uparrow, \rho\downarrow] = T_0 + V_{ext} + V_C + E_{xc}^{LSDA}[\rho\uparrow, \rho\downarrow] \tag{2.48}$$

$$T_0\ [\rho\uparrow, \rho\downarrow] = \sum_{i,\sigma}^{N} \langle \Psi_{i\sigma} | -\frac{1}{2}\nabla^2 | \Psi_{i\sigma} \rangle, \tag{2.49}$$

$$E_{xc}^{LSDA}[\rho\uparrow, \rho\downarrow] = \int \varepsilon_{xc}[\rho\uparrow, \rho\downarrow]\rho(r)\, dr, \tag{2.50}$$

and

$$\left(-\frac{1}{2}\nabla^2 + V_{ext}(r) + \int \frac{\rho(r')}{|r-r'|}dr' + \frac{\delta E_{xc}}{\delta \rho_\sigma(r)}\right)\Psi_{i\sigma}(r) = \varepsilon_{i\sigma}\Psi_{i\sigma}(r), \tag{2.51}$$

where densities can be defined by

$$\rho_\sigma(r) = \sum_{i=1}^{occupied} |\Psi_{i\sigma}(r)|^2, \sigma = \uparrow, \downarrow. \tag{2.52}$$

$$\rho(r) = \rho\uparrow(r) + \rho\downarrow(r) \tag{2.53}$$

In the inhomogeneous electron gas, the LSDA still underestimates the exchange energy while it overestimates the correlation energy.[59] The discrepancy may be too large to explain atomic properties such as the ionization and the binding energies.

The further correction of the LSDA approximation into the exact solution of the single particle limit is needed. This implies that the self-consistent one-particle equation has to have the same one particle limit. This self-interaction correction has been initiated by Perdew[60] and detailed fully by Perdew and Zunger[16]and Harrison.[61] The orbital structure of the exact DFT is self-interaction free with Perdew and Zunger's constraint,

$$V_C[\rho_{i\sigma}] + E_{xc}[\rho_{i\sigma}, 0] = 0, \tag{2.54}$$

However, the local approximation leads to a self-interaction error for the LSDA functional,

$$V_C[\rho_{i\sigma}] + E_{xc}^{LSDA}[\rho_{i\sigma}, 0] = \delta_{i\sigma}, \tag{2.55}$$

and a correction formed as an orbital-by-orbital subtraction can be included on the ground states energy from the SIC version of the LSDA:

$$E_{xc}^{SIC-LSDA} = E_{xc}^{LSDA} + U_{SIC}, \tag{2.56}$$

$$U_{SIC} = -\sum_{\sigma}^{N_\sigma}\sum_{i}\left[V_C[\rho_{i\sigma}] + E_{xc}^{LSDA}[\rho_{i\sigma}, 0]\right]. \tag{2.57}$$

This self-interaction correction gives accurate results for the ground state energy, binding energy, and ionization energy calculations in atomic systems.

From the variational principle, the one-particle equations for the orbitals can be written by

$$H_{i\sigma}\Psi_{i\sigma}(r) = \varepsilon_{i\sigma}\Psi_{i\sigma}(r) \qquad i = 1, 2, \ldots, N_\sigma, \tag{2.58}$$

with

$$H_{i\sigma} = -\frac{1}{2}\nabla^2 - \frac{Z}{r} + V_C + V_\sigma^{xc} + \Delta V_{i\sigma}^{SIC}, \tag{2.59}$$

$$V_{\sigma}^{xc} = \frac{\delta(\rho\varepsilon_{xc}[\rho_{\sigma}])}{\delta\rho_{\sigma}}, \tag{2.60}$$

$$\Delta V_{i\sigma}^{SIC} = -V_C[\rho_{i\sigma}] - v_{i\sigma}^{xc}. \tag{2.61}$$

In our approximation, we keep the SIC-LSDA scheme and extend it into the electron and positron system in the next section. The SIC-LSDA provides the accurate self-consistent electron and positron densities which are important ingredients in determining positron annihilation lifetimes.

C. The electron-positron system

Within the SIC-LSDA scheme, it is useful to introduce a three-component formalism to consider a system in which a single positron interacts with the spin-polarized electronic structure. A positron bound in an atomic system is an inhomogeneous system of N electrons and a positron, and electron densities can be denoted by $\rho_{\uparrow}$, $\rho_{\downarrow}$ and the positron by $\rho^{+}{}_{\uparrow}$. The Hamiltonian may be written as

$$H = T_0 + V_{ext} + V_C + V_{ep}, \tag{2.62}$$

where

$$T_0 = \sum_{i=1}^{N_{\sigma}} \left(-\frac{1}{2}\nabla_i^2\right) - \frac{1}{2}\nabla_j^2, \tag{2.63}$$

$$V_{ext} = \sum_{i=1}^{N_{\sigma}} \left(-\frac{Z}{r_i}\right) + \frac{Z}{r_j} = \sum_{i=1}^{N_e} V_{en}(r_i) + V_{pn}(r_j), \tag{2.64}$$

and

$$V_{ep} = -\sum_{i=1}^{N_{\sigma}} \frac{1}{|r_i - r_p|}. \tag{2.65}$$

Where T_0 is the non-interacting component of the kinetic energies for electrons and the positron, and V_{ext} is nuclear external interactions for electrons and the positron.

Following the Hohenberg-Kohn theorem,[14] basic variables as densities $\rho\uparrow$, $\rho\downarrow$, and $\rho^+\uparrow$, for the external potentials V_{en} and V_{pn} can be uniquely determined from the minimization of the energy functional. From Levy's constrained-search formalism[62] which restricts the set of wavefunctions Ψ to those that are antisymmetric under the exchange of electron coordinates, the following inequality of energy functional for trial densities exists:

$$E \leq \int dr \rho(r) V_{en}(r) + \int dr \rho_+(r) V_{pn}(r) + Q[\rho\uparrow, \rho\downarrow, \rho^+\uparrow], \tag{2.66}$$

where the universal functional is written as

$$Q[\rho\uparrow, \rho\downarrow, \rho^+\uparrow] = \langle \Psi | T + U_C + U_{ep} | \Psi \rangle . \tag{2.67}$$

Densities can be described by a set of orthonormal orbitals and occupation numbers such that

$$\rho_\sigma = \sum_{i=1}^{N_\sigma} f_{i\sigma} |\Phi_{i\sigma}(r)|^2, \sigma = \uparrow, \downarrow, \tag{2.68}$$

$$\rho^+\uparrow = |\Phi_p(r)|^2, \tag{2.69}$$

where occupation number $f_{i\sigma}$ is in the interval $0 \leq f \leq 1$. To derive a set of single-particle Kohn-Sham equations, an exchange-correlation energy functional for the SIC-trial wavefunction is defined as

$$Q[\rho\uparrow, \rho\downarrow, \rho^+\uparrow] = T_0[\rho\uparrow, \rho\downarrow, \rho^+\uparrow] + U_C[\rho] - U_{ep}[\rho, \rho^+\uparrow] + E_{xc}^{SIC-LSDA}[\rho\uparrow, \rho\downarrow, \rho^+\uparrow], \tag{2.70}$$

where the last term is the exchange-correlation energy in the SIC-local

approximation, and the non-interacting kinetic energy and the Coulomb potential energies are written as follows:

$$T_0[\rho\uparrow, \rho\downarrow, \rho^+\uparrow] = Min\left[\sum_{\sigma}\sum_{i=1}^{N_\sigma} f_{i\sigma}\langle\Phi_{i\sigma}|-\frac{1}{2}\nabla^2|\Phi_{i\sigma}\rangle + \langle\Phi_p|-\frac{1}{2}\nabla_p^2|\Phi_p\rangle\right] \tag{2.71}$$

and

$$U_C[\rho] = \frac{1}{2}\iint dr dr' \frac{\rho(r)\,\rho(r')}{|r-r'|}, \tag{2.72}$$

$$U_{ep}[\rho, \rho^+] = -\iint dr dr' \frac{\rho(r)\,\rho^+(r')}{|r-r'|}, \tag{2.73}$$

respectively. Normalization constraints are imposed on the orbitals via the Lagrange multipliers, $\varepsilon_{i\sigma}$ and ε^+, and the variational minimum in our modified functional is obtained from

$$\delta\left[E-\sum_{\sigma}\left(\sum_{i=1}^{N_\sigma}\varepsilon_{i\sigma}\langle\Phi_{i\sigma}|\Phi_{i\sigma}\rangle-\varepsilon^+\langle\Phi_p|\Phi_p\rangle\right)\right] = 0. \tag{2.74}$$

Calculating the functional derivatives gives the unique potentials for the densities in the SIC-LSDA scheme,

$$V_{e\sigma}'(r) = V_C[\rho_\sigma] - V_C[\rho_{i\sigma}] + V_{ep}[\rho^+] + V_{xc}[\rho_\sigma] - V_{xc}[\rho_{i\sigma}] + V_c^{ep-e}[\rho_\sigma, \rho^+], \tag{2.75}$$

$$V_p'(r) = V_{ep}[\rho] + V_c^{ep-p}[\rho, \rho^+]. \tag{2.76}$$

The self-consistent one-particle equations for orbitals can be written by

$$H_{i\sigma}\Phi_{i\sigma}(r) = \varepsilon_{i\sigma}\Phi_{i\sigma}(r)\,,\ i = 1, 2, \ldots, N_\sigma, \tag{2.77}$$

$$H_p\Phi_p(r) = \varepsilon^+\Phi_p(r)\,, \tag{2.78}$$

with

$$H_{i\sigma} = -\frac{1}{2}\nabla^2 - \frac{Z}{r} + \int dr' \frac{\rho(r')}{|r-r'|} - \int dr' \frac{\rho_+(r')}{|r-r'|} + V_{xc} + V_c^{ep-e} + \Delta V_e^{SIC}, \quad (2.79)$$

$$H_p = -\frac{1}{2}\nabla^2 + \frac{Z}{r} - \int dr' \frac{\rho(r')}{|r-r'|} + V_c^{ep-p}, \quad (2.80)$$

and

$$V_{xc}^{\sigma}[\rho\uparrow, \rho\downarrow] = \frac{\delta E_{xc}}{\delta \rho_\sigma} \quad (2.81)$$

$$V_c^{ep-e}[\rho\uparrow, \rho\downarrow, \rho^+\uparrow] = \frac{\delta E_c^{ep}}{\delta \rho_\sigma} \quad (2.82)$$

$$V_c^{ep-p}[\rho\uparrow, \rho\downarrow, \rho^+\uparrow] = \frac{\delta E_c^{ep}}{\delta \rho^+} \quad (2.83)$$

$$\Delta V_e^{SIC} = -(V_C[\rho_{i\sigma}] + V_{xc}[\rho_{i\sigma}]). \quad (2.84)$$

With these single-particle equations, the minimized energy functional in three-component density functional formalism can be obtained as follows:

$$E[\rho\uparrow, \rho\downarrow, \rho^+\uparrow] = \sum_i^{N_\sigma} \varepsilon_{i\sigma} + \varepsilon^+ - (E_e + E_{ep}), \quad (2.85)$$

where

$$E_e = U_C - E_{xc}[\rho\uparrow, \rho\downarrow] = \int V_{xc}(\rho\uparrow(\boldsymbol{r}) + \rho\downarrow(\boldsymbol{r}))d\boldsymbol{r} - U^e{}_{SIC}. \quad (2.86)$$

$$E_{ep} = U_{ep} - E_c^{ep} + \int V_c^{ep-e}(\rho\uparrow(\boldsymbol{r}) + \rho\downarrow(\boldsymbol{r}))d\boldsymbol{r} + \int V_c^{ep-p}\rho^+(\boldsymbol{r})\,d\boldsymbol{r}, \quad (2.87)$$

$$U^e{}_{SIC} = \sum_\sigma \sum_i^{N_\sigma} \left(U_C[\rho_{i\sigma}] - E_{xc}[\rho_{i\sigma}] + \int V_{xc}[\rho_{i\sigma}]\,\rho_{i\sigma} d\boldsymbol{r} \right). \quad (2.88)$$

In the above expression, the electron exchange-correlation energy is denoted to

$E_{xc}[\rho\uparrow, \rho\downarrow]$ and the electron-positron correlation energy to $E_c^{ep}[\rho\uparrow, \rho\downarrow, \rho^+\uparrow]$. From this three-component formalism of the DFT, the self-consistent electron and positron densities can be obtained by minimizing the energy functional. We solved these equations by means of a modified atomic structure code[20] used for the SIC-LSDA calculation of atoms interacting with a positron.

Further information about exchange-correlation for electrons and positrons is required to solve the Eqs. (2.77) and (2.78) self-consistently. These quantum many-body interactions are available for the implementation of this work by the field theoretical investigation. The details are reviewed in Appendix A. In the next Chapter, the general physical properties of positron and the annihilation characteristics on the solid materials will be described.

CHAPTER III

POSITRON ANNIHILATION

A positron, the antiparticle of the electron, can be generated from the β^+ decay process of the nuclear weak interaction of a radioactive isotope such as ^{22}Na. When a positron enters a solid, it is thermalized rapidly and is either trapped by a defect center or enters a Bloch state in a perfect crystal. The positron subsequently annihilates with an electron, and the emitted annihilation radiation is observed and analyzed with spectroscopy. The fact that positrons can be absorbed in defects and surfaces of solids and annihilate with discernibly different characteristics from those in the perfect crystal has given us a very useful method for the study of real solids. In this chapter, we will first review in detail the properties of the positron and its annihilation characteristics and its relationship to the pair correlation function.

A. General properties

The existence of positively charged states of the electron was one of the most significant predictions of relativistic quantum mechanics by Dirac.[63] Non-relativistic quantum theory is based on the correspondence principle. Space and time are not viewed equally, and the observable in quantum mechanics is based on the classical concept of dynamical variables. This involves the concept of the physical quantities at widely separated spatial points at the same instant of time, and the quantum state prescribed by the complete set of commuting observables has the lack of space-time symmetry.

In the development of the relativistic wave equation, a linear equation is required to preserve the principle of superposition of states since it is a covariant principle in the Schrödinger representation for the fermion. From the Hamiltonian of a relativistic free particle

$$H^2 = p^2c^2 + m^2c^4, \tag{3.1}$$

the Dirac equation of the relativistic particle has two solutions:

$$H\Psi = \pm\left(\sum_{i=1}^{3} \alpha_i p_i + \beta mc^2\right)\Psi = \pm E\Psi, \tag{3.2}$$

where the Dirac matrices $(\alpha_1, \alpha_2, \alpha_3, \beta)$ are defined by relations $\alpha_i^2 = \beta^2 = 1$ and $\alpha_i\beta + \beta\alpha_i = 0$ from the 2×2 Pauli matrices

$$\alpha_i = \begin{bmatrix} \mathbf{0} & \sigma_i \\ \sigma_i & \mathbf{0} \end{bmatrix} \text{ and } \beta = \begin{bmatrix} \mathbf{1} & \mathbf{0} \\ \mathbf{0} & \mathbf{-1} \end{bmatrix}. \tag{3.3}$$

The positive energy solution for the Dirac equation describes the electron, and the negative energy was interpreted as the solution of the antiparticle of the electron by the Dirac hole theory.[63]

The hole theory implies that the negative energy solution may give the occupation of the negative-energy level of the electron in accord with the Pauli exclusion principle for the different charge quantum number. The vacuum state contains all negative energy electron levels filled and all positive-energy levels empty.

A hole in the negative sea, or a positron, is a trap for a positive energy electron and leads to electron-positron pair annihilation with emission of radiation, as shown in Fig. 3.1. It is also possible for a negative-energy electron to absorb radiation and be excited into a positive-energy state. When this happens, there is a pair creation of

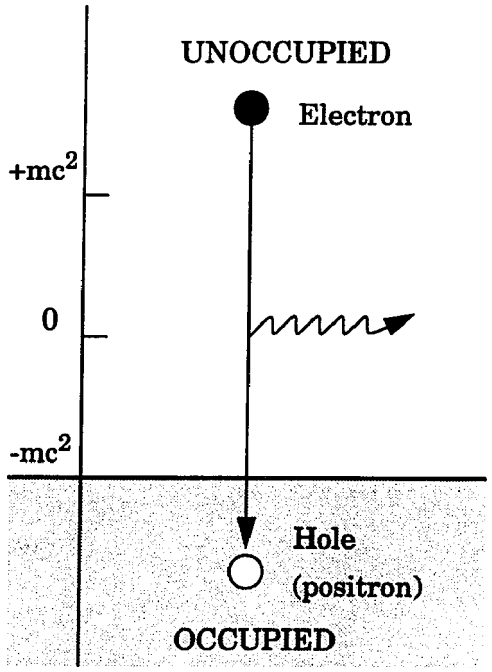

FIG. 3.1. Electron-positron pair annihilation. A positive energy electron falls into a negative energy hole emitting radiation.

an electron with charge $-|e|$ and energy $+E$, and in addition a hole in the negative-energy sea. The hole registers the absence of an electron of charge $-|e|$ and energy $-E$ and would be interpreted by an observer relative to the vacuum as the presence of a particle of charge $+|e|$ and energy $+E$, that is, the positron.

Positrons and electrons have the same mass m, the same magnitude of charge $|e|$, and the same magnetic moment $\frac{g|e|}{2mc}$. The charge quanta of positrons e^+ and electron e^- are distinguished with $e^+ = -e^- = |e|$. In addition, positrons and electrons are distinguishable from each other and thus do not comply with the exclusion principle.

In thermal equilibrium with a medium of temperature T (K), the de Broglie wavelength of positrons in a.u.

$$\lambda_+ = \frac{h}{mv_+} = \frac{2044.3}{\sqrt{T}}, \tag{3. 4}$$

is always largely compared to interatomic distances d in condensed matter where $d \approx 5$ a.u. so that

$$\frac{\lambda_+}{d} \gg 1. \tag{3. 5}$$

This implies that thermal positrons in solids and liquids have the particle-wave duality of the quantum particle. In contrast to positrons, protons have very short de Broglie wave lengths,

$$\lambda_p = \frac{\lambda_+}{1836} = \frac{1.1}{\sqrt{T}}, \tag{3. 6}$$

even at $T = 4$ K, where $\lambda_p = 0.55$ a.u., and hence still

$$\frac{\lambda_p}{d} \ll 1, \tag{3. 7}$$

thermal hydrogen and all other atoms always behave like heavy classical particles.

Since electrons and positrons each have a spin of $\frac{1}{2}$, there are two possibilities for the initial spin state. If the particle spins are antiparallel, the total spin of the system is singlet $^1S_0$; if they are parallel, the system has spin-triplet $^3S_1$. Photons, on the other hand, each have a spin of 1, so the production of two photons would necessarily result in either a spin of 0 or a spin of 2. In order to obtain a state having a total spin of 1 and satisfying the linear momentum conservation law, we must have at least three photons. Therefore, for electron-positron annihilation, two photons will be emitted in the antiparallel spin case into opposite directions with energy of $mc^2 = 0.511\text{MeV}$ each. Three photons will generally be emitted in the case of parallel spins. The distribution of the angle and 1.02 MeV energy among the three photons is more complicated than the two photon case. These modes of positron annihilation are shown in Fig. 3. 2. The statistical weight of triplet to singlet is three to one, and the ratio of the cross-section of the two annihilation modes is given by

$$\frac{\sigma_{2\gamma}}{\sigma_{3\gamma}} = 372. \tag{3. 8}$$

The positron was discovered by Anderson[64] in cloud chamber tracks of cosmic radiation. The emission of a positron also occurs from a nucleus that is proton rich compared to its more stable isobars. This radioactive decay results from the nuclear transformation of a proton p within the nucleus into a neutron n, a positron e^+, and a neutrino ν_e,

$$p \rightarrow n + e^+ + \nu_e \tag{3. 9}$$

or

$$^A_Z X \rightarrow {}^A_{Z-1}X + {}^0_{+1}e + \nu_e, \tag{3. 10}$$

where the neutrino with the spin of $\frac{1}{2}$ and no electric charge preserves the energy

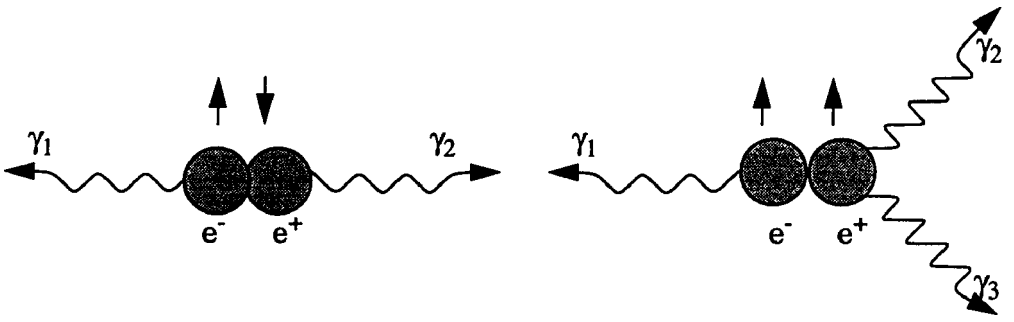

Singlet S=0
Lifetime $\tau=10^{-10}$sec
$E=2E_{\gamma}=1.02$ MeV

Triplet S=1
Lifetime $\tau=10^{-7}$sec
$E=E_{\gamma 1}+E_{\gamma 2}+E_{\gamma 3}=1.02$MeV

FIG. 3.2. Channels of positron annihilation. Two photon mode from spin singlet state and three photon mode from triplet state.

conservation and carries non-zero energy which is hard to detect with the spectrometer.[65] This neutrino spreads the energy of positron as a spectrum.

Several sources of positrons are available. The basic requirements of a positron source are emission of a prompt gamma ray photon which can serve as a birth signal of positrons, a long half life, a narrow energy spectrum, and thermal stability. The majority of investigations of electronic structure[3-5] by positrons have been done with sodium-22 or cobalt-58 positron sources as they meet most of these basic requirements. Table I lists many of the relevant properties of these and other potentially useful positron emitters.[66] It shows that both ^{22}Na and ^{58}Co produce positrons of relatively low energy which are useful for condensed matter systems. ^{58}Co is unattractive for use in sandwich sources for either energy or time measurements since it not only produces a large number of γ-rays per positron, but most of the gamma rays are not coincident with the positrons. ^{44}Ti has a complicated energy spectrum and lifetimes of metastates. ^{68}Ge and ^{64}Cu are favored for measuring energy spectra but are not feasible for lifetime measurements. Thus, the best source of the positron is ^{22}Na.

The positron energy spectrum[67] for sodium-22 shown in Fig. 3.3 is the characteristic of the decay positrons, and this energy distribution comes from the missing energy of the neutrino. Sodium-22 decays with emission of a positron of 0.544 MeV maximum energy to give an excited neon-22, which in turn decays to the ground state by the emission of a 1.28 MeV photon (Fig. 3.4). The excited neon-22 has an average lifetime of a few pico-seconds. Therefore, for all practical purposes, it can be assumed that the positron and the 1.28 MeV photon are emitted simultaneously. The use of sodium-22 as the positron source, therefore, offers distinct advantages such as its long half life (2.67 years), simultaneous emission of the gamma

TABLE I. Selected positron sources

Isotope	Half-life	Production	E_{max}(MeV)
^{22}Na	2.67y	$^{25}Mg(p, \alpha)\ ^{22}Na$	0.54
^{44}Ti	4.80y	$^{45}Sc(p, 2n)\ ^{44}Ti$	1.47
^{55}Co	18.2h	$^{58}Ni(p, \alpha)$; $^{56}Fe(p, 2n)\ ^{55}Co$	1.50
^{57}Ni	36.0h	$^{56}Fe(\ ^{3}He, 2n)\ ^{57}Ni$	0.85
^{58}Co	71.0d	$^{58}Ni(n,p)$; $^{55}Mn(\alpha, n)\ ^{58}Co$	0.48
^{64}Cu	12.8h	$^{63}Cu(n, \gamma)\ ^{64}Cu$	0.66
^{65}Zn	245d	$^{64}Zn(n, \gamma)\ ^{65}Zn$	0.33
^{65}Ge	275d	$^{66}Zn(\alpha, 2n)\ ^{68}Ge$	1.90
^{90}Nb	14.7h	$^{90}Zr(p, n)$; $^{90}Zr(d, 2n)\ ^{90}Nb$	1.50

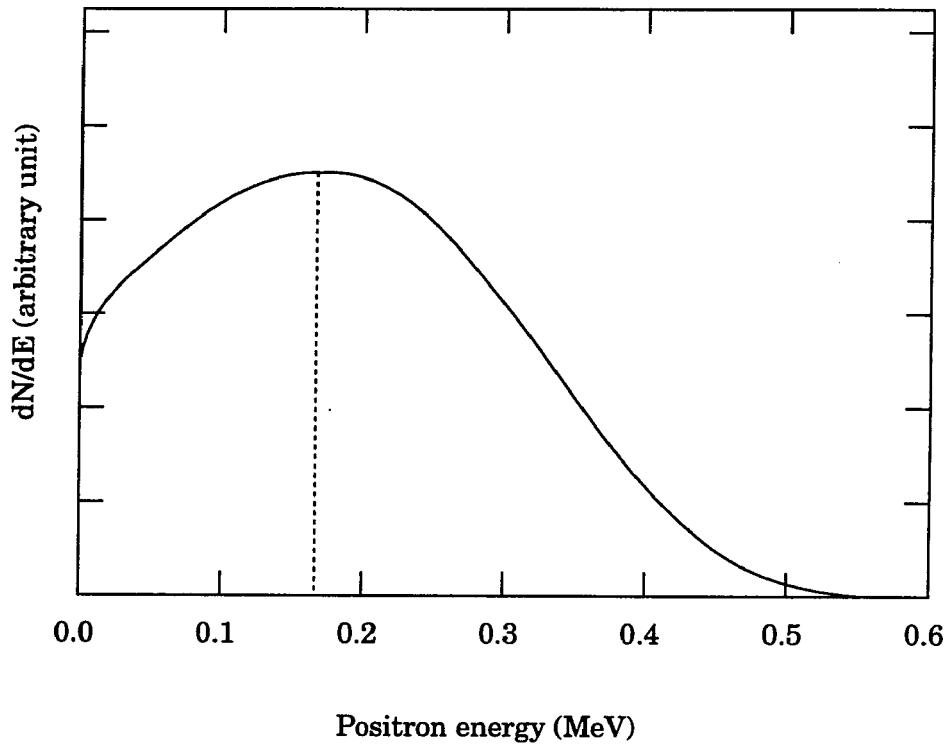

FIG. 3.3. Energy spectrum of positrons emitted from ^{22}Na. The energy distribution comes from the missing energy of the neutrino.

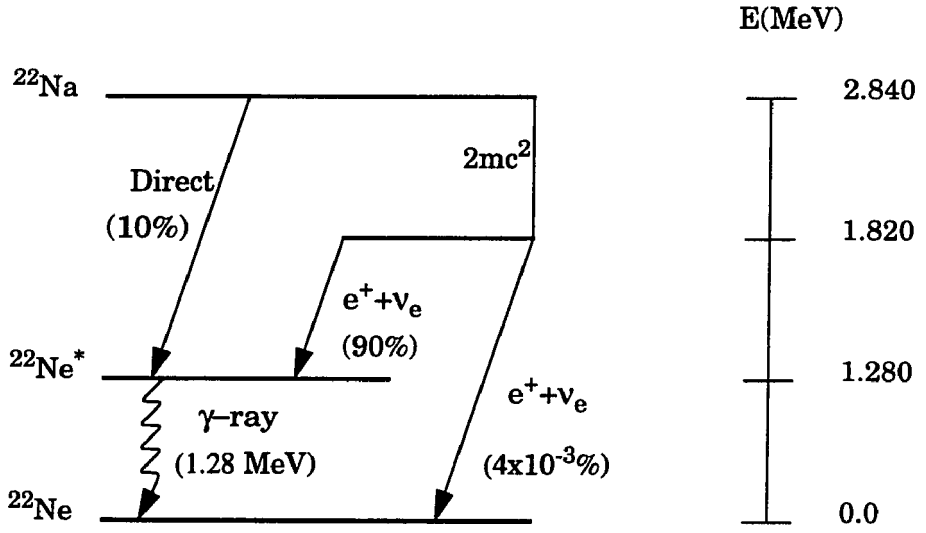

FIG. 3.4. Decay scheme for the production of the positron from ^{22}Na.

photons and the positron, easy energy discrimination of the gamma ray (1.28 MeV) and the annihilation photon (0.511 MeV), and thermal stability up to 600 °C.

In addition to radioisotope sources, slow positron beam facilities are now available.[8] In an accelerator, electrons bombard a tantalum target and the resulting forward scattering generates gamma rays (<10 MeV). These γ-rays strike tungsten target as the modulator which can create the electron-positron pairs. The generated positron can be guided to some direction and reduced in velocity by high voltage (10~120 KeV), and becomes the source of the positron beam. A small percentage of the positrons are moderated to very low energies, <3 eV. Slow positron beams[8] are available with the current as high as 10^8 sec^{-1} (c.f., 30 μCi ^{22}Na = $1.11x10^6$ sec^{-1}).[68]

When a positron is incident on condensed matter, as schematically shown in Fig. 3.5, it interacts with electrons. This positron-electron system annihilates with the emission of two or three gamma photons. The annihilation photons provide information about the electron-positron state at the moment of annihilation; therefore, the experimental studies of positron-electron annihilation as well as positron-electron interaction may provide information about the physical properties of the medium under investigation.

The positron techniques can be classified into two categories: (i) positron scattering, for example, positron energy loss spectroscopy, and low energy positron diffraction which has been developed on the basis of electron spectroscopy; and (ii) conventional positron annihilation methods that involve the use of positrons emitted from radioisotopes. Conventional positron annihilation spectroscopy (PAS) encompasses three methods: the positron lifetime technique,[69] angular momentum distribution,[70] and Doppler broadening measurements.[71]

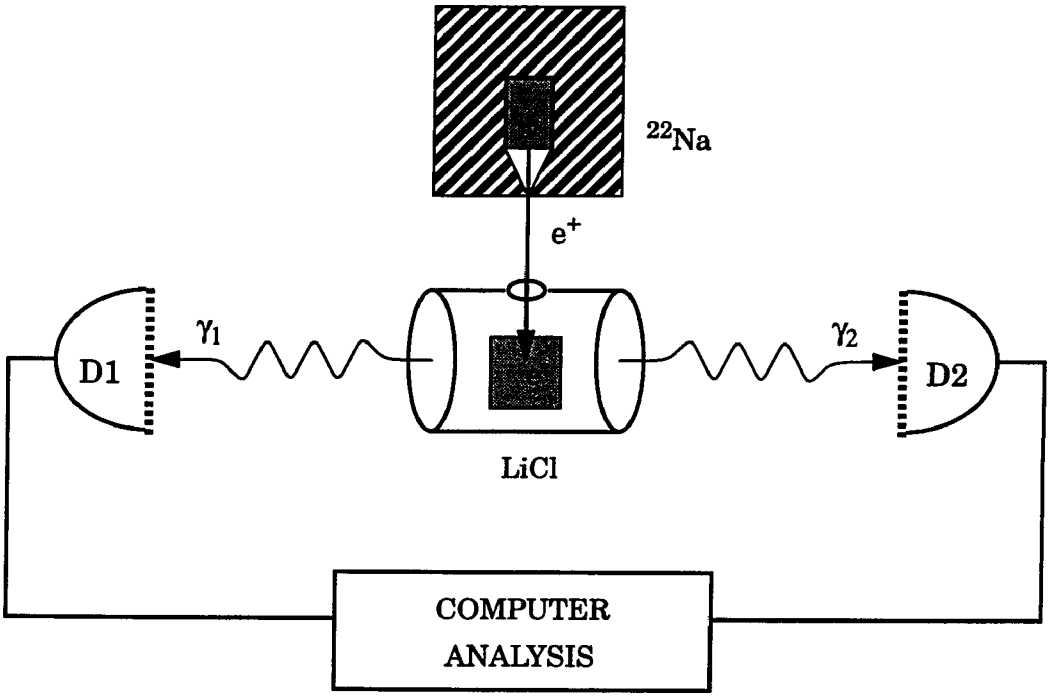

FIG. 3.5. Schematic positron annihilation technique.

The PAS is a good probe for studies of electronic structure and defect characterization in condensed matter. The angular distribution technique is based on the fact that the total momentum of the annihilation electron-positron pair is distributed between the annihilation photons. This technique is useful for understanding momentum density and Fermi surface measurements in metals. The method involves the measurement of the angle between the direction of annihilation photons, which depends on the electronic momentum. Thus, if it is different from zero, there will be a deviation of less than 180° between the directions of the emitted photons. Since the positron is thought to be thermalized before the annihilation occurs (10^{-11} sec), the angular deviation from 180°, which is in the order of a few milliradians, is mainly due to the contribution of electronic momentum. The form of angular distribution yields information about electronic momentum distribution.

In the Doppler broadening technique, the energy distribution of the annihilation photons is measured. The spreading of the annihilation peaks caused by the motion of the positron-electron pair with respect to the detector can be observed. This technique can also be used to measure the momentum distribution of the annihilating pair. It is much simpler and faster than the angular momentum distribution but has a poorer momentum resolution. The above two positron annihilation spectroscopic techniques can yield the momentum distribution of electrons. However, they cannot provide information on electron density distribution, which can be provided from the positron lifetime analysis.

In positron lifetime measurements, the incident beam of positrons thermalizes in solids and annihilates into gamma rays. The number of positrons, $N(t)$, is recorded as a function of time. The accumulated lifetime spectrum which represents the number of positrons that have lived a certain time consists of several components

relating to the properties of the material under investigation. Each component has an exponential decay form. The simple form of the lifetime spectrum can be represented as

$$N(t) = \sum_i I_i e^{-\lambda_i t} + B, \tag{3. 11}$$

where I_i is the intensity of the i-th lifetime component representing the probability of positrons that annihilate at a rate of λ_i and B is the background of the spectrum. In condensed matter, a positron interacts and may annihilate with any of electronic states, and hence the spectrum usually consists of several components. Each lifetime represents different states of the positron in electronic environments. The quantity λ_i is the annihilation rate which may represent the slopes of the lifetime spectrum. Positron lifetimes are reciprocal of λ_i. The intensity I_i can be obtained by integrating the area under the i-th lifetime component and normalizing to the total area under the lifetime curve.

The experimental data analysis is not as simple as we have abstractly explained it above. It is much more difficult to resolve lifetime spectra into two, three, or four components. Several computer programs for analyzing lifetime spectra are available, including POSITRONFIT,[72] PAL,[73] PFPOSFIT,[74] and INTERACTIVE POSITRON FIT.[75] As an example, the analyzed experimental data[76] for alkali halides is shown in Table II.

B. The pair correlation function

One of the central theoretical problems is how to properly describe the distortion of the positron wavefunction due to the electronic structure in the vicinity of the defect center or in the Bloch states of the host crystal. The positron state may be changed from the free particle state as a plane wave into the bound state or a

TABLE II. Positron lifetimes($x10^{-10}$ sec) and the corresponding intensities(%) for alkali halides.

Crystal	τ_0	τ_1	τ_2	τ_3	τ_{tail}	I_0	I_1	I_2	I_3	I_{tail}
LiF	-	1.32+/-.07	2.97+/-.09	-	11.0; 18.7*	-	31+/-2	63.1+/-3.1	-	1.8; 0.4*
NaF	-	1.93+/-.10	3.90+/-.09	-	36.0; 14.4*	-	27+/-2	66.0+/-3.2	-	0.8; 1.3*
KF	-	1.80+/-.09	4.24+/-.13	10.0+/-.30	-	-	34+/-3	50.0+/-2.5	9.0+/-0.2	-
RbF	-	1.55+/-.08	3.51+/-.11	7.44+/-.22	-	-	21+/-3	61.7+/-3.1	22.8+/-.7	-
CsF	-	1.45+/-.08	3.89+/-.12	9.38+/-.28	-	-	30+/-3	45.9+/-2.6	23.9+/-.6	-
LiCl	-	2.36+/-.12	4.35+/-.13	-	17.5	-	51+/-4	49.1+/-2.4	-	0.6
NaCl	-	3.13+/-.16	6.84+/-.20	-	28.9	-	65+/-5	27.6+/-0.9	-	1.2
KCl	-	2.75+/-.14	6.28+/-.19	-	40.5; 24.3*	-	48+/-4	41.3+/-2.0	-	1.3; 1.6*
RbCl	-	1.99+/-.10	4.56+/-.14	10.0+/-.30	-	-	27+/-3	59.3+/-3.0	7.0+/-0.3	-
CsCl	-	2.02+/-.11	4.51+/-.14	12.1+/-.30	-	-	42+/-4	54.6+/-2.7	5.0+/-0.2	-

* Powders; Single Crystals, L. Busolatti et al. (Ref. 76)

scattered state by the attraction of electrons. In this study, we are mainly concerned with the bound states of the positron. The probability of pair-annihilation increases with the increasing probability of the electron density at a positron position.

From the three-component formalism of DFT which includes the correlation terms, one can calculate the electron and positron probability densities self-consistently. The spin averaged positron annihilation rate λ, is given by the equation,[77]

$$\lambda = \frac{\pi r_0^2 c}{e^2} \int dr \rho(r) \rho_+(r) g(0;\rho, \rho_+;\zeta) = \frac{1}{\tau}, \tag{3.12}$$

where $r_0 = e^2/(4\pi\varepsilon_0 mc^2) = 2.81794092(38)$ fm is the classical electron radius, ρ is the ground-state electron charge density, and ρ_+ is the positron charge density. If the electron and positron are statistically independent, the annihilation rate just comes from the product of their densities. However, since they are not independent, especially in bound states, the rate is a sensitive measure of electron-positron probability distribution. The pair-correlation function $g(0;\rho, \rho_+;\zeta)$ gives the measure of quantum correlation effect between the electron and the positron at the origin of the positron position in any polarization mode ζ. It may be valuable to consider further detailed information on this correlation function.

For the one particle limit of the positron in the uniform electron gas, in other words, the positron concentration $x(= \rho_+/\rho) \rightarrow 0$, the function can be evaluated within the Sawada bosonic approach, which provides good accuracy for the positron annihilation rate.[26] When the positron concentrations are increased to $x = \frac{1}{2}$ and 1, the pair correlation can be analyzed by the Fermi-hypernetted chain equation (FHNC),[27] which approximately gives the same limit with the Sawada bosonic

method for the $x \to 0$. From these theoretical approaches, the computational implementation can be performed by the interpolation of the data.

The pair-correlation function reduces, in the single positron limit, to

$$g(r) = 1 + \frac{4}{3}\pi r_s^3 \langle \delta\rho(r) \rangle, \tag{3.13}$$

where the r_s is the Wigner-Seitz radius defined by $\frac{1}{\rho} = \frac{4}{3}\pi r_s^3$, and the average of the increased electron density is at the positron position $\langle \delta\rho(r) \rangle$. The electron gas is described by a set of interacting bosons representing the collective excitations of the random-phase approximation (RPA). These bosons were first defined by Sawada,[78] who showed that the RPA can be formulated in terms of non-interacting, free bosons; this was extended into the whole interacting electronic Hamiltonian being represented with a boson Hamiltonian. The Sawada bosons include not only the plasmons, which are important for the correction of the long-wavelength limit, but also the continuum of particle-hole excitations, whose oscillator strengths are suppressed in the small-momentum region in comparison with free pairs. While these various eigen-excitations are only weakly coupled to each other in a homogeneous interacting electron system, the presence of the positron has the effect of making the strongly excited collective modes also of obtaining important mutual interactions due to the induced inhomogeneity. The mutual correlation of the induced collective excitations gives the expression for the pair correlation function assumed to be spherically symmetric about the positron from the induced density of Eq. (3.12). The interpolated form for the pair-correlation function on the limit $x \to 0$ may be written in terms of the Wigner-Seitz radius as follows:[26]

$$g_0(r_s) = 1 + 1.23 r_s + 0.8295 r_s^{3/2} - 1.26 r_s^2 + 0.3286 r_s^{5/2} + \frac{r_s^3}{6}. \tag{3.14}$$

The pair correlation function can also be described by the approximate Euler-Lagrange equations for the Fermi hypernetted-chain method[79-81] for the higher positron concentration $x = \frac{1}{2}$ and 1. The basic assumption is that at the zero temperature, Fermi systems are described by the approximate Jastrow wavefunction,[82] which is modified from the usual Slater type unperturbed wavefunction including the correlational factor; that is,

$$|\Psi\rangle = \prod_{i<j=1}^{N} f(x_i, x_j)\,|\Phi\rangle, \tag{3.15}$$

where N is the number of particles of the system. The trial wavefunction consists of a product of correlation factors f which act on an unperturbed wavefunction for the independent particle motion. For Fermi systems, the unperturbed wavefunction is a Slater determinant:

$$|\Phi\rangle = \prod_{\lambda} (a_\lambda{}^\dagger)\,|0\rangle, \tag{3.16}$$

composed of single particle orbitals λ belonging to the Fermi sea. The $a_\lambda{}^\dagger$ are fermion creation operators acting on the particle vacuum $|0\rangle$.

The Jastrow wavefunctions can be applied to a model of interpenetrating fluids, each of which consists of $N_\alpha\,(\alpha = 1, 2)$ multi-component particles in a common volume V, at zero temperature, such that all the partial densities $\rho_\alpha = N_\alpha/V$ remain constant as N_α and V go to infinity. The ground state wavefunction for such a multicomponent system may be approximated by a variational trial function with the following form:[21]

$$|\Psi\rangle = \prod_{\alpha\le\beta=1}^{2} F_{\alpha\beta} \prod_{\alpha=1}^{2} |\Phi_\alpha\rangle. \tag{3.17}$$

Here each $|\Phi_\alpha\rangle$ is the Slater determinant of single particle states for N_α non-interacting particles of species α. Pairwise correlation factors are built into the many-body wavefunction through

$$F_{\alpha\beta} = \prod_{i,j} f_{\alpha\beta}(r_{\alpha i}, r_{\beta j}), \tag{3.18}$$

where $i = 1, 2, \ldots, N_\alpha$, $j = 1, 2, \ldots, N_\beta$ for $\alpha \neq \beta$ and $i = 1, 2, \ldots, N_\alpha - 1$, $j = 2, \ldots, N_\alpha$ for $\alpha = \beta$ such that each pair of particles appears only once in this product. For a two-component fluid such as electron and positron plasma, two Slater determinants and three correlation factors f_{11}, f_{12}, and f_{22} have to be determined by minimizing the energy of the system by the variational principle which leads to the Euler-Lagrange equations. By solving the equations with the Jastrow function, the correlation factors $f_{\alpha\beta}$ provide information about the pair correlation function $g_{\alpha\beta}$.

The pair correlation function g_{12} at the positron position in the electron-positron system for several positron concentrations has been obtained. The results imply that the more positrons overlap the electron gas, the fewer electrons there are to screen each positron. The numerically parameterized forms of the pair correlation functions at the positron concentrations $x = \frac{1}{2}$ and 1 are available:[27]

for $\rho_+ = \rho_-$ $(x = 1)$,

$$g_1(r_s) = 1 + 0.51 r_s + 0.65 r_s^2 - 0.51 r_s^{5/2} + 0.167 r_s^3, \tag{3.19}$$

and for $\rho_+ = \rho_-/2$ $\left(x = \frac{1}{2}\right)$,

$$g_2(r_s) = 1 + 0.6 r_s + 0.63 r_s^2 - 0.48 r_s^{5/2} + 0.167 r_s^3. \tag{3.20}$$

The correlation functions can be interpolated from both the Arponen and Pajanne data and Lantto's results.[26-27] These results provide the general form of the

pair correlation function from data at positron concentrations 0, $\frac{1}{2}$, and 1:

$$g(\rho_+ \to 0, \rho_-) = g_0(\rho_-), \tag{3.21}$$

$$g(\rho_+, \rho_-)\big|_{\rho = \rho_+ = \rho_-} = g_1(\rho), \tag{3.22}$$

$$g(\rho_+, \rho_-)\big|_{\rho_+ = \rho/2} = g_2(\rho). \tag{3.23}$$

On the basis of this knowledge, Nieminen[1] found that it was possible to construct the surface of the pair correlation functions per unit volume $g(\rho_+, \rho_-)$ throughout the (ρ_+, ρ_-) plane. For $\rho_+ \to 0$, $g(\rho_+, \rho_-)$, the slope of the surface parallel to ρ_+-axis and close to ρ_--axis is equal to $g_0(\rho_+, \rho_-)$. In turn, for $\rho_+ = \rho_- = \rho$, $g(\rho_+, \rho_-)$ equals to $g_1(\rho)$. The surface of $g(\rho_+, \rho_-)$ is of course symmetric with respect to ρ_+ and ρ_-. The derivatives of the function of contact density between electron and positron at the origin,

$$g_+(\rho_+, \rho_-) = \rho_+ \frac{\delta g(\rho_+, \rho_-)}{\delta \rho_+}, \tag{3.24}$$

$$g_-(\rho_+, \rho_-) = \rho_- \frac{\delta g(\rho_+, \rho_-)}{\delta \rho_-}, \tag{3.25}$$

become partial derivatives of $g(\rho_+, \rho_-)$ along ρ_+, ρ_- directions

$$g_+(\rho_+, \rho_-) = \rho_+ \frac{\partial}{\partial \rho_+} g(\rho_+, \rho_-), \tag{3.26}$$

$$g_-(\rho_+, \rho_-) = \rho_- \frac{\partial}{\partial \rho_-} g(\rho_+, \rho_-). \tag{3.27}$$

Taking this fact into account and assuming the continuity of partial derivatives throughout the (ρ_+, ρ_-) plane, the surface of correlation function may be symmetric

for the equal densities

$$g_-(\rho_+,\rho_-)\big|_{\rho_+=\rho_-=\rho} = g_+(\rho_+,\rho_-)\big|_{\rho_+=\rho_-=\rho} = \rho\frac{\partial}{\partial\rho}g_1(\rho) = k(\rho)\,. \qquad (3.28)$$

On this analytic plane, it is possible to assume the following analytic form of the pair correlation function for $\rho_+ \le \rho_-$:

$$g(0;\rho_>,\rho_<) = a(\rho_>)\rho_<^3 + b(\rho_>)\rho_<^2 + c(\rho_>)\rho_< + g_0(\rho_>)\,, \qquad (3.29)$$

where $\rho_<(\rho_>)$ denotes the smaller (greater) of the densities ρ_+ and ρ_-. Then the unknown coefficients $a(\rho), b(\rho), c(\rho)$ can be found by solving the above Eqs. (3.21-23) and (3.28). The solution is

$$a(\rho) = \rho^{-3}[2k(\rho) - 6g_1(\rho) + 8g_2(\rho) - 2g_0(\rho)]\,, \qquad (3.30)$$

$$b(\rho) = \rho^{-2}[-3k(\rho) + 11g_1(\rho) - 16g_2(\rho) + 5g_0(\rho)]\,, \qquad (3.31)$$

and

$$c(\rho) = \rho^{-1}[k(\rho) - 4g_1(\rho) + 8g_2(\rho) - 4g_0(\rho)]\,. \qquad (3.32)$$

The interpolated result has proper asymptotic behavior for the high density limit ($r_s \to 0$) and the low density limit ($r_s \to \infty$) which corresponds to pairs of Ps atoms.

CHAPTER IV

CRYSTAL FIELD EFFECTS

When investigating positron annihilation phenomena in crystalline material, the crystal field effect on the self-consistent electron and positron densities needs to be included. The crystal effect is generally represented with the crystal potential which provides information about the periodicity of the crystalline structure. The crystal potential keeps the electron bound in the Bloch states. However, the positron in the Bloch states is repulsed by those regions of the crystal potential which are attractive to electrons. The Hamiltonian of the atom can be extended to the solid system by including the crystal potential:

$$H_{i\sigma} = H_{i\sigma}^{atom} + V_{crys} - V_{center} \tag{4. 1}$$

$$H_{p} = H_{p}^{atom} - V_{crys} + V_{center}. \tag{4. 2}$$

In this chapter, the crystal field treatment is described in detail for simple ionic cubic crystals such as alkali-halides (LiF, NaF, LiCl, and NaCl) with octahedral symmetry (O_h^5) as shown in Fig. 4.1.

In a perfect crystal, at T = 0 K, the nuclei are supposed to be located at the equilibrium positions. The alkali-halide lattice is constructed from two inter-penetrating sublattices of face-centered cubic (fcc) structure with the halide ion located at the position $\boldsymbol{R}_\nu$; the alkali ion on $\boldsymbol{R}_\nu + \boldsymbol{t}$. $\boldsymbol{R}_\nu$ is a translational vector of

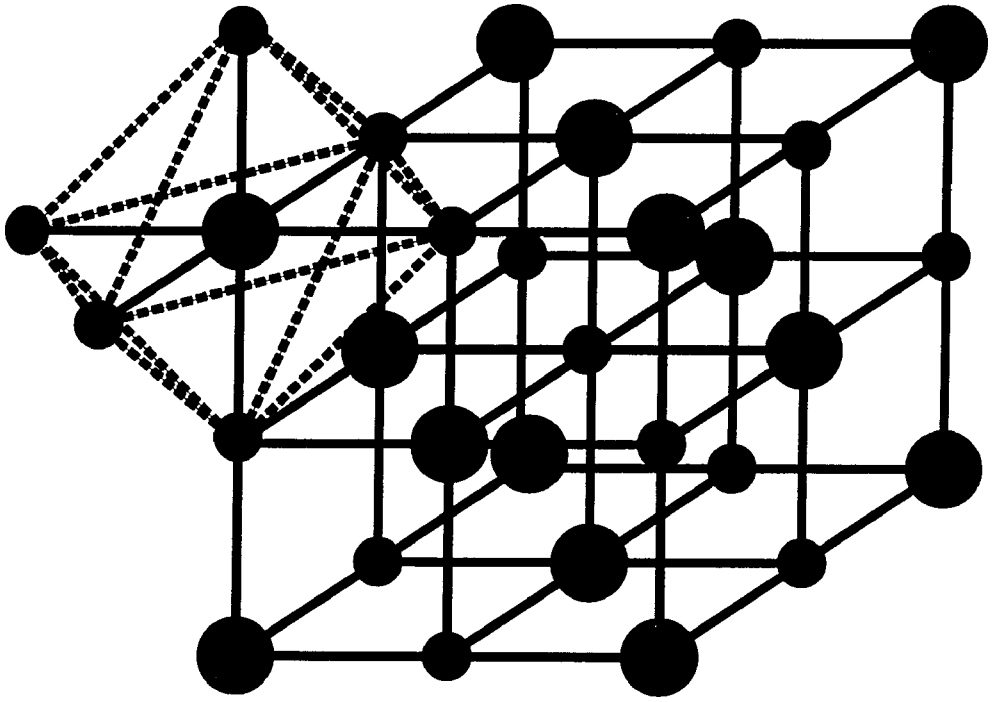

FIG. 4.1. Octahedral structure of alkali halides.

the fcc lattice with lattice constant a [7.611816282 (LiF), 8.756990231 (NaF), 9.713191581 (LiCl), 10.65805458 (NaCl)],[83]

$$\boldsymbol{R}_v = n_1\boldsymbol{a}_1 + n_2\boldsymbol{a}_2 + n_3\boldsymbol{a}_3 , \tag{4. 3}$$

where n_1, n_2, n_3 are all integers, and $\boldsymbol{a}_1, \boldsymbol{a}_2, \boldsymbol{a}_3$ are fcc basis vectors:

$$\boldsymbol{a}_1 = \frac{a}{2}(1, 1, 0) , \tag{4. 4}$$

$$\boldsymbol{a}_2 = \frac{a}{2}(1, 0, 1) , \tag{4. 5}$$

$$\boldsymbol{a}_3 = \frac{a}{2}(0, 1, 1) . \tag{4. 6}$$

Thus,

$$\boldsymbol{R}_v = \frac{a}{2}(n_1 + n_2, n_1 + n_3, n_2 + n_3)$$

$$= \frac{a}{2}(m_x, m_y, m_z) \tag{4. 7}$$

where $m_x + m_y + m_z = 2(n_1 + n_2 + n_3)$ is even. $t = \frac{a}{2}(1, 0, 0)$ is a translational vector from a halide site to a nearest neighbor alkali cation.

We are concerned with the electronic structure of a halide ion at the anion center in our density functional calculation, and the rest of the crystal lattice is simplified into point-like or full ions. The long range interaction between ions with repetitive charge $\pm e$ is the electrostatic interaction, attractive between ions of opposite charge and repulsive between ions of the same charge. The ions arrange themselves in such a way so that the crystal structure gives the strongest attractive interaction compatible with the repulsive interaction at short distances between ion cores. In ionic solids, the major part of the cohesion comes from the Coulomb

interaction. The simple point-ionic approximation for this ionic crystal is given by

$$V_{crys}(\boldsymbol{r}) = \sum_{\nu=0}^{\infty}\left(\frac{1}{|\boldsymbol{r}-\boldsymbol{R}_\nu|}-\frac{1}{|\boldsymbol{r}-\boldsymbol{R}_\nu-\boldsymbol{t}|}\right), \tag{4. 8}$$

and the point-ionic crystal potential at the halide center is called the Madelung potential

$$V_{Ma}(\boldsymbol{r}) = V_{crys}(\boldsymbol{r}) - \frac{1}{r}, \tag{4. 9}$$

where one point-like halide ion at the origin is removed in order to assess the crystal field effect from the rest of the crystal lattice on the anion center. The Madelung potential can be expressed in terms of the lattice constant

$$V_{Ma}(0) = \frac{-2\alpha}{a}, \tag{4. 10}$$

where the Madelung constant[84] is defined by

$$\alpha = \sum_{j=1}\frac{(\pm 1)}{p_{ij}}, \tag{4. 11}$$

where p_{ij} is the distance of the j-th ion from the reference ion i in units of the nearest-neighbor distance, and the plus sign is for alkali sites and minus sign is for halides sites with the halide ion as the reference ion.

The evaluation of the Madelung constant is of central importance in the theory of ionic crystals. One of the direct methods is that of Evjen,[85] where one treats successive shells, going outward from the origin, each one being exactly neutral in total electrostatic charge. This method was utilized by Frank[86] by introducing a cuboid which contains one ion at its center and 8 point charges of e/8 at the corners of the cell. This direct sum of the Madelung constant gives the periodic potential at a lattice point due to the rest of the ions in an infinite crystal. Madelung[84] evaluated

this as 1.74(2) and Emersleben[87] as 1.74755(7±2). The four-term sum of cuboid shells from the Frank method[86] gives 1.747626 and is sufficiently accurate for most physical applications.

However, the series of the Madelung constant is conditionally convergent, but even then only slowly. This slow convergence of $V_{Ma}(\boldsymbol{r})$ may be associated with the singularities of the point-charge potential which behave like $\pm 1/r$ about each site as shown in Fig. 4.2. In order to overcome the problem of slow convergence in the lattice sums of an ionic crystal, there is a very elegant general procedure developed by Ewald.[88] Ewald's method can be applied to two models of the crystal potential. In our current study, we employ a modified point-ionic potential and a full ionic potential determined from an energy-band calculation.

A. The modified point-ionic potential

To improve the convergence of the Madelung potential, the singularities can be removed by introducing a Gaussian cut-off potential to cut the long range Coulomb interaction and calculate the $\pm 1/|\boldsymbol{r}-\boldsymbol{R}_{\nu}|$ contribution to the potential integral by a direct space integration.[89] The Madelung potential at the anion center can be written as

$$V_{Ma}(\boldsymbol{r}) = V_{crys}(\boldsymbol{r}) - V_{center}(\boldsymbol{r}) , \tag{4.12}$$

where the crystal potential has been slightly modified from the point-ionic potential by introducing the ionic radius. This can be written as

$$V_{crys}(\boldsymbol{r}) = \sum_{\nu=0}^{\infty} \left[V^{H}_{ion}(\boldsymbol{r}-\boldsymbol{R}_{\nu}) + V^{A}_{ion}(\boldsymbol{r}-\boldsymbol{R}_{\nu}-t) \right] \tag{4.13}$$

with a spherical approximation for ionic potentials

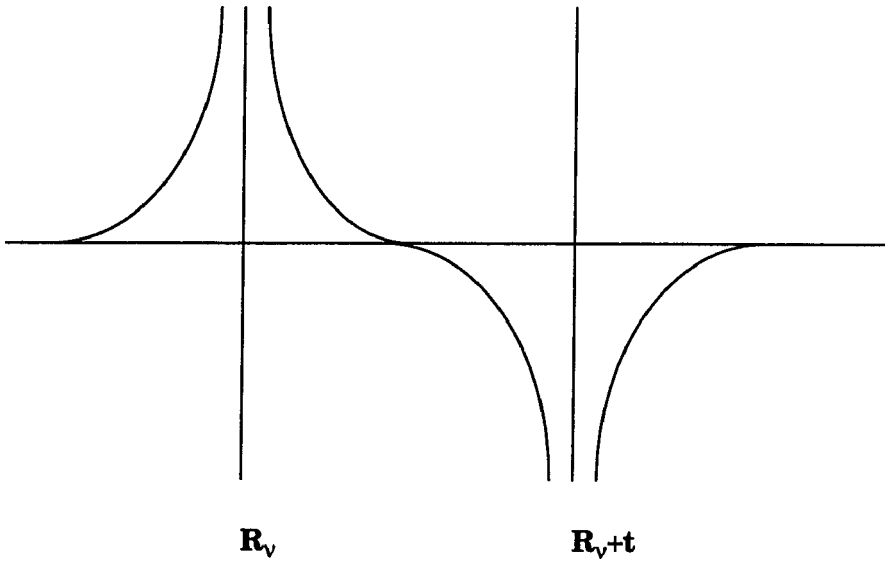

FIG. 4.2. Schematic point-ionic potential for alkali halides.

$$V^{H}_{ion}(\boldsymbol{r}) = \frac{1-\left(Z^{H}+1\right)\exp\left(-\alpha^{H}r^{2}\right)}{r} \tag{4. 14}$$

$$V^{A}_{ion}(\boldsymbol{r}) = \frac{-1-\left(Z^{A}-1\right)\exp\left(-\alpha^{A}r^{2}\right)}{r}, \tag{4. 15}$$

where the exponential terms are negligible beyond the ionic radius R_{ion} [1.10 (Li^+), 1.81 (Na^+), 2.57 (F^-), and 3.42 (Cl^-)], and thus the relation $\exp\left(-\alpha R^{2}_{ion}\right) = \Delta = 10^{-6}$ gives the parameter α [10.74 (Li^+), 4.29 (Na^+), 2.09 (F^-), and 3.42 (Cl^-)].

The periodicity for the ionic crystal potential provides the potential form of the Fourier series:

$$V_{crys}(\boldsymbol{r}) = \sum_{\nu} V_{crys}(\boldsymbol{k}_{\nu})\, e^{i\boldsymbol{k}_{\nu}\cdot\boldsymbol{r}}, \tag{4. 16}$$

so the Fourier coefficients of these potentials can be derived from

$$V_{crys}(\boldsymbol{k}_{\nu}) = \frac{1}{N\Omega}\int V_{crys}(\boldsymbol{r})\, e^{-i\boldsymbol{k}_{\nu}\cdot\boldsymbol{r}} d^{3}\boldsymbol{r}, \tag{4. 17}$$

where Ω is the volume of unit cell, N is the number of cells in the crystal, and $N\Omega$ is the entire crystal volume:

$$\boldsymbol{k}_{\nu} = m_1\boldsymbol{b}_1 + m_2\boldsymbol{b}_2 + m_3\boldsymbol{b}_3$$

$$= \frac{2\pi}{a}[l_x, l_y, l_z], \tag{4. 18}$$

where l_x, l_y, and l_z are all even or all odd for the O^5_h group of fcc crystals, and $\boldsymbol{b}_1$, $\boldsymbol{b}_2$, $\boldsymbol{b}_3$ are basis vectors of the reciprocal lattice for fcc, that is, a bcc lattice:

$$\boldsymbol{b}_1 = \frac{2\pi}{a}(1, 1, -1), \tag{4. 19}$$

$$\boldsymbol{b}_2 = \frac{2\pi}{a}(-1, 1, 1), \tag{4. 20}$$

and

$$\boldsymbol{b}_3 = \frac{2\pi}{a}(1,-1,1)\,. \tag{4.21}$$

After changing the variables of the Fourier integrations and using $\boldsymbol{k}_\nu \cdot \boldsymbol{R}_\nu = 2m\pi$ and $\boldsymbol{k}_\nu \cdot \boldsymbol{t} = l_x\pi$, there exist the following relations:

$$\frac{1}{N}\sum_{\nu} e^{-i\boldsymbol{k}_\nu \cdot \boldsymbol{R}_\nu} = 1\,, \tag{4.22}$$

$$e^{-i\boldsymbol{k}_\nu \cdot \boldsymbol{t}} = (-1)^{l_x}. \tag{4.23}$$

Fourier coefficients can be obtained as

$$V_{crys}(\boldsymbol{k}_\nu) = \frac{4\pi}{\boldsymbol{k}_\nu \Omega}\left\{\left[\frac{1}{\boldsymbol{k}_\nu} - \frac{Z_H+1}{\sqrt{\alpha_H}} D\left(\frac{|\boldsymbol{k}_\nu|}{2\sqrt{\alpha_H}}\right)\right] - (-1)^{l_x}\left[\frac{1}{\boldsymbol{k}_\nu} + \frac{Z_A-1}{\sqrt{\alpha_A}} D\left(\frac{|\boldsymbol{k}_\nu|}{2\sqrt{\alpha_A}}\right)\right]\right\}, \tag{4.24}$$

where the following integrals have been used:

$$\int_0^\infty \sin k_\nu r dr = \lim_{\lambda \to 0}\int_0^\infty e^{-\lambda r}\sin k_\nu r dr = \frac{1}{k_\nu}, \tag{4.25}$$

$$D(x) = \int_0^\infty e^{-t^2}\sin 2xt dt\,. \tag{4.26}$$

The convergence of the matrix element:

$$V_{ij}^{crys} = \int \Phi_i^*(\boldsymbol{r})\, V_{crys}(\boldsymbol{r})\, \Phi_j(\boldsymbol{r})\, d^3\boldsymbol{r}\,, \tag{4.27}$$

for the crystal potential can be examined. As an example, for an s-type basis function, $\Phi_i(\boldsymbol{r}) = Nexp(\alpha_i r^2)$, the normalization factor and the matrix element of the crystal potential integral are, respectively, written as

$$\int \Phi_i^*(\boldsymbol{r})\,\Phi_j(\boldsymbol{r})\,d^3\boldsymbol{r} = N^2\left(\frac{\pi}{\alpha_i+\alpha_j}\right)^{3/2} = 1 \tag{4.28}$$

and

$$\langle \Phi_i | V_{crys}(\boldsymbol{r}) | \Phi_j \rangle = N^2 \int e^{-\alpha_i r^2}\left(\sum_{\nu} V_{crys}(\boldsymbol{k}_\nu)\cos(\boldsymbol{k}_\nu\cdot\boldsymbol{r})\right)e^{-\alpha_j r^2} d^3\boldsymbol{r}$$

$$= \sum_{\nu} V_{crys}(\boldsymbol{k}_\nu)\, e^{-k_\nu^2/4(\alpha_i+\alpha_j)}. \tag{4.29}$$

The convergence of the Fourier expansion is primarily determined by the two factors, the Fourier coefficients $V_{crys}(\boldsymbol{k}_\nu)$ and the exponential term. The Fourier coefficients, $V(\boldsymbol{k}_\nu)$, of the crystal potential drop like $1/\boldsymbol{k}_\nu^2$, but the number of terms grows as $\boldsymbol{k}_\nu^2$ and will not converge unless the exponent helps. When $\alpha_i+\alpha_j$ is small, $(\alpha_i+\alpha_j<20)$, the matrix element Eq. (4.29) will converge quickly since the exponential term becomes smaller when $\boldsymbol{k}_\nu$ increases.

When $\alpha_i+\alpha_j$ is large, $(\alpha_i+\alpha_j>20)$, the convergence of the Madelung potential is not rapid; since the exponential term is too large to neglect, the convergence depends on the Fourier coefficients $V_{crys}(\boldsymbol{k}_\nu)$. So the convergence of the coefficients can be improved with Ewald's method in which the long range summation can be cut by introducing a short-range Gaussian screened potential V_{cut} which gives zero potential at the nearest neighbor. Now the crystal potential $V_{crys}(\boldsymbol{r})$ can be written as two parts:

$$V_{crys}(\boldsymbol{r}) = V_{cut}(\boldsymbol{r}) + V_E(\boldsymbol{r}), \tag{4.30}$$

where the Ewald potential is defined by

$$V_E(\boldsymbol{r}) = V_{crys}(\boldsymbol{r}) - V_{cut}(\boldsymbol{r}), \tag{4.31}$$

and the cut-off potential is introduced as

$$V_{cut}(\boldsymbol{r}) = \sum_{\nu=0} \left[V^{H}_{cut}(\boldsymbol{r}-\boldsymbol{R}_\nu) + V^{A}_{cut}(\boldsymbol{r}-\boldsymbol{R}_\nu-\boldsymbol{t}) \right], \tag{4.32}$$

with

$$V^{H}_{cut}(\boldsymbol{r}) = \frac{-Z^{H}\exp\left(-\gamma r^{2}\right)}{r}, \tag{4.33}$$

$$V^{A}_{cut}(\boldsymbol{r}) = \frac{-Z^{A}\exp\left(-\gamma r^{2}\right)}{r}. \tag{4.34}$$

The potential V_{cut} behaves like $-Z/r$ about each nucleus. It is a short ranged function dropping off to zero before r approaches the nearest neighbor distance. The Ewald potential V_E is a relatively smooth function shown schematically in Fig. 4.3. It can be expanded in a Fourier series which converges with much fewer terms.

From the same periodicity for the Ewald and cut-off potentials, Fourier coefficients and the matrix element for the s-type basis function can be obtained, respectively,

$$V_{cut}(\boldsymbol{k}_\nu) = \frac{4\pi}{\Omega k_\nu \sqrt{\gamma}} D\left(\frac{|\boldsymbol{k}_\nu|}{2\sqrt{\gamma}}\right)\left[Z_H - (-1)^{lx} Z_A\right], \tag{4.35}$$

$$V_E(\boldsymbol{k}_\nu) = V_{crys}(\boldsymbol{k}_\nu) - V_{cut}(\boldsymbol{k}_\nu), \tag{4.36}$$

$$V^{E}_{ij} = \sum_{\nu} V_E(\boldsymbol{k}_\nu)\, e^{-k_\nu^2/4(\alpha_i+\alpha_j)}. \tag{4.37}$$

From the above equation, it is implied that while $V_{crys}(\boldsymbol{k}_\nu)$ and $V_{cut}(\boldsymbol{k}_\nu)$ decrease as $1/k_\nu^2$, $V_E(\boldsymbol{k}_\nu)$ decreases more rapidly, as shown in Fig. 4.4. By substituting potential Fourier coefficients $V_{crys}(\boldsymbol{k}_\nu)$ and $V_E(\boldsymbol{k}_\nu)$ into Eqs. (4.29) and (4.37), respectively, then the lattice sum rapidly converges. The $V^{H}_{cut}(\boldsymbol{r})$ potential with the parameter γ gives the $-Z^{H}/r$ behavior on the near halide site and goes to zero for

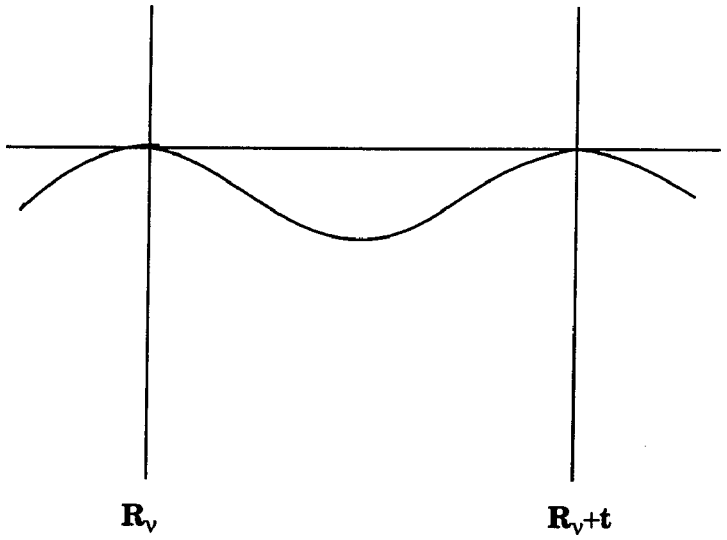

FIG. 4.3. Schematic Ewald potential for ionic crystals.

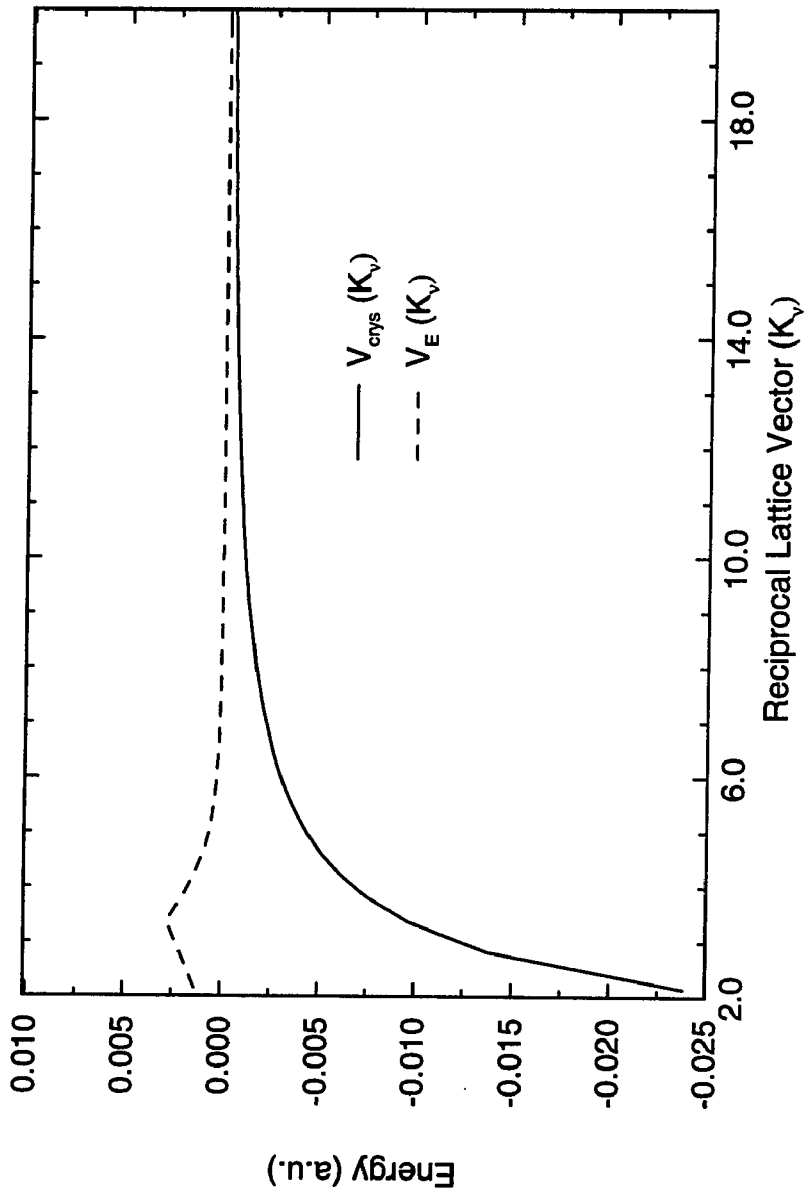

FIG. 4.4(a) Convergence of Fourier coefficients; the point-ionic and corresponding Ewald potentials for LiCl.

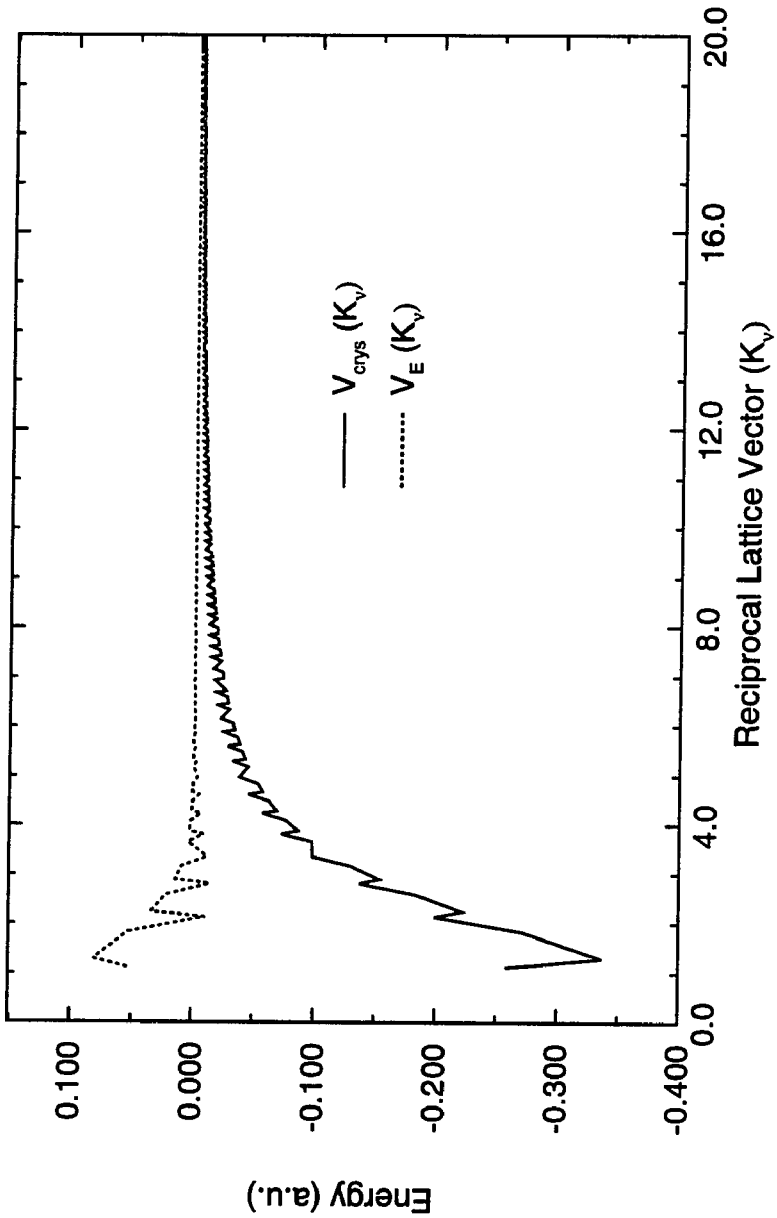

FIG. 4.4(b) Convergence of Fourier coefficients of the Ewald potential in the modified point-ionic potential for LiCl with $\gamma = 1.0$

the near neighbor distance:

$$\frac{Z^H \exp\left(-\gamma|R_1|^2\right)}{R_1} \leq \frac{Z^A \exp\left(-\gamma|t|^2\right)}{t} \cdot \Delta. \tag{4. 38}$$

From the relation $R_1 = \sqrt{2}t$, this condition sets the following criterion:

$$\gamma \geq -\frac{4}{a^2} ln\left(\frac{Z^A}{Z^H}\sqrt{2} \cdot \Delta\right), \tag{4. 39}$$

where the tolerance factor is set to $\Delta = 10^{-6}$.

In the next section, information about making the band structure into this point-like ionic potential will be introduced, leading to a better approximation for the crystal potential.

B. The energy band-ionic potential

The approximation of the crystal potential can be modified for the point-ionic crystal potential by including input from an energy-band structure calculation. The fit of the crystal potential from a band structure calculation takes the form

$$V_{ion}^H(\boldsymbol{r}) = \frac{-Z^H}{r}\exp\left(-\alpha_0^H r^2\right) + \sum_{i=1}^{12} C_i^H \exp\left(-\alpha_i^H r^2\right), \tag{4. 40}$$

$$V_{ion}^A(\boldsymbol{r}) = \frac{-Z^A}{r}\exp\left(-\alpha_0^A r^2\right) + \sum_{i=1}^{12} C_i^A \exp\left(-\alpha_i^A r^2\right), \tag{4. 41}$$

where Z^A and Z^H are atomic numbers of the alkali and the halide ions, respectively, and Gaussian fitting parameters $Z^H, C_i^H, \alpha_0^H, \alpha_i^H$, and $Z^A, C_i^A, \alpha_0^A, \alpha_i^A$ are given in Tables III-VI for calculation of the energy bands.[90] The total band crystal potential $V_{crys}(\boldsymbol{r})$ can be written as

TABLE III. Gaussian fit for the energy-band potential of LiF.

C_i (LiF)	α_i
-9.00000000	0.593632250
2.65038652	346555.700
0.709481713E-01	6297.96120
-0.349654661	1260.15930
520.230614	127.555410
-516.116613	126.909920
-6.78560619	159.184100
5.35082174	73.3755010
2.87783165	16.7435040
3.42824464	6.64249770
3.71815494	2.35684430
7.10673327	0.840146010
-0.731319177E-01	0.230894750
-3.00000000	1.28316320
-0.183981087E-02	38405.0470
-0.699622298E-02	5129.04920
-0.158189199E-01	706.593800
0.100616809	12.0139200
0.671184348E-01	51.3046000
0.337808976	15.4597090
1.20517430	1.19836730
0.424860264	7.85149220
2.28748657	2.85814160
-2.36366034	0.157813380
-1.65457470	0.517409070
1.82297807	0.352311700

TABLE IV. Gaussian fit for the energy-band potential of NaF.

C_i (NaF)	α_i
-9.00000000	0.387101050
1.03490513	336767.850
-0.354141154	2497.16750
-0.259079486	489.937640
6.42794220	81.8034750
-6.17139972	75.0246890
3.30109169	42.9767420
5.52376122	11.9109270
-1.89804287	15.1261670
3.43488041	3.53691520
4.45679578	1.11975010
5.00654651	0.476072390
-0.807798830	0.582518210E-01
-11.0000000	9.92310960
0.591820560E-01	107370.560
0.879976081E-01	40834.7850
-29.9062778	1528.71450
29.9334996	1473.17790
1.40824049	2958.47600
9.11477229	53.8230220
3.29900922	190.906290
1.10245655	176.151470
22.9664052	15.5803140
-9.00704817	3.31253430
-2.52490068	0.837923250
-0.439520463	0.277395710

TABLE V. Gaussian fit for the energy-band potential of LiCl.

C_i (LiCl)	α_i
-17.0000000	0.756517250
1.38700319	1598418.60
-1.11021999	5361.02470
0.639391821	937.194170
5.69044146	177.931760
8.76181173	41.3527380
-23.4585639	7.88611970
31.9592987	8.97134910
13.3156337	3.59601320
13.8951663	1.16092410
1.63876390	0.587777500
-0.167295817E -02	0.262445690E-01
-1.94709179	0.926992820E-01
-3.00000000	10.850328350
-0.521379165E-0 1	1761.23770
-0.746168130	342.623710
0.634605110	384.557850
0.914634717E-01	165.177470
0.533045372	10.8869830
1.01199487	3.61923480
-3.11894912	1.25827800
3.53486155	1.56462970
1.93679141	0.884166550
0.455585250	0.507662630
-3.48232971	0.221795510
2.81710626	0.156329790

TABLE VI. Gaussian fit for the energy-band potential of NaCl.

C_i (NaCl)	α_i
-17.0000000	0.372068210
0.346088514	552645.710
-1.18596156	6474.38450
2.05155519	361.428080
-14.7340189	94.4305110
17.7986718	106.049140
9.40054548	42.1475860
-0.879296342	16.4124030
11.5436361	10.1836770
8.39611594	3.01224870
6.26471649	1.55143470
11.5737169	0.533509050
-0.244790538	0.455824190E-01
-11.0000000	1.47355070
-0.425372850	4355.58650
-0.156129398	1509.50790
0.475480520	124.129750
2.81040842	109.226210
6.41453274	23.2664020
10.2676604	5.07722010
28.2765606	2.18969170
-18.8346932	2.63095900
-1.37528867	1.40107800
5.79074546	0.253607140
-5.80440190	0.302293340
-1.97042777	0.100396510

$$V_{crys}(\boldsymbol{r}) = \sum_{\nu}\sum_{m=0}^{1} V_{ion}[\boldsymbol{r} - (\boldsymbol{R}_{\nu} + m\boldsymbol{t})]$$

$$= \sum_{\nu}\left[V^{H}_{ion}(\boldsymbol{r} - \boldsymbol{R}_{\nu}) + V^{A}_{ion}(\boldsymbol{r} - \boldsymbol{R}_{\nu} - \boldsymbol{t})\right]. \qquad (4.42)$$

From the same procedure used with the modified point-ionic case, it is possible to handle the singularities at the periodic lattice points, which behave like $-Z/r$ about each site as illustrated in Fig. 4.5. The Gaussian cut-off potential V_{cut} can be written as

$$V_{crys}(\boldsymbol{r}) = V_{cut}(\boldsymbol{r}) + V_{E}(\boldsymbol{r}), \qquad (4.43)$$

where the Ewald potential is defined as

$$V_{E}(\boldsymbol{r}) = V_{crys}(\boldsymbol{r}) - V_{cut}(\boldsymbol{r}) \qquad (4.44)$$

and

$$V_{cut}(\boldsymbol{r}) = \sum_{\nu}\left[V^{H}{}_{cut}(\boldsymbol{r} - \boldsymbol{R}_{\nu}) + V^{A}{}_{cut}(\boldsymbol{r} - \boldsymbol{R}_{\nu} - \boldsymbol{t})\right], \qquad (4.45)$$

$$V^{H}{}_{cut}(\boldsymbol{r}) = -\frac{Z^{H}}{r}\exp\left(-\gamma^{H} r^{2}\right) + \sum_{i=1}^{5} C_{i}^{H}\exp\left(-\alpha_{i}^{H} r^{2}\right), \qquad (4.46)$$

$$V^{A}{}_{cut}(\boldsymbol{r}) = -\frac{Z^{A}}{r}\exp\left(-\gamma^{A} r^{2}\right) + \sum_{i=1}^{5} C_{i}^{A}\exp\left(-\alpha_{i}^{A} r^{2}\right). \qquad (4.47)$$

In the above equations, γ^{H} and γ^{A} are chosen in such a way that $V_{cut}(\boldsymbol{r})$ reproduces $-Z^{H}/|\boldsymbol{r} - \boldsymbol{R}_{\nu}|$ near the site; it becomes negligibly small before $\boldsymbol{r}$ goes to the nearest neighborhood site $-Z^{A}/|\boldsymbol{r} - \boldsymbol{R}_{\nu} - \boldsymbol{t}|$, and $V_{E}(\boldsymbol{r})$ becomes a relatively smooth function.

The energy-band potential can thus be used to generate the following Fourier coefficients from the periodicity of the crystal like the modified point-ionic potential:

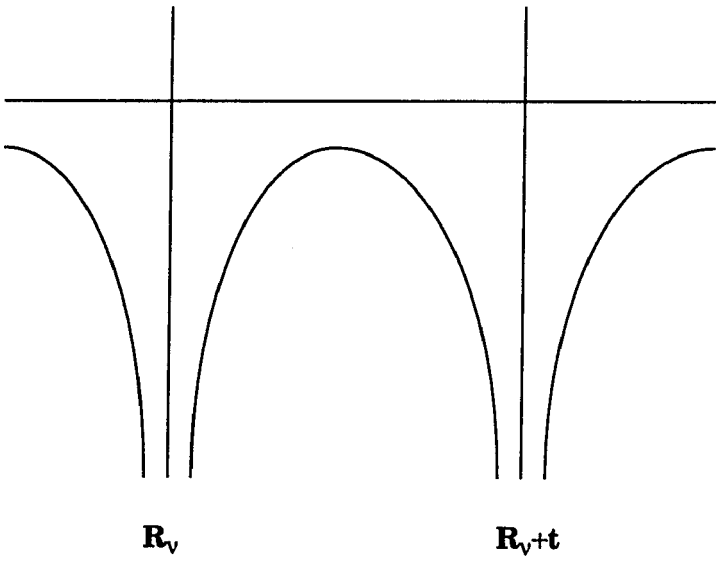

FIG. 4.5. Schematic energy-band ionic potential

$$V_{crys}(\boldsymbol{k}_\nu) = \frac{4\pi}{k_\nu \Omega}\left[V_H(\boldsymbol{k}_\nu) + (-1)^{l_x} V_A(\boldsymbol{k}_\nu)\right], \text{ for } \boldsymbol{k}_\nu \neq 0 \tag{4.48}$$

$$= \frac{4\pi}{\Omega}\left[\sum_{i=1}^{12} C_i^H \frac{1}{4\alpha_i^H}\sqrt{\frac{\pi}{\alpha_i^H}} + \sum_{i=1}^{12} C_i^A \frac{1}{4\alpha_i^A}\sqrt{\frac{\pi}{\alpha_i^A}}\right], \text{ for } k_\nu = 0 \tag{4.49}$$

with

$$V_H(\boldsymbol{k}_\nu) = \frac{-Z^H}{\sqrt{\alpha_0^H}} D\left(\frac{|\boldsymbol{k}_\nu|}{2\sqrt{\alpha_0^H}}\right) + \sum_{i=1}^{12} C_i^H \frac{|\boldsymbol{k}_\nu|}{4\alpha_i^H}\sqrt{\frac{\pi}{\alpha_i^H}} e^{-k_\nu^2/\left(4\alpha_i^H\right)}, \tag{4.50}$$

$$V_A(\boldsymbol{k}_\nu) = \frac{-Z^A}{\sqrt{\alpha_0^A}} D\left(\frac{|\boldsymbol{k}_\nu|}{2\sqrt{\alpha_0^A}}\right) + \sum_{i=1}^{12} C_i^A \frac{|\boldsymbol{k}_\nu|}{4\alpha_i^A}\sqrt{\frac{\pi}{\alpha_i^A}} e^{-k_\nu^2/\left(4\alpha_i^A\right)}, \tag{4.51}$$

and

$$V_E(\boldsymbol{k}_\nu) = V_{crys}(\boldsymbol{k}_\nu) - V_{cut}(\boldsymbol{k}_\nu), \tag{4.52}$$

where $V_{cut}(\boldsymbol{k}_\nu)$ has a form similar to $V_{crys}(\boldsymbol{k}_\nu)$ after replacing α_0 and 12 exponents of band data with the γ–parameter and 5 short-range potential exponents. In the Eq. (4.52) of Fourier coefficients, while $V_{crys}(\boldsymbol{k}_\nu)$ and $V_{cut}(\boldsymbol{k}_\nu)$ decrease as $1/\boldsymbol{k}_\nu^2$, $V_E(\boldsymbol{k}_\nu)$ decreases more rapidly, as shown in Fig. 4.6.

By neglecting the terms in exponential summation of the cut-off potentials, the criterion of the parameters γ^H andγ^A for the V_{cut} potential, which has the $-Z^H/r$ (or $-Z^A/r$) behaviors on the near halide site and goes to zero for the near neighbor distance, is

$$2\gamma^H - \gamma^A \geq -\frac{4}{a^2} ln\left(\frac{Z^A}{Z^H}\sqrt{2}\cdot\Delta\right), \tag{4.53}$$

from the condition of

$$\frac{Z^H}{R_1}\exp\left(-\gamma^H |R_1|^2\right) \leq \frac{Z^A}{t}\exp\left(-\gamma^A |t|^2\right)\cdot\Delta, \tag{4.54}$$

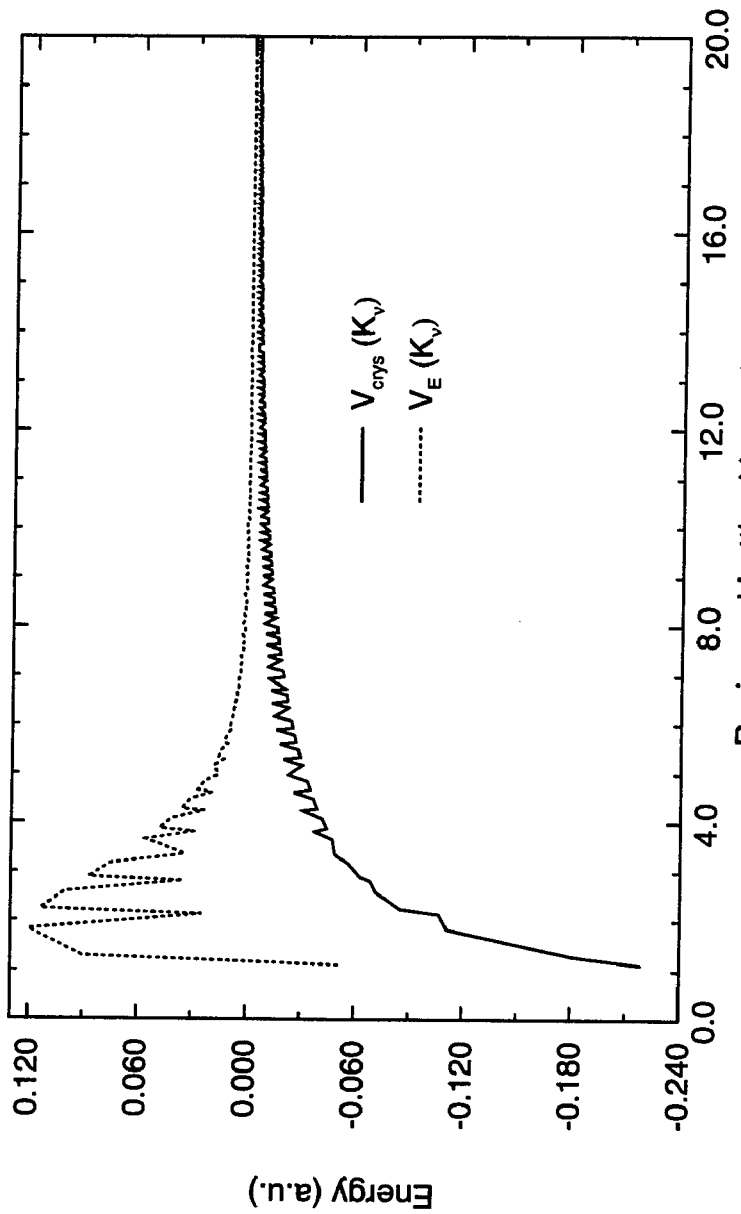

FIG. 4.6. Convergence of Fourier coefficient of the Ewald potential in the energy-band ionic potential in LiCl with $\gamma^H = 1.842$ and $\gamma^A = 1.2$

where the tolerance factor generating the convergence is set to $\Delta = 10^{-6}$. The values obtained for the parameter γ are shown in the Table VII.

To simplify the calculation of the matrix elements with the analytical form of the matrix elements, we use the linear combination of the Gaussian type orbitals which can be optimized from the results of atomic calculation by an atomic structure code. With this orbital basis set, we can solve the self-consistent one-particle equations in the crystal system. The detailed computational procedure will be amplified in the next Chapter.

TABLE VII. The γ–parameter for cut-off potentials. The modified point ionic and the energy-band ionic potentials.

Crystal	Model	γ_{limit}	γ_{used}
LiF	Point	1.005	2.0
	Band		(1.83 / 1.08)*
NaF	Point	0.692	1.5
	Band		(1.5 / 0.713)
LiCl	Point	0.645	1.0
	Band		(1.842 / 1.2)
NaCl	Point	0.490	1.0
	Band		(1.45 / 0.54)

* $(\gamma^{Halide} / \gamma^{Alkali})$

CHAPTER V

COMPUTATIONAL METHODOLOGY

This chapter provides a brief description of some of the important elements incorporated in the execution of programs. We want to carry out self-consistent electronic structure calculations for the positron bound states in systems such as isolated negative and neutral atoms, alkali halide pure crystals, and F-centers in those crystals. Basically we use two numerical algorithms. For the atomic system, we use a numerical atomic structure code which is a modified Herman-Skillman code.[31, 91] For the crystal system, we use a simplified embedded cluster method using linear combinations of Gaussian type orbitals (LC-GTO) because of the analytical management of the complicated multi-center integrals. After optimizing the basis set by using the potential of the atomic numerical calculation by the SIMPLEX algorithm [92] and including the crystal field effect on the Hamiltonian matrix element, the convergence of crystal calculation can be achieved by using the self-consistent field (SCF) iteration. It is helpful to start with a brief description of the atomic numerical codes for the SCF iteration and then take up the simplified embedded cluster.

A. SCF iteration in atomic structures

Before the iteration is started, the nucleus external potential can be used for a crude potential in order to build up initial orbital densities from the Kohn-Sham equation. The orbital density can be used for the evaluation of the orbital Coulomb

potential from the Poison equation. After summing up the occupied orbital densities, the total density can be obtained from the same equation. The exchange-correlation energy and potential can be obtained from the orbital and total densities by calling appropriate subroutines. The orbital by orbital subtraction for the residual self-interaction can modify the effective potential within the SIC-LSDA scheme. On each iteration, the old effective potential is averaged with the new created effective potential from the new trial density. If the maximum difference between the old and new potentials is smaller than a chosen tolerance ($\Delta = 5 \times 10^{-5}$), the self-consistent field iteration can be stopped.

The positron orbital can also be generated from the iteration after the Schrödinger equation is called. The electron-positron Coulomb potential generated from the Poison equation for the electron and positron densities may perturb both electron and positron orbitals. The electron and positron correlation potentials are separately generated in appropriate subroutines. These effective one-body calculations give the self-consistent eigenvalues and total energy for the atomic system with bound positron. The eigenfunctions provide the self-consistent electron and positron densities which are useful for the information of the characterization of the positron annihilation. For the crystal system, another code is required to generate the crystal potential for use in the following embedded cluster method.[92-99]

B. One-site approximation of the embedded-cluster method

The code of the Gaussian-type orbital of the SIC-LSDA for periodic crystal system can be modified to investigate the positron annihilation process in alkali halides (LiF, LiCl, NaF, and NaCl) within a simplified cluster embedding scheme shown in Fig. 5.1. The system can be approximated as a halide-centered cluster with basis functions only on the center. The rest of the crystal is simplified with modified

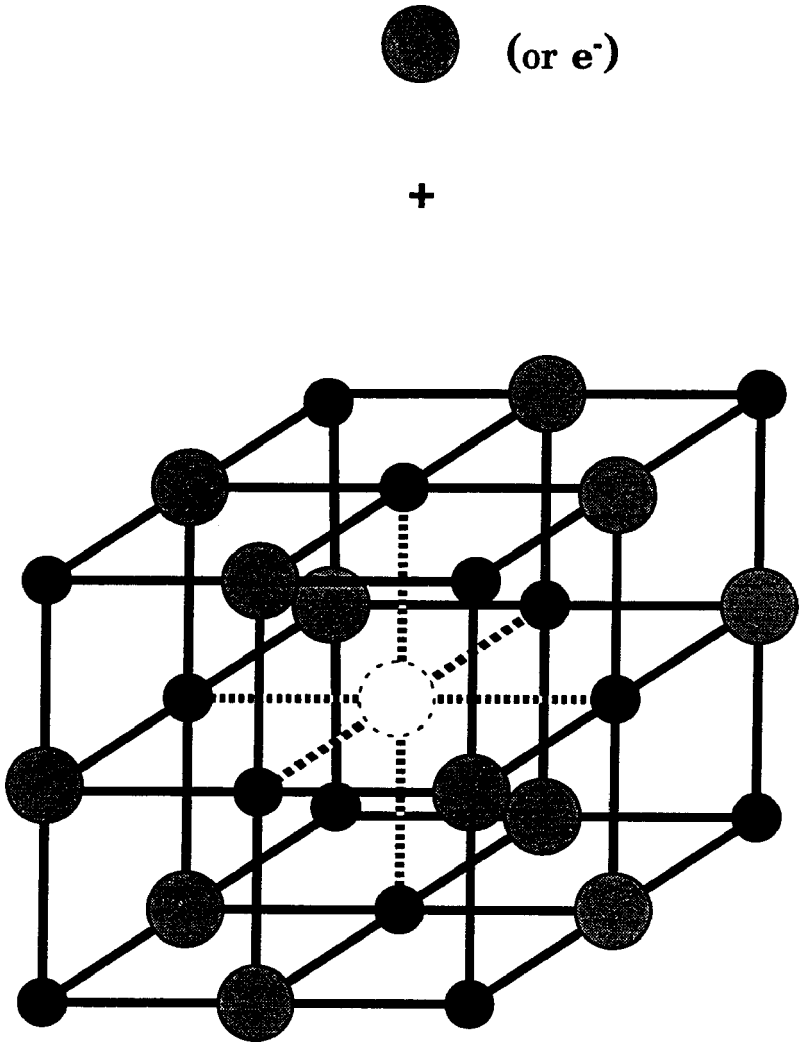

FIG. 5.1. The point-embedded cluster: The halide-ion or the electron on the F-center of alkali halides.

point-ions, or frozen-orbital ions derived from an LCAO energy-band calculation of the pure crystal located on the lattice positions.

The energy functional may be written as the sum of the atomic part including the atomic potential of the halide at the center, and the Madelung potential energy of periodic crystal lattice. From the variational principle, the self-consistent formalism of DFT leads to the one-particle Kohn-Sham equations:

$$H_{i\sigma}\Psi_{i\sigma}(r) = \varepsilon_{i\sigma}\Psi_{i\sigma}(r)\,,\ i = 1, \ldots, N_{\sigma} \tag{5.1}$$

$$H_{p}\Psi_{p}(r) = \varepsilon^{+}\Psi_{j\sigma}(r)\,, \tag{5.2}$$

and Hamiltonian can be written as

$$H_{i\sigma} = H_{i\sigma}^{atom} + V_{Ma}, \tag{5.3}$$

$$H_{p} = H_{p}^{atom} - V_{Ma}. \tag{5.4}$$

Here the Madelung potential is defined at the halide center by $V_{Ma} = V_{crys} - V_{center}$ and the total Hamiltonian includes the ionic crystal field on the atomic Hamiltonian.

The matrix elements can be integrated by using GTO basis functions and the matrix form of the Hamiltonian can be diagonalized to solve the Kohn-Sham equations. The eigenvalue is what is of interest in this eigensystem; also important are the corresponding eigenvectors which are essential for determining the self-consistent electron and positron densities as inputs for the calculation of the positron annihilation rates and lifetimes in bulk state and defect state of F-center in alkali halides.

As a convenience, a simplified version of the LCAO embedded-cluster method[95-97] can be adopted for the analysis of the electron/positron structure of pure crystals.

This code is also useful for the analysis of the defect system of F-center related positron bound states. The essence of this method is that the eigensystem has the Hamiltonian of an infinite pure crystal and a basis set of a finite number of shells of ions around the halide-position. This implies that while our expansion of wavefunction in GTO's is limited to a finite number of shells, the Hamiltonian, corresponds to the infinite system. Our simplified system is a halide-centered cluster with basis functions only on the first shell (central site) and is used to model positron bound states on the negative ion of the bulk site and the F-center of colored crystals. The rest of the crystal potential in the Hamiltonian can be modeled and determined in the context of the modified point-ions located at the lattice positions or the frozen-orbital ions derived from an LCAO energy-band calculation of the pure crystal.[98, 99]

In the context of the concept of the point-defect center in a crystal, the halide ion with a bound positron can be considered as a kind of defect center in the pure crystal as the local limit of the positron state in the perfect crystals. From this viewpoint, Eqs. (5.1) and (5.2) can be solved with the LC-GTO embedded-cluster method by the construction of the point-defect at the positron bounded halide ion site. In other words, the Hamiltonian for the positron bounded system may be analyzed from the viewpoint of the pure crystalline system with an embedded potential at the halide center. The pure crystal Hamiltonian H_{pc} includes the crystal kinetic energy and the crystal potential for the electron and the positron, respectively,

$$H^{e}_{pc} = -\frac{1}{2}\nabla^2 + V_{crys}, \tag{5. 5}$$

$$H^{p}_{pc} = -\frac{1}{2}\nabla^2 - V_{crys}, \tag{5. 6}$$

and the extra potential V_{emb} is the effective potentials of the electron and the positron at the halide center, respectively, written by

$$V^{e}_{emb} = -\frac{Z}{r} + \int dr' \frac{\rho(r')}{|r-r'|} - \int dr' \frac{\rho_{+}(r')}{|r-r'|} + V_{\sigma}^{xc} + V_{c}^{ep-e} + \Delta V_{i\sigma}^{SIC} - V_{center}, \quad (5.7)$$

$$V^{p}_{emb} = \frac{Z}{r} - \int dr' \frac{\rho(r')}{|r-r'|} + V_{c}^{ep-p} + V_{center}. \quad (5.8)$$

The density functional self-consistent iterative loop can be initiated from the zeroth-order approximation of the defect-crystal Hamiltonian matrix $\langle H_{dc} \rangle$ such as

$$\langle H^{e(0)}_{dc} \rangle = \langle H^{e(0)}_{pc} \rangle + \langle V^{e(0)}_{emb} \rangle, \quad (5.9)$$

$$\langle H^{p(0)}_{dc} \rangle = \langle H^{p(0)}_{pc} \rangle + \langle V^{p(0)}_{emb} \rangle. \quad (5.10)$$

In the computational procedure, the perfect crystal Hamiltonian matrix element $\langle H^{(0)}_{pc} \rangle$, as well as $\langle V^{(0)}_{emb} \rangle$, is required to initiate the iterations. The calculation for the infinite pure-crystal potential can be carried out by using the BANDAID package.[90] The Fourier coefficients for the Coulomb and Ewald potential for the periodic infinite crystal have been installed into the perfect Hamiltonian matrix element.

The single-GTO basis functions have been used with the finite number of exponents;

$$\Phi_i(r) = N_0 X exp\left(-\alpha_i r^2\right) . \quad (5.11)$$

Here N_0 is a normalization constant, α_i is the Gaussian exponent (Tables VIII and IX), and X specifies the type (s, p, or d) of Gaussian function, X is 1 for s-type Gaussians, x, y, or z for p-type Gaussians. In the main density functional routine of the self-consistent iterative loop, the same SCF method has been used. The size and

TABLE VIII. Gaussian basis exponents for the fluorine ion. These sets are optimized from the numerical atomic structure results and the re-optimized number of basis sets have been used for crystal calculation for LiF and NaF.

i	Electron (s, p)	Positron (s, p)
1	0.1509536E+05	0.1766448E+02
2	0.2168112E+04	0.7637861E+01
3	0.3568040E+03	0.2433052E+01
4	0.1006477E+03	0.1470892E+01
5	0.3042323E+02	0.7389733E+00
6	0.9723098E+01	0.1850153E+00
7	0.6612085E+00	0.8130870E-01
8	0.6056460E+00	0.3953731E-01
9	0.2556460E+00	0.7297975E-02
10	0.1008263E+00	
11	0.7054373E-01	
12	0.1187524E-01	
13	0.5000000E-02	

TABLE IX. Gaussian basis exponents for the chlorine ion. These have been selectively used for the pure crystals (LiCl, NaCl) and for the associated F-center calculations.

i	Electron (s, p)	Positron (s, p)
1	0.7184573E+06	0.1712508E+03
2	0.2333152E+05	0.5114676E+02
3	0.3268139E+04	0.3927008E+02
4	0.5998057E+03	0.1369680E+02
5	0.1712508E+03	0.4545725E+01
6	0.5114676E+02	0.8099507E+00
7	0.1068252E+02	0.4814303E+00
8	0.2519048E+01	0.3964695E+00
9	0.5952765E+00	0.9662527E-01
10	0.1397643E+00	0.3748278E-01
11	0.9662527E-01	0.2369135E-01
12	0.2369135E-01	0.7220000E-02
13	0.7220000E-02	0.1158693E-02

composition of the basis set can be optimized by energy minimization as shown in Fig. 5.2 for the self-consistent density functional calculation.

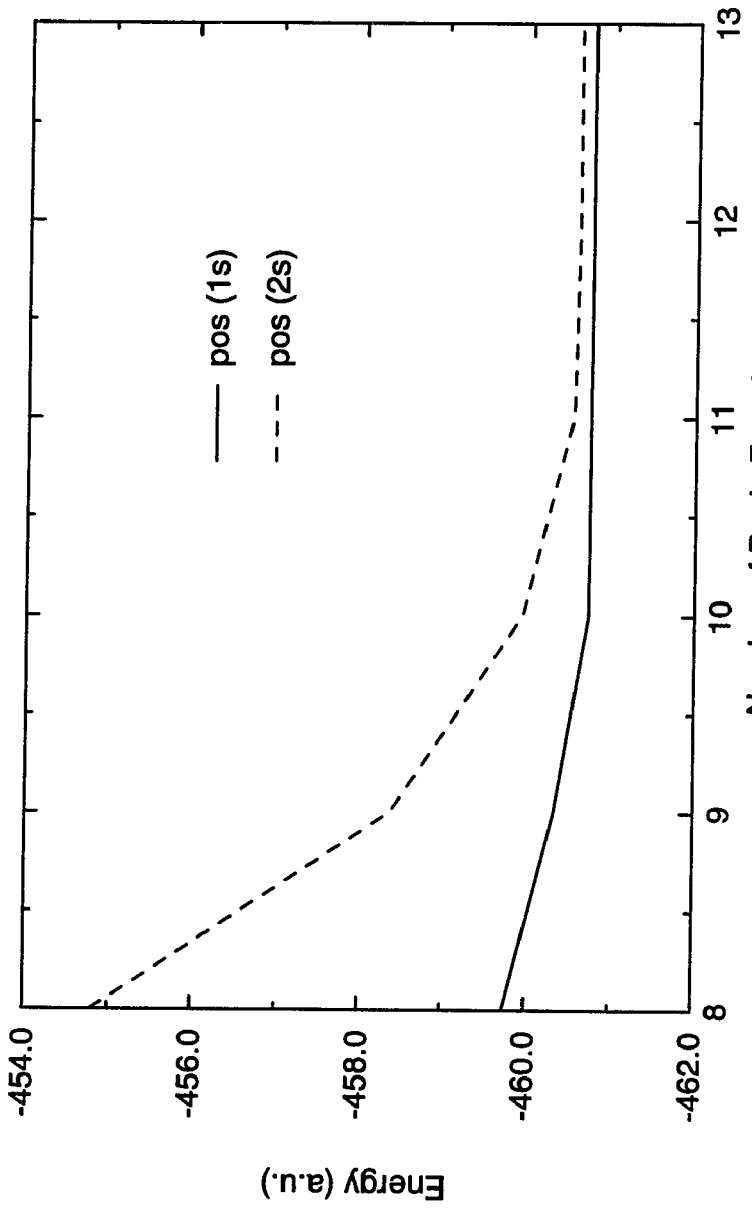

FIG. 5.2. Energy minimization from optimized electron basis sets in the modified point ionic potential of LiCl.

CHAPTER VI

APPLICATIONS

We have performed density functional calculations in the SIC-LSDA scheme of DFT for positron bound states in atomic systems, pure alkali halide crystals, and the F-centers of alkali halides. The positron is fixed with the polarized spin state for each positron orbital, and only the two-photon annihilation process has been considered. The self-consistently calculated electron and positron densities have been used in the evaluation of positron lifetimes at three levels of theory: (i) no correlation included (X-O), (ii) electron-electron correlation included (EC-O), and (iii) electron-electron and electron-positron correlation included (EPC). The X-O calculation for atom-positron systems are compared to *ab-initio* calculations by the restricted Hartree-Fock method.[9]

For the crystalline systems, the lifetimes have been calculated after including the crystal field effect by using the Gaussian basis sets optimized for energy-band calculations. The pure crystalline system and F-center systems are modeled as an anion and a vacancy-bound electron embedded in a pure crystal, respectively, with basis functions only on the halide side in a simplified cluster-embedding scheme. The rest of the crystal is modeled: (i) as point-ions located on the lattice positions and (ii) frozen-orbital ions derived from an LCAO energy band calculation of the pure crystal. The calculated theoretical lifetimes are compared with experimental data.[76] The positron annihilation from bound states associated with F-center defects in alkali

halides has been analyzed with the above first-principles crystal field and compared with other model calculations[36] and available experimental results.[100] We begin with our results for atomic systems.

A. Positron bound states in atomic systems

1. Negative ions

The positron can readily interact with the negatively charged atomic system because the net negative charge of the atom can attract the positron to create bound states. It is known that in H-F calculations, the result of the positron annihilation lifetime for the fully relaxed orbitals of both the electron and positron is 10% smaller than that for the frozen core orbitals. This implies that the core region of electron orbits can only contribute a small portion to the positron lifetime. Therefore, in both H-F and X-O calculations, the positron could not be well localized by the electron. Inclusion of electron-electron correlation also gives a negligible contribution to decreasing the positron lifetime from the EC-O calculation in Table X. This also implies that the positron density is not significantly distorted by this electron-electron correlation of the electron density.

However, as remarked early by Farazdel and Cade,[9] the inclusion of the electron-positron correlation is the important ingredient for the positron annihilation in atomic systems. This is demonstrated from the EP-O and EPC calculations, which include the electron-positron correlation potential. Both electron and positron probability densities are treated as statistically independent in the EP-O calculation in order to investigate the role of the correlation potential. The positron correlation potential in the vicinity of the nuclear site strongly attracts positron density inward, as shown in Fig. 6.1. Furthermore, the inclusion of the pair-distribution function as the annihilation enhancement factor (g) [see Eq. (3.12)] in the EPC calculation

TABLE X . Positron annihilation lifetimes τ (nsec) for negative atoms [A^-:e^+].

A^-	nl(e^+)	X-O	EC-O	EP-O	EPC	Exp.ave.[a]
F^-	1s	1.767	1.722	0.614	0.225	0.161
	2s	7.102	6.944	3.417	1.225	0.894
	2p	9.825	9.627	2.396	0.649	0.354
Cl^-	1s	4.324	4.180	1.192	0.326	0.245
	2s	15.207	14.768	5.708	1.514	1.105
	2p	13.253	12.864	2.552	0.565	0.531

[a] The experimental values are averaged from alkali halides (Ref. 76).

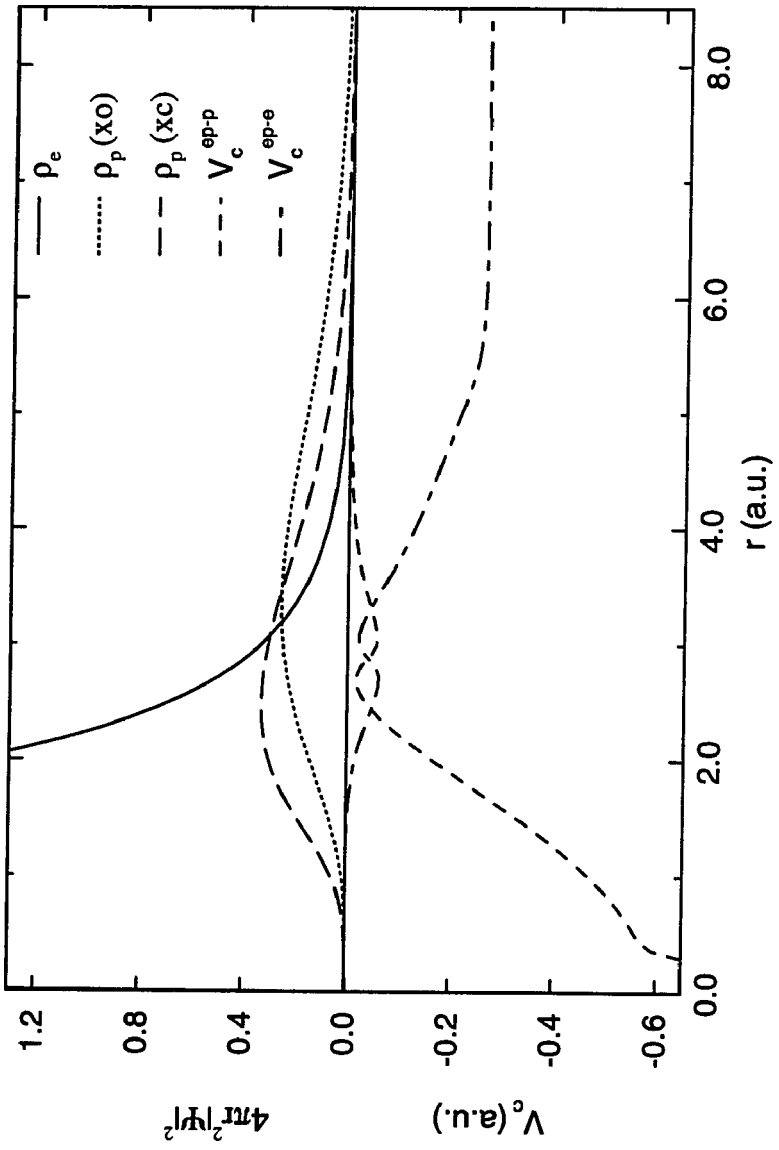

FIG. 6.1. Positron-correlation effect in the negative fluorine atom (F^-:e^+).

strongly reduces positron lifetimes. The increased electronic charge density at the position of the positron increases the probability of the pair annihilation, and thus also the annihilation rate. This correspondingly decreases the positron lifetimes. This means that the neutral core density of electrons is not completely screened any more but can be seen to the interacting positron by means of the quantum correlation between electron and positron.

If it is supposed that the experimental average can be resolved into lifetime components corresponding to the ground, first, and second excited states,[76] the order of annihilation rates for the positron (inverse of positron lifetimes) would be dramatically changed into the proper positron orbitals (1s, 2p, and 2s), as shown in Table X. The eigenvalues of positron bound states are consistently corresponding to the positron lifetimes of both calculation and experiment with the order, [(1s), (2p, 2s), and (3d, 3p, 3s)], as shown in Table XI. This reflects that the annihilation of the positron is a process sensitive to the inclusion of the pair-correlation effect. This may be related to the fact that the higher angular quantum states have fewer nodal points in the density and the nodal point reduces the positron density overlap with the density of outside electrons in atoms.

The fully calculated EPC case, in which we include the enhancement factor between electron and positron densities with the electron-positron correlation potential, agrees relatively well with the experimental averaged values for alkali halides.[76] Larger negative ions usually are associated with longer lifetimes of the 1s state of positrons because the total potential well of positrons becomes shallower and wider in larger atoms due to the competition between both electron-positron Coulomb potential and electron-positron correlation potential and the repulsive nucleus potential as shown in Fig. 6.2. It is interesting to compare our result for negative

TABLE XI. Positron eigenvalues (- eV) in the negative fluorine and chlorine atoms. The restricted Hartree-Fock (RHF) shows the same results with the X-O calculations.

Atom	nl(e^+)	X-O[a]	RHF[b, c]	EC-O	EPC
F^-	1s	4.959	5.048	4.976	6.948
	2s	1.913	1.936	1.914	2.508
	2p	2.965	2.992	2.965	3.874
	3s	1.011	-	1.010	1.252
	3p	1.365	-	1.363	1.809
	3d	1.501	-	1.496	1.684
Cl^-	1s	3.845	3.922	3.867	5.943
	2s	1.621	1.644	1.626	2.236
	2p	2.651	2.687	2.658	3.887
	3s	-	-	0.895	1.177
	3p	1.258	-	1.259	1.739
	3d	1.478	-	1.476	1.842

[a] J. G. Harrison (Ref. 31).
[b] P. E. Cade and A Farazdel (Ref. 9).
[c] A. J. Patrick and P. E. Cade (Ref. 10).

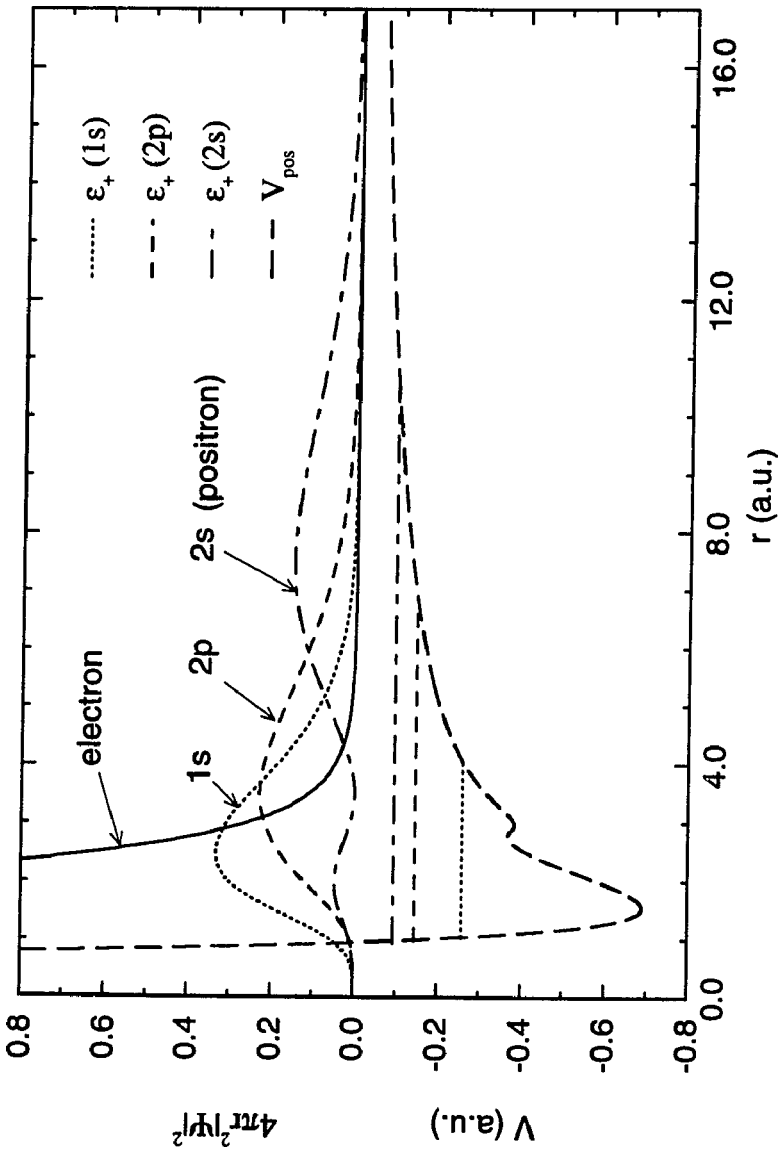

FIG. 6.2. Positron bound states in negative fluorine atom ($F^-:e^+$).

hydrogen to other results. This density functional calculation of the annihilation rate for the H^- gives the value 2.403 GHz, as shown in Table XII. This is comparable to 2.220 GHz[11] and 2.459 GHz [13] provided from the laborious method of the extensive Hylleraas-type wavefunctions. These free-anion results for positron annihilation can not be properly compared to experimental data of alkali halides. For a better model of positron annihilation in alkali halides, it is desirable to consider the anion in the crystalline system. This crystal field effect will be examined in the next section. We will next consider the neutral alkali atomic system.

2. Positron annihilation from neutral atoms

In the negative atomic system, it has been noticed that the portion of the neutral core of electrons does not contribute to the positron annihilation in the H-F calculation of Farazdel and Cade.[9] This suggested that the existence of positron bound states in neutral atoms is not clear. However, it is known that the electron cloud surrounding the nucleus supports an induced-dipole attraction to the positron by means of the density correlation.[12] The positron correlation potential for the neutral atom mimics this additional correlation effect and may succeed in pulling the positron inward and localizing the positron wavefunction to create bound states.

In Table XII, density functional calculations show that even though there is a strong nuclear repulsion to the positron from the core of the neutral atoms, the electron-positron correlation would make bound states of the positron in neutral alkali atoms such as Li and Na for 1.805 nsec and 1.531 nsec, respectively. The contribution of electron-electron correlation to these bound states are comparably small, and the enhanced effect of the electron-positron correlation is more crucial. This implies that the electron-positron correlation reflects the larger polarizabilities for alkali atoms.

TABLE XII. Positron annihilation rates (GHz) for the negative hydrogen and the neutral lithium and the sodium atoms. The importance of the electron-positron correlation is shown from the comparison of EP-O and EPC in the SIC-LSDA, the Hartree-Fock (H-F), and extensive Hylleraas-type wave-function method (HTW).

Atom	nl(e^+)	EP-O	EPC	H-F	HTW
H^-	1s	0.576	2.403	0.300[a]	2.220[b]
				0.437[c]	2.459[d]
Li	1s	0.352	0.554	0.030[c]	0.880[c]
Na	1s	0.066	0.653	-	-

[a] A. Farazdel and P. E. Cade (Ref. 9).
[b] P. Navin et al. (Ref. 11).
[c] D. C. Clary (Ref. 12).
[d] Y. K. Ho (Ref. 13).

The EP-O calculation of the annihilation rates without the pair distribution function shows that the larger atom has much less overlap in the density. The positron potential well may be established by competition between the repulsive nucleus potential, the attractive electron-positron Coulomb potential, the electron-positron correlation potential. However, the EPC calculation, in which both the electron-positron correlation potential and the pair distribution function are included, shows that the larger atom has a shorter lifetime than that of the smaller atom due to the dramatic increase of the annihilation rate by including the correlation enhancement factor. This reflects the critical importance of the role of the positron correlation effect on the neutral atom.

This result is consistent with the viewpoint of Clary[12] that the positron bound state is stable with respect to the single positron dissociation from the neutral atom but not stable with respect to the dissociation of positronium (Ps). It is noted that electron binding to a neutral atom requires a large polarizability of the atom, which for atoms often means a small ionization potential. Therefore, this leads to Clary's idea because the low-energy cost of removing e^- from the neutral alkali atom is probably offset by the energy gain in forming Ps,

$$E_{A:e^+} > E_{A^+} + E_{Ps}. \qquad (6.1)$$

Since the ionization energy of alkali atom is usually $E_{ioniz} \leq 5$ eV and the positronium formation energy is $E_{Ps} \cong -6.8$ eV, we see the cause of the instability. However, this raises an intriguing question as to the possibility of molecular systems which can bind e^+ stably against Ps dissociation.

B. Positron bound states in alkali halides

We present results of density functional calculations of bulk positron lifetimes in the alkali-halide crystals LiF, NaF, LiCl, and NaCl. The abbreviations X-O, EP-O, and EPC have the same meaning as in the atomic cases with the inclusion of the crystal potential. The potential is modeled in two ways: (i) point-ions located at the lattice positions and (ii) frozen orbital ions derived from an LCAO energy-band calculation of the pure crystal.

The crystal system is modeled as the one-site embedded cluster for the infinite crystal discussed in Chapter V. The equilibrium structures of crystal lattices and lattice constants are used for the alkali-halides.[83] For this one-site approximation, the defined Hamiltonian represents the infinite crystal lattice and the basis functions for the system are centered on the central anion site. The GTO basis set consists of the s and p single GTO's. This Gaussian set has been used in the calculations of the pure Hamiltonian matrix elements and the Madelung potential matrix element of both electron and positron. And also this set has been used for the self-consistent density functional calculation of the anion system; however, the electron and positron have been represented with a different basis set for each crystal.

The energy, which is dependent on the choice of the Gaussian basis set, is minimized, and then the positron lifetimes are determined with the self-consistent densities of both electron and positron. The Madelung potential lowers the electron eigenstates with a relative contribution to the redistribution of electron states of the anion. For the positron, however, it is possible that the shape of the potential on the neighbor lattices has a strong influence because the positron is localized in the interstitial region due to the strong Coulomb repulsion between the nucleus and the positron.

The long-ranged Gaussian basis set of the electron spans on the same interstitial region with the positron. Therefore, there is a strong correlation between the two densities so that the annihilation rate is sensitive to the long range Gaussian basis. This also implies that the contribution of the valence electron to the annihilation rate should be more carefully considered in this interstitial region. However, our one-site approximation of the embedded cluster method cannot take into account this contribution of non-spherical density distribution of the positron, in which the valence electron and the next site of the electron density distribution may contribute to the annihilation rates. Thus our embedded cluster results beyond the 1s-ground state for the positron must be treated with caution.

1. Modified point-ionic potential model

The point-ionic potential has been modified to yield a repulsive potential at each lattice point because the thermalized positron in the crystal is strongly repelled by the nucleus on lattice points. The model potential becomes negative inside of the ionic radius and becomes the usual form of the point-ionic potential outside the radius.

It is valuable to note that in the negative atomic system, the positron lifetimes in the X-O Gaussian calculation without the crystal field is close to the result of the X-O numerical calculation by the modified Herman-Skillman atomic structure code. We have optimized the Gaussian basis set from the potential generated by the numerical atomic code. The Gaussian basis set has some limitation in its ability to reproduce exactly the numerical result of the atomic system, as shown in Tables X and XIII.

However, since we need to deal with the multi-center contributions of the crystal system, we need to implement the Gaussian code; we, therefore, chose the

TABLE XIII. Gaussian calculations of positron lifetimes (nsec) in negative atoms with atomic structure information for X-O cases.

Atom	nl(e^+)	X-O	EP-O	EPC	H-F[a]	Exp.ave.[b]
F^-	1s	1.941	0.901	0.501	1.662	0.161
	2p	9.688	3.251	1.274	9.435	0.354
	2s	7.565	5.079	2.365	-	0.894
Cl^-	1s	4.247	1.260	0.581	4.018	0.245
	2p	12.63	2.819	1.066	12.46	0.531
	2s	13.92	7.592	3.581	-	1.105

[a] A. Farazdel and P. E. Cade (Ref. 9).
[b] C. Bussolati et al. (Ref. 76).

optimized basis set for the X-O calculation by using the potential of the numerical atomic structure calculation. Within this limitation, the atomic results with this Gaussian basis set give a reference for assessing the crystal effect. The overall trends of the Gaussian atomic results qualitatively agree with those of the numerical atomic calculations.

Now we will analyze the crystal system. The X-O calculation including the Madelung potential shows a large change of the positron lifetime from the Gaussian atomic results and it shows positron orbitals with the order (1s, 2p, and 2s) in Table XIV. The electron-positron correlation potential in the EP-O calculation reduces the lifetimes of the X-O results by shifting the density as shown in Fig. 6.3. The strong attraction of the positron density inward by the positron correlation potential in the vicinity of the nucleus is also true in the crystal calculation with a different degree of the strength of the potential compared to the free ionic results.

Another way to view the EP-O comparison between the atomic system an the crystal system is that the crystal effect becomes smaller than that in the X-O calculation when we introduce the electron-positron correlation effect. This implies that the crystal Madelung potential is competing with the positron correlation potential. This is shown in Fig. 6.4. The detail information of the depth and width of the potential for a specific crystal gives the detailed difference of the positron annihilation lifetimes. The EPC calculation shows reduced lifetimes from the Gaussian atomic results to a different degree for each of the states of positron orbitals shown in Fig. 6.5. This corresponds to the fact that each positron orbital sees a different correlation potential.

For the 1s positron orbital in LiF, the contribution of the crystal effect on the lifetime is slightly larger than that of the pair-correlation effect, and it is the same

TABLE XIV. Positron annihilation lifetimes (nsec) from bound states of positron in alkali halides with the modified point-ionic and the energy-band potentials. Shaded areas represent results outside the limitation of one-site approximation of the embedded cluster method.

Crystal	nl(e^+)	Point-ion			Band-ion			Exp.[a]
		X-O	EP-O	EPC	X-O	EP-O	EPC	
LiF	1s	0.792	0.458	0.326	0.199	0.172	0.135	0.132
	2p	2.225	1.218	0.764	0.331	0.277	0.204	0.297
	2s	0.293	0.300	0.230	0.077	0.079	0.073	1.10/1.87[b]
NaF	1s	1.211	0.526	0.358	0.344	0.292	0.198	0.193
	2p	2.131	1.207	0.693	0.556	0.462	0.282	0.390
	2s	3.536	3.456	2.064	0.954	0.644	0.458	1.44/3.60[b]
LiCl	1s	1.464	1.011	0.452	0.585	0.491	0.262	0.236
	2p	2.435	1.686	0.633	0.789	0.645	0.317	0.435
	2s	6.979	6.812	3.096	0.636	0.491	0.316	1.75
NaCl	1s	1.499	1.002	0.449	0.873	0.707	0.335	0.313
	2p	2.649	1.852	0.668	1.303	1.029	0.427	0.684
	2s	5.846	7.980	3.528	7.788	1.713	0.912	2.89

[a] C. Bussolati et al. (Ref. 76)
[b] Samples for powders/ single crystals

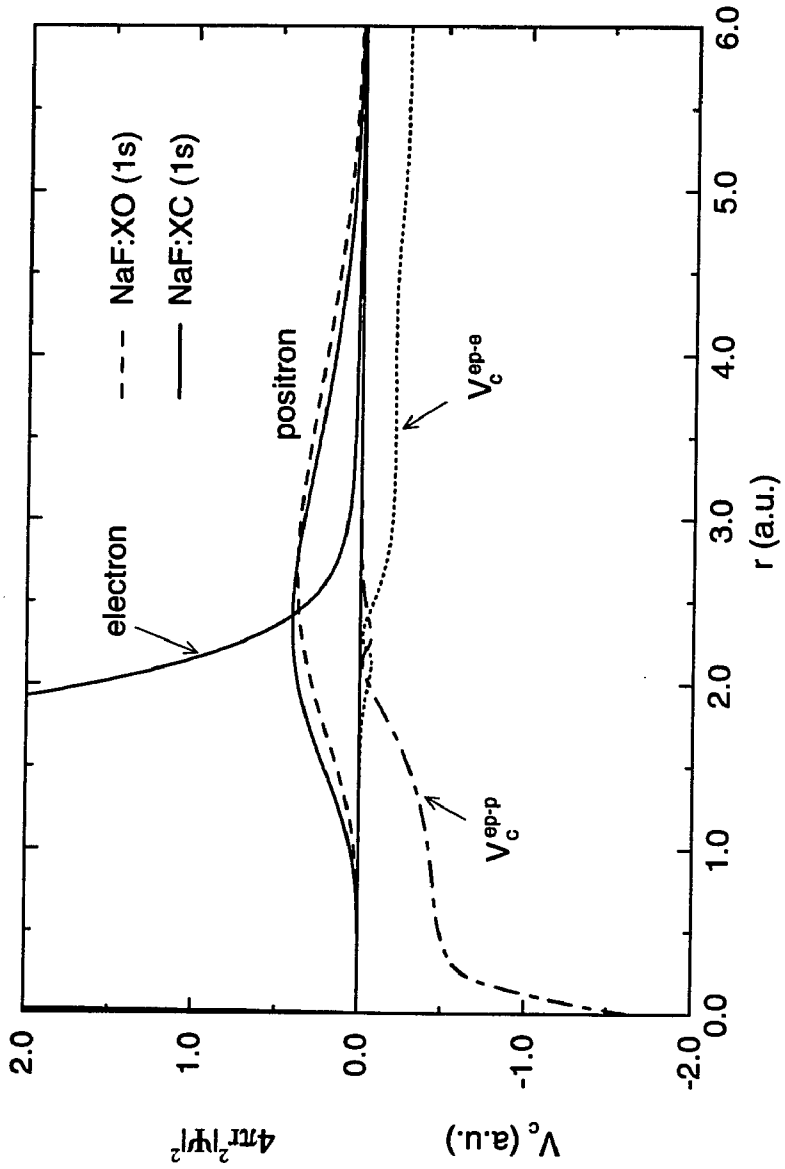

FIG. 6.3. Positron-correlation effect in the point-ion model of NaF.

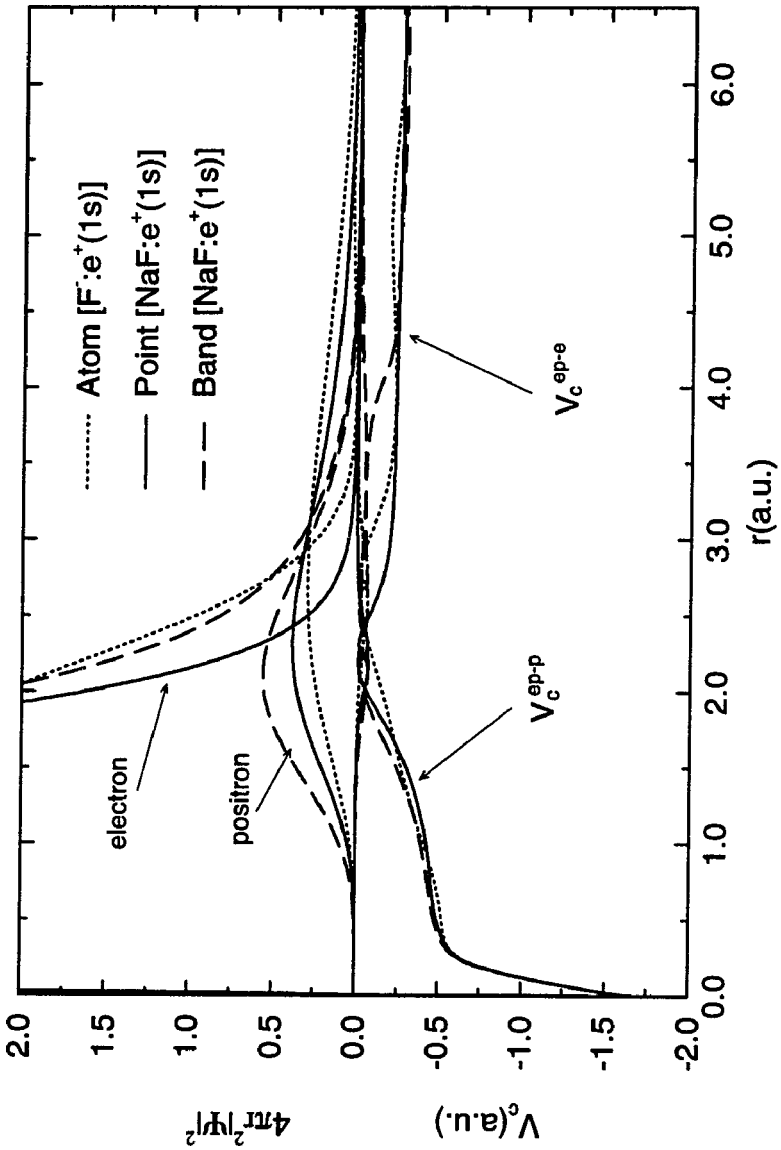

FIG. 6.4. Competition between the positron correlation and crystal effects

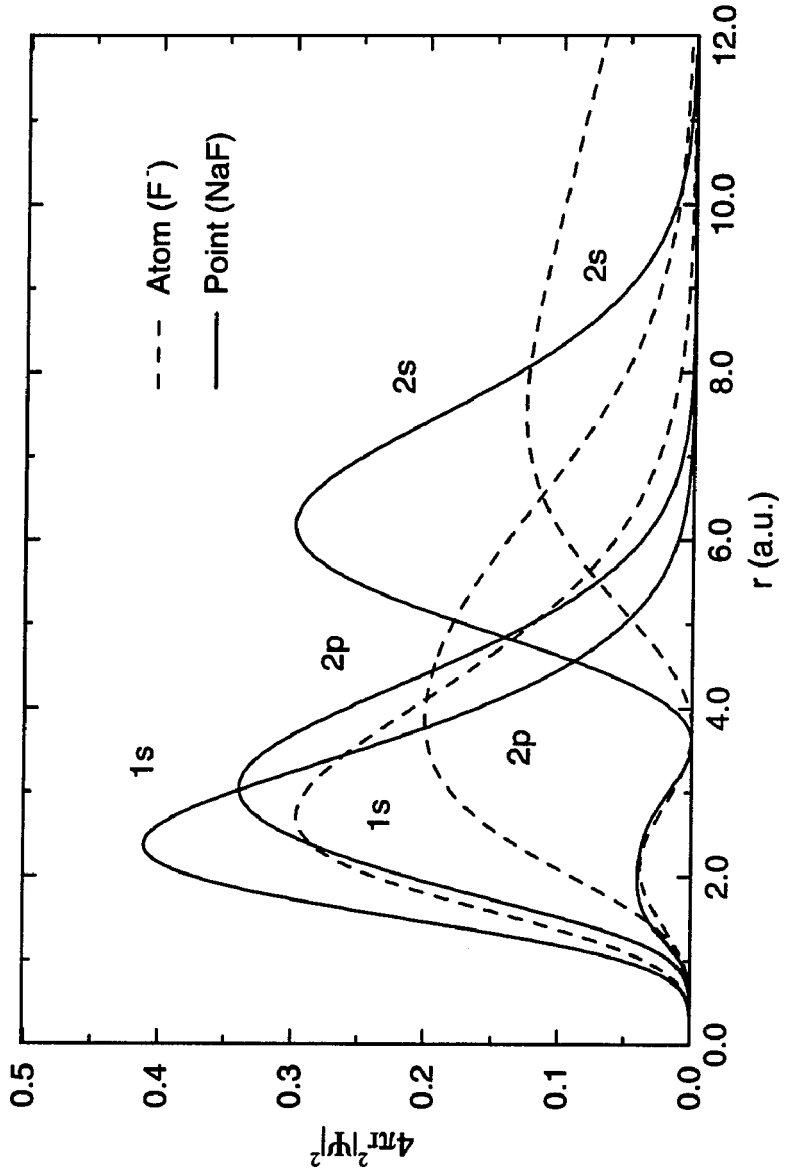

FIG. 6.5. The crystal field effect on the bulk states of positron orbitals.

order in NaF. However, for both LiCl and NaCl, the pair-correlation effect becomes larger. These reflect that the shape of crystal potential also influences the correlation effect. As the Madelung potential becomes shallower and wider, the correlation effect becomes more competing with the crystal effect by the correlation potential as shown in Fig. 6.6. For the 2p state of positron, the contribution of the crystal effect to the LiF and NaF crystals is comparable to the correlation effect, but the correlation effect becomes dominant for the LiCl and NaCl crystals. For the 2s state, there is no contribution from the crystal effect effectively except for LiF.

It should be mentioned that the point ionic crystal model has the limitation on the explanation of the 2s orbital of positron in LiF crystal within one-site approximation. The long ranged 2s orbit cannot be represented accurately due to the modeling of the point-ionic repulsive potential for the next lattice site and to the limitation of the basis set to just those on the center site. Because the lattice constant of LiF is the shortest among the crystals considered, the model cannot provide enough space for the positron in the 2s state. Therefore, the 2s state of the positron in LiF may meet the strong repulsion and be repelled back to the original position of the anion site rather than expanding to more distant regions. The density of the positron in the 2s state has been severely distorted and gives the unphysical result shown in the shaded area in Table XIV, which should be regarded as an artifact of the point ionic model.

As the lattice constant becomes large in alkali-fluorides, the lifetime becomes large in the ground state of positron (1s). This is also true for the alkali-chlorides. This is shown in Table XIV. The point-ionic calculations have been shown with the same order of the positron lifetimes with the experimental data. However, there is still a large discrepancy between them.

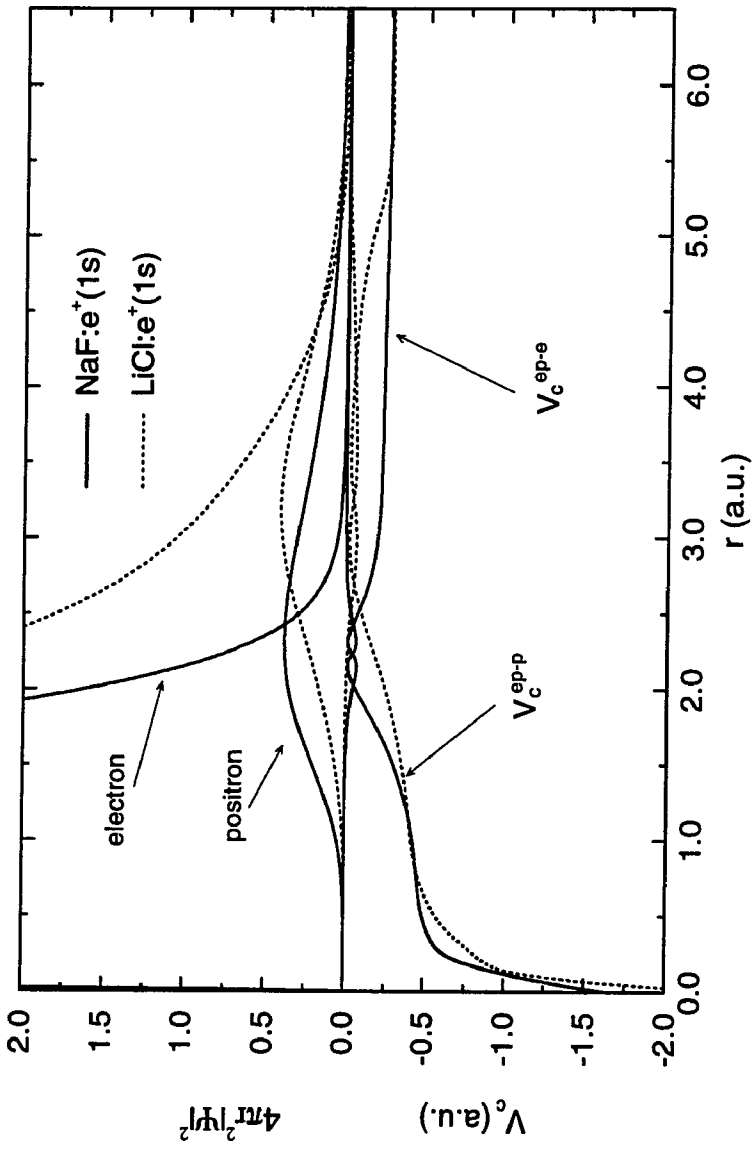

FIG. 6.6. Comparison of positron correlation potential forms in different crystals. As decreasing crystal potential, the correlation effect enhances without the change of the correlation potential.

2. Energy-Band Ionic Potential Model

The crystal potential is constructed by the superposition of the individual ions centered at the appropriate sites of the lattice. In the band crystal potential, each ionic site has been represented by the full ionic potential from band information of the LCAO-band structure calculation.

The energy bands of alkali-halides are either completely filled or completely empty and separated by a large energy gap (>5 eV). Alkali halides have the ionic characteristic of strong localization of electron density; for example, the Na^+ ions lose their 3s electron, which is transferred to make the Cl^- ion, thereby completing the chlorine 3p shell. The 1s, 2s, and to a large extent also 2p levels for the Na^+ ions are so localized at the ion that at the equilibrium interatomic spacing, no overlap arises, and these levels, therefore, remain atomic-like and sharp. On the other hand, there is sufficient overlap of 3s states of Na^+ ions that these build a band of levels, but this is empty. Because the Cl^- ions have a large ionic radius, there is a much greater tendency for their orbitals to overlap. Although the more tightly bound electrons remain in sharp atomic-like states, the 3s and 3p levels of Cl^- ions are spread into relatively narrow bands. In the occupied states, there is a quite small Na^+- Cl^- orbital interaction. This indicates that the bands of 3s and 3p occupied levels are essentially confined wholly to the Cl^- ions.

This band information has been implemented on the positron annihilation calculation by using band-ionic crystal potential in the embedded cluster method. The one-site approximation of this method facilitates this calculation just as in the point-ionic potential model. The positron annihilation at the anion center with the band crystal potential has been shown in Table XIV. By comparison with the experimental results, the positron lifetime calculation shows relatively good

agreement in the 1s state, but there are discrepancies in the 2s and 2p states of positron, which are similar to the distortion phenomenon in the 2s state of LiF in the point-ionic potential model shown in Fig. 6.7. This may imply that the more extensive band potential at the lattice sites cannot reserve enough space in the interstitial region even for the 2p and 2s states of positron of all the crystals considered.

Let us analyze the results for 1s states of calculated positron lifetimes. In the X-O calculations of the positron annihilation in LiF and NaF crystals, the lifetimes are shorter than those of the EPC calculations in point-ionic potential. In LiCl and NaCl crystals which have the larger crystal lattice constants than those of LiF and NaF crystals, the details of the crystal effect are less pronounced and the X-O results are comparable with the EPC results of the point-ionic potential. When the positron correlation potential in EP-O is taken into account in the band model, the results are only slightly changed. The inclusion of the pair-correlation function in EPC calculation also does not change the positron lifetimes much. They agree with the experimental values well with the fully energy-minimized basis set. This implies that the strong crystal effect from the band structure information is the main contribution to the electron and positron states, with the positron correlation potential and the pair-correlation function modifying the final states and slightly changing the positron lifetimes.

Our calculated 2p states have smaller lifetimes than those referred to as "secondary components" in the experimental data. However, the 2s states are orders of magnitude different in calculated lifetimes because annihilation rates are strongly increased due to the shift of the positron density by the strong repulsion of the band crystal potential surrounding the anion center at the cation sites. The degree

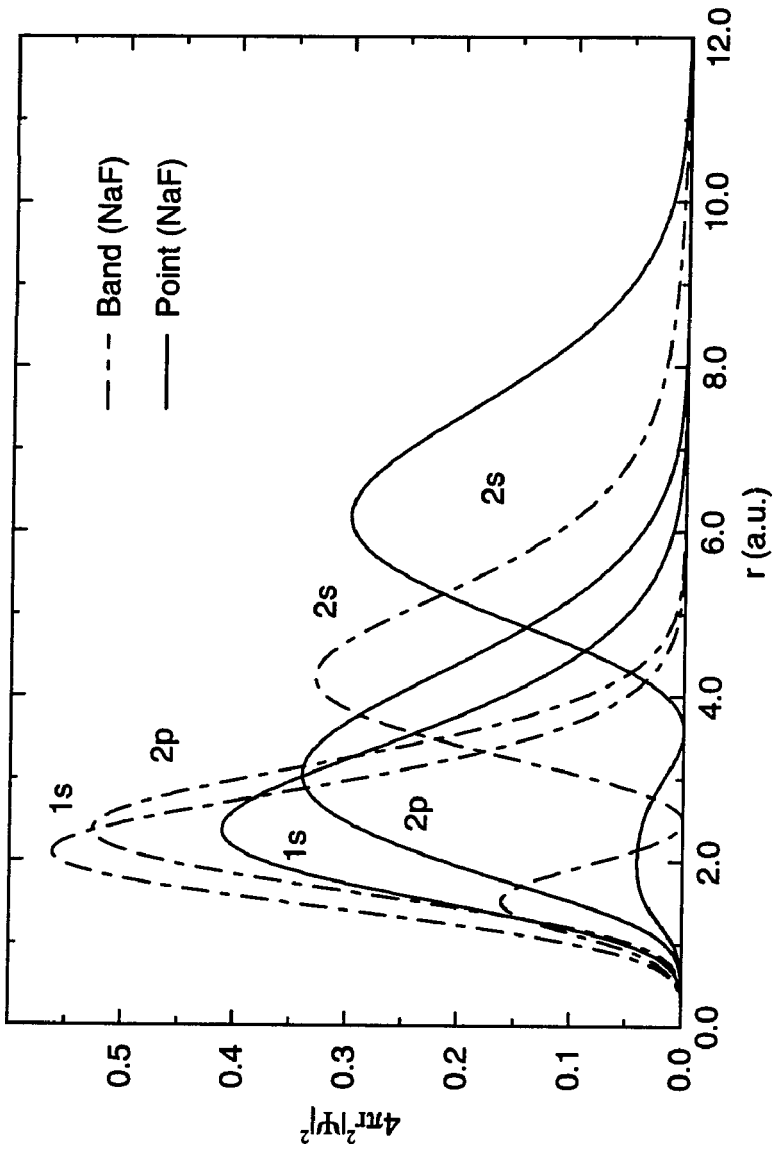

FIG. 6.7. Model dependent crystal effect on the bulk states of positron orbitals in alkali halides.

of density distortion in the higher positron states may be unrealistic due to the limitation of the one-site approximation. If both the valence electron and the core electron at the cation sites can be included, positrons may be attracted in both ways from anion sites and cation sites. They tend to be located in the interstitial region especially for the high positron states. This implies that the whole range of the lifetime components should be more properly analyzed by going beyond the single-site embedded cluster method.

In spite of the limitation of the one-site approximation, the band potential provides an appropriate model for the 1s bound state of the positron which is well-localized around the anion site. There is an interesting spectral analysis by Bertolaccini et al. of the experimental data[101, 102] for the annihilation rate of the shortest lived positron state. In their view, the crystal volume can be classified into two regions: one occupied by positive ions and the other occupied by negative ions. The density of negative ions whose region can be assessed by the positron is linearly dependent on the positron annihilation rate of this 1s state in highly ionic crystals. However, the similar study of a possible relationship between crystal properties and the second component of the annihilation rate is less conclusive with the implication that the long-lived positron states may depend on the crystal properties of both the positive and negative ions. This analysis consistently agrees with the one-site approximation.

Finally, we finish this section with the relationship between the positron annihilation rates and the crystal properties in terms of the lattice constants. As shown in Fig. 6.8, the annihilation rates of the ground state of positron can be expressed with the following relation of the power law

$$\Gamma_{theory} = 1.306a^{-2.538} \text{ [THz]} \qquad (6.2)$$

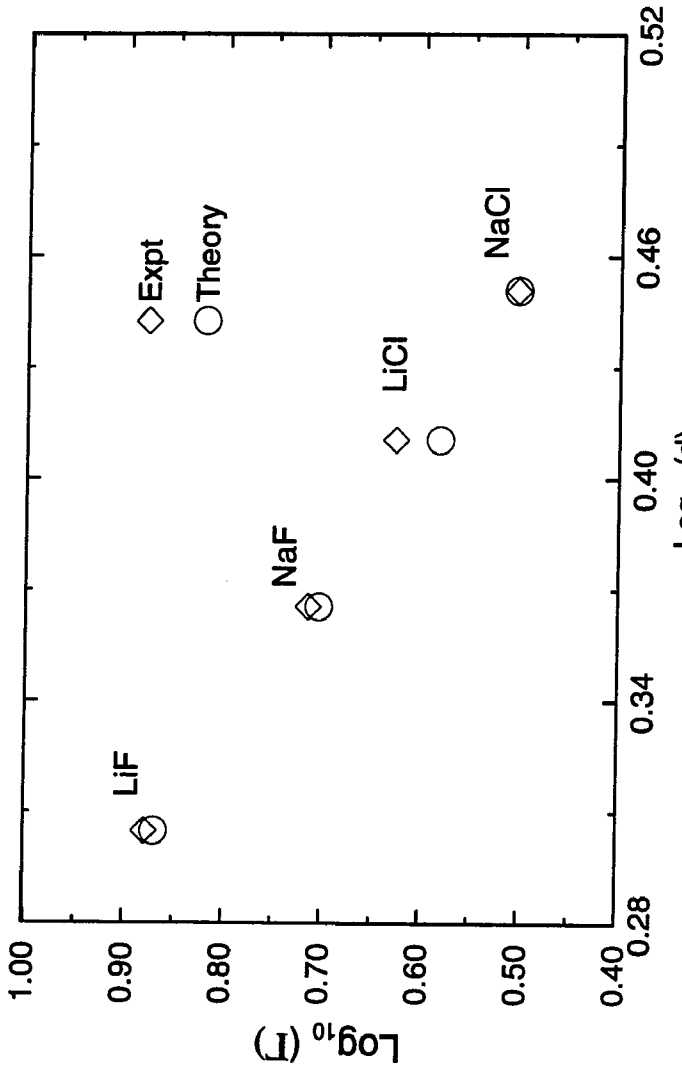

FIG. 6.8. Power law relation of positron annihilation rates in alkali halides. d (a.u.) is the nearest neighbor distance and Γ (nsec) is the annihilation rate.

$$\Gamma_{expt} = 1.084a^{-2.433} \text{ [THz]}, \tag{6. 3}$$

where a is the lattice constant. The larger the lattice constant results in less overlapping of electron-positron densities because the positron may reside in the larger interstitial region.

C. Positron annihilation in F-center related bound state

The electronic structure for the F-center in alkali-halides which consists of an electron which is bound to a halide ion vacancy by the electrostatic forces of the remainder of the crystal will be briefly reviewed. This center has a number of electronic states, and optical absorption produces a transition of the electron from the ground state to its first excited state. There is a characteristic absorption band for the F-center in each alkali-halide. Often, this falls in the visible part of the spectrum so that the crystals appear colored. As an example, the NaCl becomes yellow by the absorption of the opposite color. Once in the excited state, the F-center may return to the ground state by the emission of light or by radiationless transitions. These optical properties of F-centers are sensitive to temperature.[103] Although the temperature effect may have some effect on the annihilation characteristics of the ther-malized positron, we only consider the system of an ideal F-center plus a positron, an F_c:e^+ center at absolute zero temperature.

1. Empirical model calculations

The conventional calculations[35, 36] are based on the empirical model formalism. For the electron and positron in this model of the F_c:e^+ center, the Schrödinger equation can be written as

$$H\Psi(r_+, r_-) = E\Psi(r_+, r_-) \tag{6. 4}$$

with the Hamiltonian

$$H = -\frac{1}{2}\nabla_+^2 - \frac{1}{2}\nabla_-^2 + V(r_+) - V(r_-) - \frac{1}{|r_+ - r_-|}. \qquad (6.5)$$

For electron bound states in the F-center, the potential $V(r)$ is the effective potential of an anion vacancy of the host alkali halide crystal. The ground state has been modeled as an isotropic potential for both the electron and the positron in two empirical models[35, 104, 105]: the hydrogenic model and the cavity model. The effective potential in the hydrogenic model is written in the form $V(r) = Z^*/r$, where the parameter Z^* is empirically determined to reproduce the experimental F band of the 1s-2p transition of the F-center.[104] Another empirical potential from the cavity model is of the form, $V(r) = V_0$ for the radius of the cavity $r < R$, and $1/(k_0 r)$ otherwise, as shown in Fig. 6.9 schematically, where the radius R, potential depth V_0, and the static dielectric constant k_0 of the crystal are also determined as empirical parameters.[107] In spite of the well-known electronic structure of the F-center, the annihilation characteristics vary greatly with the model potentials. This may come from the electron density distortion at the position of the positron. This was noted before in connection with the importance of the proper electron-positron correlation in the F_c:e^+ center.[36]

It is instructive to note that the positron bound state in an F-center may be viewed as a free-positronium state perturbed by the crystal potential. In order to gain further insight into this point of view, we apply the first-order perturbation theory to calculate the positron lifetime by simplifying the Madelung potential as a square well potential. The results are discussed in Appendix B.

2. Density functional calculations

Our density functional formalism as a first-principles calculation of the positron annihilation lifetime for the F_c:e^+ center will be addressed now. From the

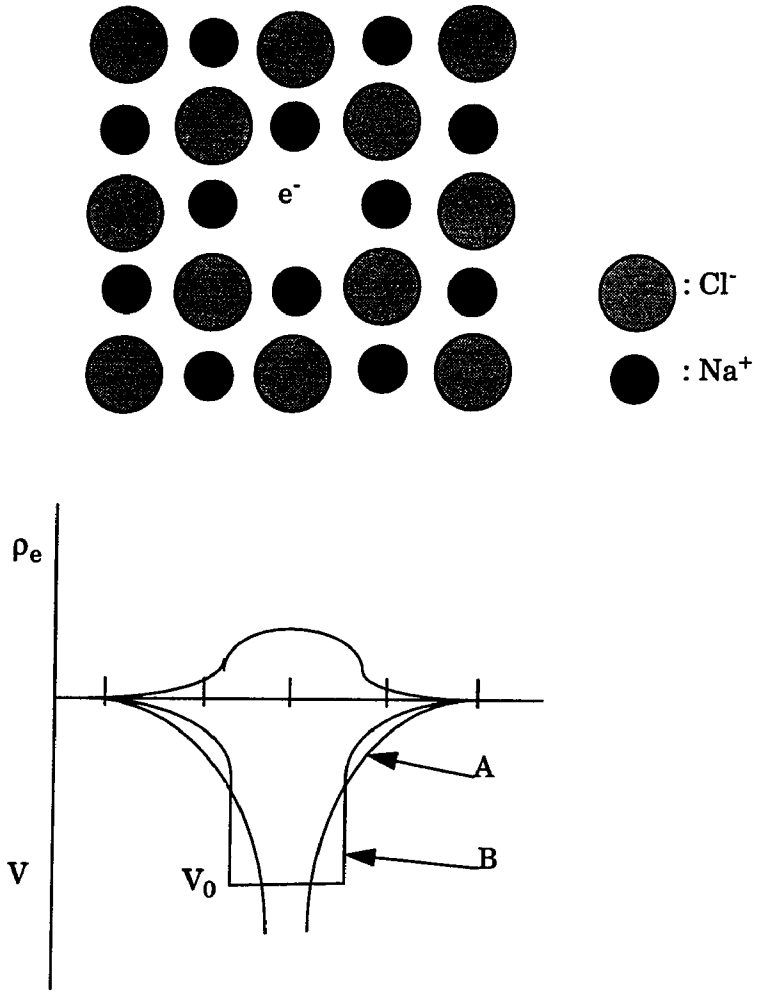

FIG. 6.9. Electron charge cloud in F-center and empirical model potentials in the (001) plane; the hydrogenic model (A) and the cavity model (B).

two-component formalism[1] of the self-interaction corrected-local spin density approximation of density functional theory, we have a parameter-free potential form for the interaction between an electron and a positron in an F_c:e^+ center. The single-particle Kohn-Sham equations for the defect crystal are expressed as

$$H_e \Psi_e(\boldsymbol{r}) = \varepsilon_e \Psi_e(\boldsymbol{r}) , \tag{6. 6}$$

$$H_p \Psi_p(\boldsymbol{r}) = \varepsilon_p \Psi_p(\boldsymbol{r}) , \tag{6. 7}$$

with

$$H_e = -\frac{1}{2}\nabla^2 - \int d\boldsymbol{r}' \frac{\rho_+(\boldsymbol{r}')}{|\boldsymbol{r}-\boldsymbol{r}'|} + V_c^{ep-e} + V_{Ma}, \tag{6. 8}$$

$$H_p = -\frac{1}{2}\nabla^2 - \int d\boldsymbol{r}' \frac{\rho_-(\boldsymbol{r}')}{|\boldsymbol{r}-\boldsymbol{r}'|} + V_c^{ep-p} - V_{Ma}, \tag{6. 9}$$

where V_c^{ep-e} and V_c^{ep-p} are electron-positron correlation potentials for the electron and the positron, respectively. These potentials can be derived from Nieminen's parametrization[2] of the electron-positron correlation functional for the data of Arponen and Pajanne,[26] and Lantto.[27] V_{Ma} is the Madelung potential as the crystal field for the rest of the F-center. As shown in Fig. 6.10 the system is defined as a single-site cluster at the F-center within the embedded cluster method. This means that our system is an electron at the anion vacancy within the one-site approximation. The first-principles calculation of the crystal field has already been discussed in Chapters IV and V.

a. Point-ionic potential model of F-center. We begin the discussion with our results obtained for the point-ionic potential in F-centers. The same point ionic potential as in the pure crystal calculation has been used. This crystal potential provides enough space for both the electron and the positron in F-center of alkali

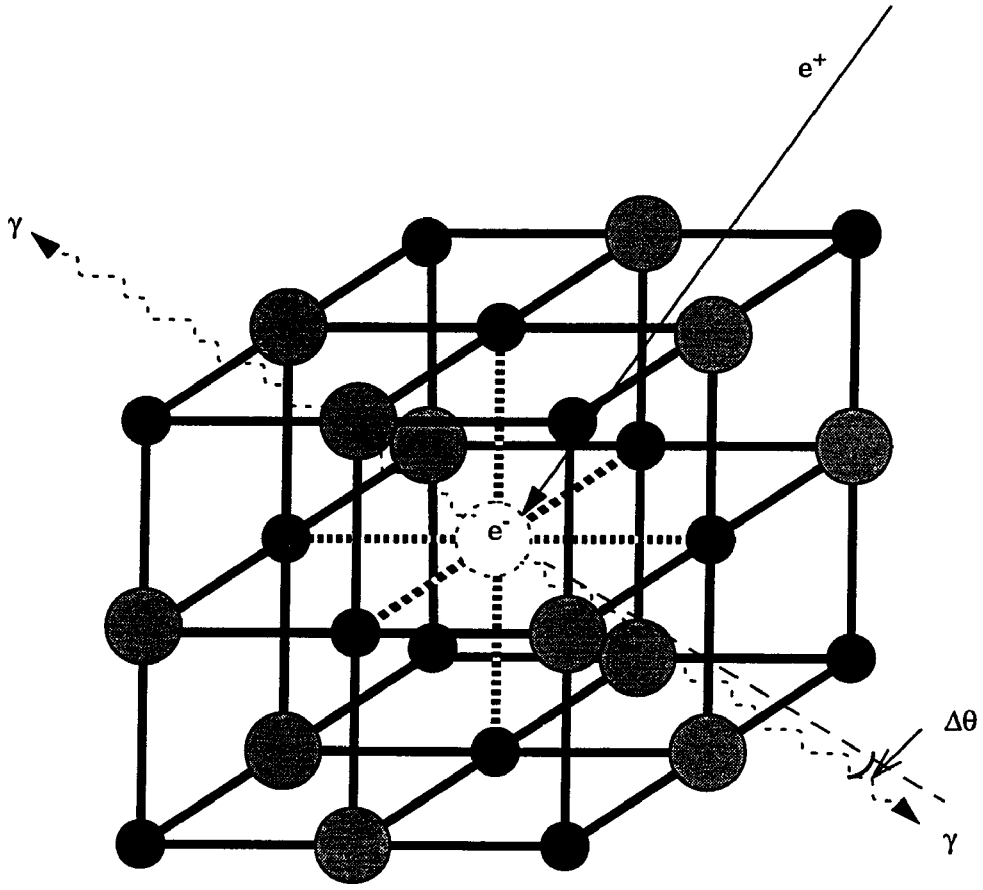

FIG. 6.10. The defect cluster model of the F-center of alkali halides.

halides because these densities are localized in the anion vacancy. This should mean that the one-site approximation of the embedded cluster method is sufficient to describe the positron bound state in F-center for this model. The positron bound state in an F-center can be considered equivalently as free positronium perturbed by the crystal potential at the anion vacancy. In Table XV, there is a comparison for several calculations such as the free positronium, the first-order perturbation model, the correlated hydrogenic model and Krumhansl-Schwarz cavity model, and our first-principles calculations with the available experimental data.

The XO calculation for NaCl:Fc shows that the electron-positron density overlap is very small, or so that the positron bound in an F-center lives 100 times longer than in free positronium and 10 times longer than the experimental value for the F-center in NaCl. Even after including the positron correlation potential, the positron lifetime is not much different from the X-O case, indicating that the positron correlation potential is not a significant factor for the F-center system at least in our point-ionic model, as shown in Fig. 6.11. However, the pair-correlation function significantly enhances the annihilation probability by up to 10 times the EP-O case. This implies that the most crucial ingredient is the pair-correlation function between the electron and the positron in the F-center related positron annihilation. This result for NaCl:Fc is in relatively good agreement with the experimental data.

In our simple perturbation calculation, the crystal effect reduces the annihilation rate from the positronium value. As the lattice constant increases, the thermalized positron at F-center shows corresponding reduction of lifetime; thus the depth of the Madelung potential which is inversely proportional to the lattice constant is directly proportional to the positron lifetime. The better correlated hydrogen model and the correlated cavity model give the longer lifetimes.[36] These

TABLE XV. Positron annihilation lifetimes (nsec) from the F-center bound state of positron in alkali halides. The free positronium (Ps), first-order perturbation (H′) of Ps, and the other empirical calculations; the hyrogenic (Z^*) and Krumhansl-Schwarz cavity (K-S) models are compared to our first-principle calculations and experiments.

Crystal	nl(e^+)	Ps[a]	H′	Point-ion			Band-ion			Others[b, c]		Exp.[d]
				X-O	EP-O	EPC	X-O	EP-O	EPC	Z^*	K-S	
LiF	1s	0.125	0.693	10.940	11.118	1.012	18.556	13.750	1.456	1.118	1.31	-
NaF	1s		0.659	8.033	8.161	0.904	10.386	9.556	1.330	0.767	1.11	-
LiCl	1s		0.632	14.106	13.737	1.055	9.747	8.824	1.188	0.684	0.98	-
NaCl	1s		0.608	11.390	12.469	0.997	11.674	8.967	1.063	0.595	0.831	1.09±0.02 1.1±0.1

[a] P. A. M. Dirac (Ref. 63) and R. N. West (Ref. 102)
[b] A. Farazdel and P. E. Cade (Ref. 35)
[c] D. G. Kanhere, A. Farazdel, and V. H. Smith, Jr. (Ref. 36)
[d] A. Bisi, A. Bosi, A. Dupasquier, and L. Zappa (Ref. 100)

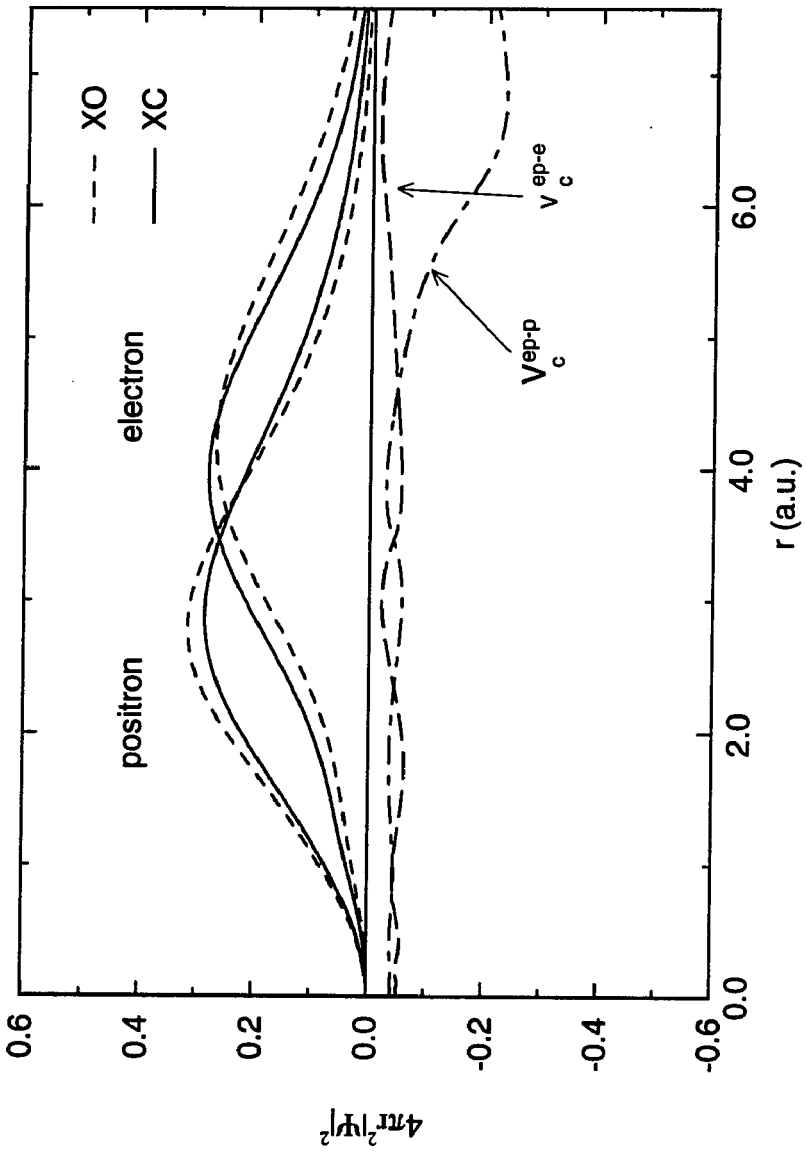

FIG. 6.11. Positron-correlation effect in LiCl:Fc with the point-ionic crystal potential.

empirical calculations also emphasize the importance of the inclusion of electron-positron correlation in the wavefunction of the (F_c:e^+) system.

The alkali-fluorides (LiF, NaF) have longer lifetimes than those of the alkali chlorides (LiCl, NaCl). This is also consistent with the relationship to the crystal properties within the same halide class of the crystals. However, there are only small differences of lifetimes among the crystals considered. This is reflected in the difference in average radial separation between electron and positron densities in Table XVI.

b. Energy-band potential model. The calculation of the positron lifetimes in F-center using the energy-band crystal potential gives results similar to the point ionic calculation. As mentioned already, the band potential provides the more extensive potential form at the cation sites than that of the point ionic potential. This energy band potential on the cations adjacent to the vacant site pulls electron density to be distributed largely and pushes positron density into the center of the vacancy. In the context of the perturbation theory, the band results should therefore have longer lifetimes than those of the point-ionic calculation, because the lifetimes are inversely proportional to the lattice constant and are directly proportional to depth of the Madelung potential.

The X-O calculations show slightly different results compared to the EP-O calculations with the small but obvious contribution of the positron correlation potential which makes negligible contributions in our point ionic calculation shown in Figs. 6.11 and 6.12. In LiF:Fc and NaF:Fc, the density distribution is sensitive on the crystal potential model. The energy-band potential allows the electron to spread out to close to the cation sites and strongly repels the positron to the halide vacancy center. However, in the point ionic case for these crystals, the electron persists to be

TABLE XVI. Averaged separations Δr (a.u.)* of densities of electron and positron in F-center of alkali halides. The Ps denotes the free positronium and H′ is for the positronium with the first-order perturbation of square well potential.

crystal	positronium		point-ion		band-ion	
	Ps	H′	X-O	EP-O	X-O	EP-O
LiF:Fc	3.000	2.963	-0.773	-0.713	2.420	2.324
NaF:Fc		2.913	-0.673	-0.885	2.272	2.179
LiCl:Fc		2.883	1.228	0.885	1.430	1.824
NaCl:Fc		2.867	1.210	0.676	1.503	1.251

* $\Delta r = \langle r\rho_e \rangle - \langle r\rho_p \rangle$

** The negative sign denotes that the electron density at the vacancy center is surrounded by the positron density

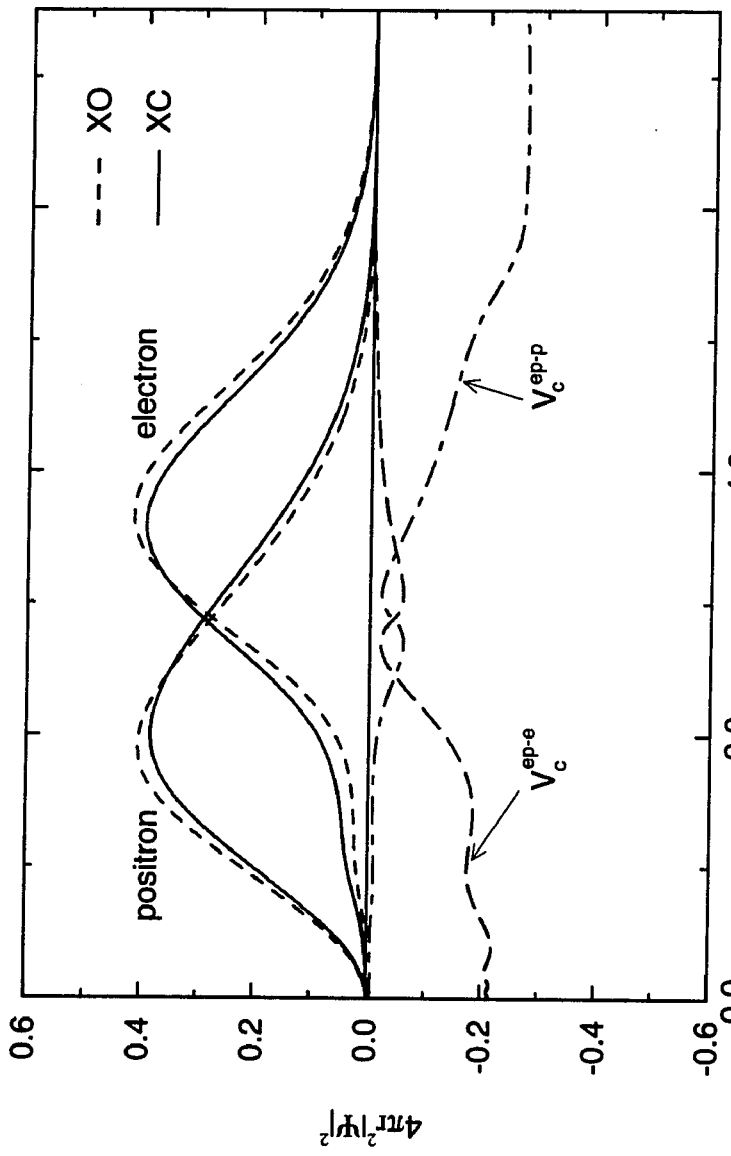

FIG. 6.12. Positron-correlation effect on the positron bound state in the F-center of NaCl within the energy-band ionic model.

located on the vacancy center. Although these X-O and EP-O results for positron lifetimes are around the same order as the point-ionic results, the electron and positron densities totally redistribute and reshape their positions as shown in Fig. 6.13. This phenomenon is reflected on the average separation of densities between electron and positron as shown in Table XVI.

The EPC calculations show longer lifetimes than those of the point ionic results and other empirical calculations, as shown in Table XV. For NaCl, the lifetime calculation in F-center gives excellent agreement with the available experimental data. This suggests that the experimental results purely come from the positron annihilation of the F-center related bound states because this agreement comes from the calculation of the one-site approximation which includes only one valence electron as the system of the density functional calculations. However, the other crystals do not have any available experimental values. For the small lattice crystal such as an LiF crystal, the positron lifetimes increase in a different way to the point-ionic calculation.

For the irradiated LiF crystal, which may include the F-center, there is an experimental observation[106] about the change of the second component (τ_2 = 0.33 nsec) intensity from that of the pure crystal. This change might be attributed to the occurrence of F-centers in the irradiation process. Our calculations also cannot exclude the following fact that the positron spreads out to touch the electron cloud surrounding the F-center from cation or more distant anion sites. This may increase the possibility of the contribution of the F-center into the second or high core states of positron in the positron annihilation from colored alkali halides.

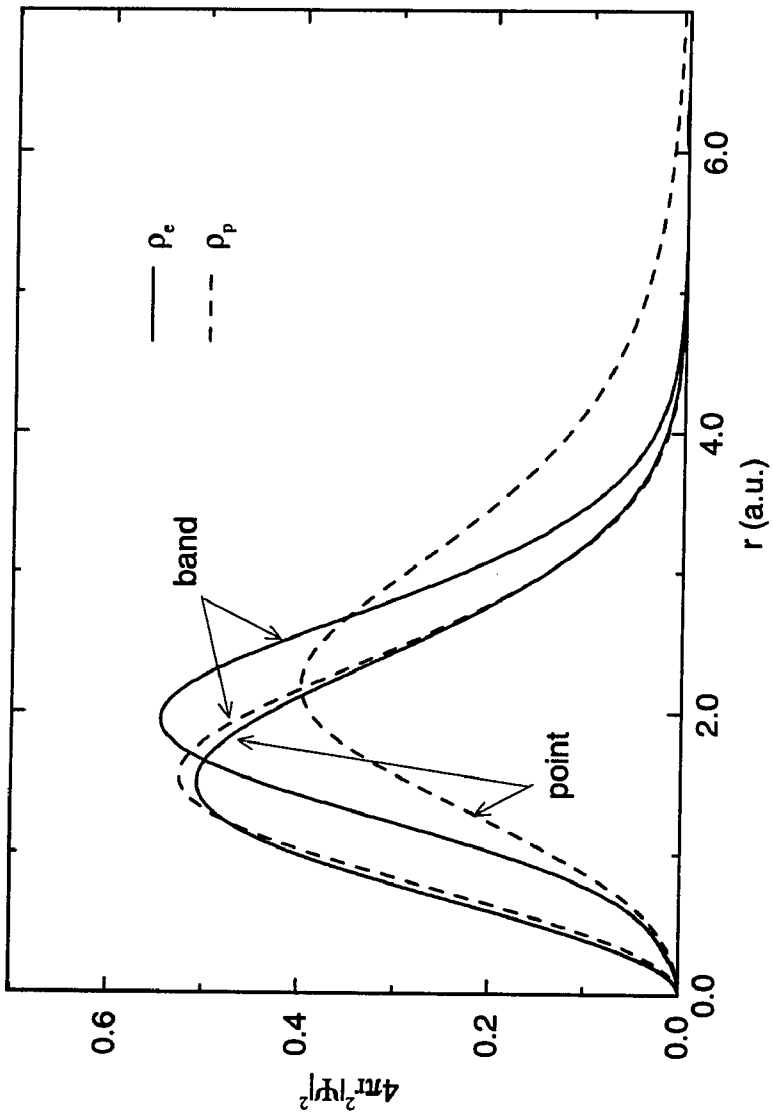

FIG. 6.13. Position of electron and positron densities in F-center of NaF. The radial density of electron shifts from inside of the point-ionic model to outside of the energy-band ionic model.

CHAPTER VII

CONCLUSIONS

Positron annihilation as a useful probe for the analysis of electron structures has been demonstrated by the theoretical first-principles calculations for positron bound states in atomic systems, pure alkali halides, and the F-center of those crystals.

In summary, in Chapter II, we have reviewed the theoretical background for the density functional theory and implemented the self-interaction corrected local spin density approximation for positron bound states in the systems. The many-body interactions have been included in the self-consistent density functional calculations such as the electron-electron exchange energy, the electron-electron correlation energy, and the electron-positron correlation energy. The phenomenology of the positron annihilation has been described in Chapter III, especially, for the two-photon annihilation. The thermalized positron as a quantum particle in matter annihilates into photons with the strong attraction of the electron-positron Coulomb interaction and the electron-positron correlation. The number of photons per annihilation event can be determined by the spin alignment of the positron and electron at the position of the positron. Our calculation has been based on the spin-averaged annihilation rate which characterizes condensed matter systems based on two-photon positron annihilation.

The other theoretical ingredient for the crystal system has been considered in Chapter IV. The crystal potential provides the attractive regions to the electron which are at the same time repulsive to the positron. This Madelung potential has been determined by considering the lattice sum with either the point-ionic potential or the band-ionic potential. The convergence of the crystal potential matrix element has been facilitated by the use of Ewald's method. In Chapter V, the computational procedure has been briefly described. The self-consistent field method has been used for the atomic structure calculation. The embedded cluster method in the single-site approximation has been applied to models: the pure crystal and F-center of alkali halides. The Gaussian basis set is included only on the anion or the electron at F-center, but the Hamiltonian corresponds to infinite lattices in the one-particle self-consistent Kohn-Sham equations. From these calculations, we have reached the results on Chapter VI.

In the atomic system, the electron and positron densities have been calculated to analyze the lifetime of positron annihilation for the several situations: (i) no correlation included (X-O), (ii) electron correlation included (EC-O), and (iii) electron-positron correlation included (EP-O, EPC). Results of the X-O and the EC-O calculations are similar to that of the Hartree-Fock calculation. However, EP-O and EPC calculations show the dramatic shifts of densities. On the EP-O calculation, the positron correlation potential attracts positron density inward, leading to an increase in the annihilation rate. Furthermore, the inclusion of the pair-correlation function in EPC calculation enhances the probability of the pair annihilation and correspondingly reduces the positron lifetimes in negative atomic systems. The increasing eigenvalues of positron bound states correspond to the increasing positron lifetimes with the order [(1s), (2p, 2s), and (3d, 3p, 3s)]. In the neutral atomic

system, there is strong evidence for the positron bound states in our density functional calculations, and the accuracy of the SIC-LSDA method is demonstrated by the agreement of the calculated annihilation rates for the negative hydrogen atom with other calculations at higher levels of theory.

In the pure crystal system of alkali halides, the crystal potential has been incorporated in the modeling of the ionic potentials in two ways: (1) the modified point-ionic potential including information of the ionic radius and (2) the full-ionic potential derived from electronic energy-band structure calculations. The density functional calculation has been performed on the anion center in the one-site embedded scheme which includes the Hamiltonian for the infinite lattices and the Gaussian-basis set on the center. The contribution of the crystal effect competes with the positron correlation effect. The positron annihilation lifetimes are found to be sensitive to the crystal model potential used. The positron forms the bound states with substantial density in the interstitial lattice positions, and the density of positron in higher state may be also distributed through interstitial region including both anion and cation sites.

However, the 1s (ground) state of positron is not seriously affected by this limitation and it can be explained within the one-site approximation. This implies that the positron ground state may be formed on the electron-rich anion site and finally annihilates into two photons in alkali halides. The result agrees relatively well with experimental data and gives a power law relationship between annihilation lifetimes and lattice constants. In the realistic band potential, especially, the improper distortion of densities in high positron states is severe within the limitation of the one-site approximation of the embedded cluster method. This implies that excited experimental components may be attributed to the contribution from both the

anion site and the cation site. Therefore, detailed comparison with experimental components for higher states will be deferred to another theoretical calculation such as the multi-shell embedded cluster method.

For the F-center as the defect center of alkali halides, the system for the density functional calculation is defined as a trapped electron and a positron. The infinite crystalline lattice has been computed with the first-principles method as described in the pure crystal system. The positron-correlation potential does not contribute significantly to the positron structure in the point-ionic potential treatment, but it does in the band-ionic potential. The significant factor in the F-center is the pair-correlation function for the positron annihilation.

Positron lifetimes are compared with other empirical calculations and the a vailable experimental data. Within our one-site approximation, the first-principles calculations of the positron annihilation from the ground state of positron in the F-center of NaCl agrees with the experiment result. Unfortunately, other crystals do not have any available experimental results for the on-center positron annihilation of F-centers. However, the available experimental results[106] for colored crystals which associate with either bulk state or defect state of positron bound states may be properly analyzed by the multi-shell band calculation of the embedded cluster method, which can address the phenomenon of the pick-off annihilation from the surrounding F-center.[107]

In conclusion, we analyzed the positron annihilation at the F-center of alkali halides from the systematic searches for the positron correlation effect and crystal field effects in the series of atomic systems and pure crystalline systems. In future work, it would be useful to implement the positron analysis in defect systems with the multi-shell embedding cluster and also to extend this work to molecular systems.

REFERENCES

[1]R. M.Nieminen, E. Boronski, and L. Lantto, Phys. Rev. B **32**, 1377 (1985).

[2]E. Boronski and R. M. Nieminen, Phys. Rev. B **34**, 3820 (1986).

[3]A. Dupasquier, *Positrons in solids* Vol. 12 of Topics in Current Physics, edited by P. Hautojärvi (Springer-Verlag, Berlin, 1979) p. 197 and references therein.

[4]L. Dorikens-Vanpraet, M. Dorikens, and D. Segers, *Positron Annihilation* (World Scientific, Singapore, 1989).

[5]Z. Kajcsos and C. Szeles, *Material Science Forum* **105-110** pt1, pt2, and pt3 (Positron Annihilation) (Trans Tech Publications, Switzerland, 1992).

[6]R. Krause, K. Saarinen, P. Hautojärvi, A. Polity, G. Gärtner, and C. Corbel, Phys. Rev. Lett. **65,** 3329 (1990).

[7]K. Saarinen and P. Hautojärvi, Phys. Rev. B **43**, 4249 (1991).

[8]J. Xu, L. D. Hulett, Jr., T. A. Lewis, D. L. Donohue, S. A. McLuckey, and G. L. Glish , Phys. Rev. A **47**, 1023 (1993).

[9]P. E. Cade and A. Farazdel, J. Chem. Phys. **66**, 2598 (1977); A. Farazdel and P. E. Cade, *ibid.* **66**, 2612 (1977).

[10]A. J. Patrick and P. E. Cade, J. Chem. Phys. **75**, 1893 (1981).

[11]P. Navin, D. M. Schrader, and C. F. Lebeda, Appl. Phys. **3**, 159 (1974); Phys. Rev. A **9**, 2248 (1974).

[12]D. C. Clary, J. Phys. B **9**, 315 (1976).

[13]Y. K. Ho, Phys. Rev. A **34**, 609 (1986).

[14]P. Hohenberg and W. Kohn, Phys. Rev. B **6**, 13864 (1964).

[15]W. Kohn and L. J. Sham, Phys. Rev. A **140**, 1133 (1965).

[16]J. P. Perdew and A. Zunger, Phys. Rev. B **23**, 5048 (1981).

[17]A. Zunger and A. J. Freeman, Phys. Rev. B **16**, 2901 (1977).

[18]L. Hedin, Phys. Rev. **139**, A 796 (1965).

[19]R. W. Godby, M. Schlüter, and L. J. Sham, Phys. Rev. B **36**, 6497 (1987).

[20]J. G. Harrison, J. Chem. Phys. **78**, 4562 (1983).

[21]D. M. Ceperley and B. L. Alder, Phys. Rev. Lett. **45**, 566 (1980).

[22]B. Chakraborty, Phys. Rev. B **24**, 7423 (1981).

[23]B. Chakraborty and R. W. Siegel, Phys. Rev. B **27**, 4535 (1983).

[24]C. H. Hodges and M. J. Stott, Solid State Commun. **12**, 1153 (1973).

[25]R. H. Nieminen and C. H. Hodges, Phys. Rev. B **18**, 2568 (1978).

[26]J. Arponen and E. Pajanne, Ann. Phys.(N.Y.) **121**, 343 (1979).

[27]L. J. Lantto, Phys. Rev. B **36**, 5160 (1987).

[28]P. Vashishta, P. Bhattacaryya, and K. S. Singwi, Phys. Rev. B **10**, 5108 (1974).

[29] J. H. Rose and H. B. Shore, Phys. Rev. B **17**, 1884 (1978).

[30]E. Boronski, Cryst. Res. Technol. **22**, 1505 (1987).

[31]J. G. Harrison, J. Chem. Phys. **84**, 1659 (1986).

[32]M. R. Pederson, R. A. Heaton, and J. G. Harrison, Phys. Rev. B **39**, 1581 (1989).

[33]F. H. Gertler, H. B. Snodgrass, and L. Spruch, Phys. Rev. **172**, 110 (1968).

[34]S. Golden and I. R. Epstein, Phys. Rev. A **10**, 761 (1974).

[35]A. Farazdel and P. E. Cade, Phys. Rev. B **9**, 2036 (1974).

[36]D. G. Kanhere, A. Farazdel, and V. H. Smith, Jr., Phys. Rev. B **35**, 1313 (1987).

[37]L. D. Landau, *Mechanics* 3rd Edition (Pergamon Press, Oxford, 1976).

[38]H. S. Bethe and R. W. Jackiw, *Intermediate Quantum Mechanics* 2nd Edition (Benjamin Inc., New York, 1968).

[39]S. Weinberg, *Gravitation and Cosmology: Principles and Applications of the General Theory of Relativity* (Wiley, New York, 1972).

[40]J. D. Bjorken and S. D. Drell, *Relativistic Quantum Mechanics*, McGraw-Hill Inc., New York, 1964).

[41]C. Itzykson and J. B. Zuber, *Quantum Field theory* (McGraw-Hill Inc., New York, 1980).

[42]S. Tomonaga, Prog. Theor. Phys. **1**, 27 (1946).

[43]J. Schwinger, Phys. Rev. **75**, 651; *ibid.* **76**, 790 (1949).

[44]R. P. Feynman, Phys. Rev. **76**, 749; *ibid.* 769 (1949).

[45]P. Nozieres and D. Pines, *The theory of quantum liquids I* (Benjamin, New York, 1966).

[46]M. Born and J. R. Oppenheimer, Ann. Physik **84**, 457 (1927).

[47]D. R. Hartree, Proc. Cambridge Phil. Soc. **24**, 89; *ibid.* 111 (1928).

[48]V. Fock, Z. Phys. **61**, 126; **62**, 795 (1930).

[49]L. H. Thomas Proc. Camb. Phil. Soc. **23**, 542 (1927).

[50]E. Fermi Rend. Accad. Lincei **6**, 602 (1927); Z. Phys. **48**, 73 (1928); Rend. Accad. Lincei **7**, 342 (1928).

[51]P. A. M. Dirac Proc. Camb. Phil. Soc. **26**, 376 (1930).

[52]C. F. von Weizsäcker Z. Physik **96**, 431 (1935).

[53]J. C. Slater, Phys. Rev. **34**, 1293 (1929).

[54]J. C. Slater, Phys. Rev. **81**, 385 (1951); *ibid.* **91**, 528 (1953).

[55]J. C. Slater, *Quantum Theory of Molecules and Solids* (McGraw-Hill, New York, 1974).

[56]B. Y. Tong and L. J. Sham, Phys. Rev. **144**, 1 (1966).

[57]U. von Barth and L. Hedin, J. Phys. C **5**, 1629 (1972).

[58]J. G. Rajagopal and J. Callaway, Phys. Rev. B **7**, 1912 (1973).

[59]R. G. Parr and W. Yang, *Density-Functional Theory of Atoms and Molecules* (Oxford University Press, 1988) p. 57.

[60]J. P. Perdew, Chem. Phys. Lett. **64**, 127 (1979).

[61]J. G. Harrison, J. Chem. Phys. **79**, 2265 (1985).

[62]M. Levy, Phys. Rev. A **26,** 1200 (1982).

[63]P. A. M. Dirac, Proc. Roy. Soc. (London), A **126**, 360 (1930).

[64]C. D. Anderson, Phys. Rev. **44**, 406 (1933).

[65]J. S. Allen, *The Neutrino* (Princeton University Press, Princeton, NJ 1958).

[66]K. Venkateswaran, Ph. D. Thesis (University of Missouri, Kansas City, 1985) (unpublished).

[67]K. S. Krane, *Introductory Nuclear Physics* (John Wiley & Sons, New York, 1988)p. 296.

[68]F. H. Hsu, W. C. Mallard, and J. H. Hadley, Jr., Appl. Phys. **4**, 83 (1974).

[69]L. T. Dillman, MIND, Pamphlet No. 4, J. Nucl. Med. Suppl., No. 2 (1969).

[70]M. Mourino, H. Löbl, and R. Paulin, Phys. Lett. A **71**, 106 (1979).

[71]G. Z. Gleason, I. D. Taylor and D. L. Tabern, Nucleonics **8**, 12 (1951).

[72]P. Kirkegaard and M. Eldrup, Comput. Phys. Commun. **3**, 240 (1972); P. Kirkegaard and M. Eldrup, Comput. Phys. Commun. **7**, 401 (1974).

[73]W. J. Madia, A. L. Nichols, and H. J. Ache, J. Am. Chem. Soc. **97**, 5041 (1975).

[74]W. Puff, Comput. Phys. Commun. **30**, 359 (1983).

[75]C. J. Virtue, K. J. Douglas, and B. T. A. Mckee, Comput. Phys. Commun. **15**, 97 (1978).

[76]C. Bussolati, A. Dupasquier, and L. Zappa, Nuovo Cimento (Ser.X) **52** B 529 (1967).

[77]W. Brandt and J. Reiheimer, Phys. Lett. A **35**, 109 (1971).

[78]K. Sawada, Phys. Rev. **106,** 372 (1957).

[79]S. Fantoni and S. Rosati, Nuovo Cimento A **25**, 593 (1975).

[80]E. Krotscheck and M. L. Ristig, Nucl. Phys. A **242**, 389 (1975).

[81]G. Ripka, Phys. Rep. **56**, 1 (1979).

[82]R. Jastrow, Phys. Rev. **98**, 1479 (1955).

[83]C. Kittel, *Introduction to Solid State Physics* (John Wiley & Sons, Inc., New York 1991) p. 71.

[84]E. Madelung, Z. Phys. **19**, 524 (1918).

[85]H. M. Evjen, Phys. Rev. **39**, 675 (1932).

[86]F. C. Frank, Philos. Mag. **41**, 1287 (1950).

[87]O. Emersleben, Phys. Zeits. **24**, 73 (1923).

[88]P. Ewald, Ann. Phys. (Leipzig) **64**, 253 (1921).

[89]C. S. Ho, Ms. Thesis (North Dakota State University, 1986) (unpublished).

[90]S. C. Erwin, R. A. Heaton, and C. C. Lin, BANDAID Software Package, (University of Wisconsin, 1986).

[91]F. Herman and S. Skillman, *Atomic Structure Calculations* (Prentice_Hall, Englewood Cliffs, NJ, 1963).

[92]J. A. Nedler and R. Mead, Computer Journal **7**, 308 (1968).

[93]W. P. Menzel, Ph. D. Thesis (University of Wisconsin, 1974) (unpublished).

[94]J. W. Hsu, Ph. D. Thesis (University of Alabama at Birmingham, 1991) (unpublished).

[95]J. G. Harrison and C. C. Lin, Phys. Rev. B **24**, 6060 (1981).

[96]R. A. Heaton, J. G. Harrison, and C. C. Lin, Phys. Rev. B **31**, 1077 (1985).

[97]K. A. Jackson and C. C. Lin, Phys. Rev. B **38**, 12171 (1988).

[98]R. C. Chaney and C. C. Lin, Phys. Rev. B **13**, 843 (1976).

[99]R. A. Heaton and C. C. Lin, Phys. Rev. B **22**, 3629 (1980).

[100]A. Bisi, A. Bosi, A. Dupasquier, and L. Zappa, Phys. Status Solidi B **69**, 515 (1975).

[101]M. Bertolaccini, A Bisi, G. Gambarini, and L. Zappa, J. Phys. C **4**, 734 (1971).

[102]R. N. West, *Positron Studies of Condensed Matter* (Taylor & Francis LTD, London 1974) p. 76.

[103]T. T. Basiev and S. B. Mirov, *Room Temperature Tunable Color Center Lasers*, Laser Science and Technology--An International Handbook Vol. 16, edited by V.S. Letokhov, C. V. Shank, Y. R. Shen and H. walther (Harwood Academic Publishers, 1994).

[104]D. Zahrt and S. H. Lin, Theor. Chim. Acta **12**, 256 (1968).

[105]A. Krumhansl and N. Schwarz, Phys. Rev. **89**, 1154 (1953).

[106]F. H. Hsu, W. C. Mallard, and J. K. Fu, Appl. Phys. **4**, 75 (1974).

[107]U. Lauff, J. Major, A. Seeger, H. stoll, A. Siegle, Ch. Deckers, H. Greif, K. Maier, and M. Tongbhoyai, Phys. Lett. A **182**, 165 (1993).

[108]S. H. Vosko, L. wilk, M. Nusair, Can. J. Phys. **58**, 1200 91980).

[109]M. Gell-Man and K. A. Brueckner, Phys. Rev. **106**, 364 (1957).

[110]S. Misawa, Phys. Rev. A **140**, 1645 (1965).

[111]S. Kahana, Phys. Rev. **129**, 1622 (1963).

[112]A. Sjölander and M. J. Stott, Solid State Commun. **8**, 1881 (1970); Phys. Rev. B **5**, 2109 (1972).

[113]G. Ferrante, Phys. Rev. **170**, 76 (1968).

APPENDIX A

EXCHANGE-CORRELATION ENERGY FUNCTIONAL

Many-body interactions in a fermionic system consisting of N-electrons and a single positron are considered in detail. The many-body interactions in terms of the exchange-correlation energy functional needed in the local density approximation of the DFT have been studied in the context of the quantum field theory. The field theoretical approach has been implemented in two cases: one is for the homogeneous gas and the other is for the inhomogeneous gas. The GW-approximation, a recently developed method for the inhomogeneous gas, gives better results for electronic structures of semiconducting materials.[19] The homogeneous gas method is the most widely used method for density functional calculations including many-body interactions between electron and electron, and also between electron and positron. Exchange and correlation energy in the uniformly distributed homogeneous gas are reviewed next.

1. Electron-electron exchange energy[51]

The electron-electron exchange-correlation energy functional for the local approximation of the Eq. (2.40) can be decomposed into the exchange and the correlation energy functionals. The exchange energy functional can be written in the following form,

$$E_x[\rho_\sigma] = \int dr \rho_\sigma \varepsilon_x[\rho_\sigma] \,. \tag{A. 1}$$

From the Hartree-Fock equations, Eq. (2.14) for a free-electronic homogeneous gas, the exchange energy can be cast into the above form of the local density functional. It is convenient to simplify the Eq. (2.15) by neglecting the nuclear interaction and the Coulomb repulsion in order to address the local exchange energy functional. For the free-electron system, the normalized plane wave can be used as the eigenfunctions,

$$\phi_k(r) = \frac{1}{\sqrt{V}} e^{ik\cdot r}, \tag{A. 2}$$

where V is the volume of the electron gas, and so the states i, j can be distinguished by the momentum states k and k' from Eq. (2.17). The Hartree-Fock equation for the orbital ϕ_k thus becomes

$$-\frac{1}{2}\nabla_1\phi_k(r_1) - \sum_{k'}\left[\int \frac{\phi^*_{k'}(r_2)\,\phi_{k'}(r_2)\,\phi_{k'}(r_1)\,dr_2}{r_{12}\phi_{k'}(r_1)}\right]\phi_k(r_1) = \varepsilon(k)\,\phi_k(r_1). \tag{A. 3}$$

The sum over k' is a sum over all the occupied orbital states, so that, at the absolute zero of temperature, when each of these states contains two electrons with opposite spins, the sum over k' is the same as a sum over all electrons with one kind of spin, and a sum over all electrons with the other kind of spin would be precisely the same. The exchange term in Eq. (A.3) with the plane wavefunctions becomes

$$-\frac{1}{V}\sum_{k'}\left[e^{-i(k-k')\cdot r_1}\int \frac{e^{i(k-k')\cdot r_2}}{r_{12}}dr_2\right]\phi_k(r_1). \tag{A. 4}$$

From Poisson's equation, the potential V_x at the point r due to a distribution of charge whose density is given by the function $e^{i(k-k')\cdot r}$ can be written by

$$\nabla^2 V_x(r) = -4\pi e^{i(k-k')\cdot r}, \tag{A. 5}$$

and the required solution may be written as

$$V_x(r) = \frac{4\pi e^{i(k-k')\cdot r}}{|k-k'|^2}. \tag{A. 6}$$

The potential at the point r_1 due to the all charge distribution at r_2

$$V_x(r_1) = \int \frac{e^{i(k-k')\cdot r_2}}{r_{12}}dr_2 \tag{A. 7}$$

has the value

$$V_x(r_1) = \frac{4\pi e^{i(k-k')\cdot r_1}}{|k-k'|^2}, \tag{A. 8}$$

and the eigenvalue and the exchange term (A.4) can be rewritten as

$$\varepsilon(k) = \frac{k^2}{2} + \varepsilon_x(k), \tag{A. 9}$$

$$\varepsilon_x(k) = -\frac{4\pi}{V}\sum_{k'}\frac{1}{|k-k'|^2}. \tag{A. 10}$$

For the evaluation of $\varepsilon_x(k)$, a volume element d^3k of k-space contains $Vdk/(8\pi^3)$ orbital states. The exchange sum can be expressed with the integral form

$$\varepsilon_x(k) = -\frac{4\pi}{V}\left(\frac{V}{8\pi^3}\right)\int\frac{d^3k'}{|k-k'|^2}. \tag{A. 11}$$

The integral is taken throughout the Fermi sphere. From the spherical coordinates (k', θ, ϕ), where θ is the angle between k' and k, the exchange term is

$$\varepsilon_x(k) = -\frac{1}{2\pi^2}\int_0^{k_0}dk'\int_0^{\pi}d\theta\int_0^{2\pi}\frac{k'^2\sin\theta}{|k-k'|^2}d\phi$$

$$= -\frac{1}{\pi}\int_0^{k_0}dk'\int_{-1}^{1}\frac{k'^2 d(\cos\theta)}{k^2+k'^2-2kk'\cos\theta}$$

$$= -\frac{1}{\pi k}\int_0^{k_0}k'\left(\log\left|\frac{k+k'}{k-k'}\right|\right)dk'$$

$$= -\frac{1}{2\pi}\left[2k_0 + \frac{k_0^2-k^2}{k}\log\left(\frac{k_0+k}{k_0-k}\right)\right]. \tag{A. 12}$$

Where the integrand becomes infinite when $k'(\leq k_0) = k$ so that, for $k < k_0$, the integral can be expressed as the sum of the integral from 0 to k and the integral from k to k_0.

The total exchange energy for the spectra of k is the sum of the $\varepsilon_x(k)$ and can be evaluated by replacing the sum by an integral over the Fermi sphere. This gives

$$\sum_k \varepsilon_x(k) = -\frac{1}{2\pi}\left(\frac{V}{8\pi^3}\right)\int_0^{k_0}\left[2k_0 + \frac{k_0^2-k^2}{k}\log\left(\frac{k_0+k}{k_0-k}\right)\right]4\pi k^2 dk$$

$$= -\frac{V}{4\pi^3}\int_0^{k_0}\left[2k_0k^2 + k\left(k_0^2-k^2\right)\log\left(\frac{k_0+k}{k_0-k}\right)\right]dk$$

$$= -\frac{V}{4\pi^3}k_0^4. \qquad \text{(A. 13)}$$

The total exchange energy per electron becomes

$$E_x = -\int\frac{V}{4\pi^3}k_0^4 dr$$

$$= -\frac{3}{4}\left(\frac{6}{\pi}\right)^{1/3}\int dr\,(\rho_\uparrow^{4/3}+\rho_\downarrow^{4/3}), \qquad \text{(A. 14)}$$

where the density of states, $2V/(8\pi^3)$ within the Fermi sphere, $\frac{4\pi}{3}k_0^3$ for each spin orbital states gives the total number of states N, and the spin densities are defined as $N/(2V) = \rho_\uparrow$ and $N/(2V) = \rho_\downarrow$.

2. Electron-electron correlation energy

The local density form of the correlation energy functional can be written by the following form:

$$E_C = \int dr\rho_\sigma\varepsilon_c[\rho_\uparrow, \rho_\downarrow], \qquad \text{(A. 15)}$$

where ε_c denotes the correlation energy per electron for an electron gas with uniform

spin densities has been simulated by Ceperley and Alder[21] and parametrized by Vosko et al.[108] and Perdew and Zunger.[16]

In Perdew and Zunger's parametrization, the correlation energy ε_c and the corresponding potential V_c can be classified into the high and the low limits of the density after using the following derivatives at the point $r_s = 1$,

$$v_c(\rho, \zeta = 0, 1) = \left\{1 - \frac{r_s}{3}\frac{d}{dr_s}\right\}\varepsilon_c(\rho, \zeta = 0, 1). \quad \text{(A. 16)}$$

For the low density $r_s \geq 1$, the correlation energy and the corresponding potential are written as the following:

$$\varepsilon_c(\zeta) = \frac{\gamma(\zeta)}{\left(1 + \beta_1(\zeta)\sqrt{r_s} + \beta_2(\zeta) r_s\right)} \quad \text{(A. 17)}$$

$$v_c(\zeta) = \left(1 + \frac{7}{6}\beta_1(\zeta)\sqrt{r_s} + \frac{4}{3}\beta_2(\zeta) r_s\right)\frac{\varepsilon_c^2(\zeta)}{\gamma(\zeta)}, \quad \text{(A. 18)}$$

where $\beta_1(\zeta)$, $\beta_2(\zeta)$, and $\gamma(\zeta)$ are fit-parameters,[16] the index ζ is for the polarized $(\zeta = 1)$ or the unpolarized $(\zeta = 0)$ case, and the Wigner-Seitz radius is $r_s = (3/4\pi)^{1/3}\rho^{-1/3}$ in atomic units. The parameters used to represent the Ceperley and Alder results are $\beta_1(0) = 1.0529$, $\beta_1(1) = 1.3981$, $\beta_2(0) = 0.3334$, $\beta_2(1) = 0.2611$, $\gamma(0) = -0.1423$, and $\gamma(1) = -0.0843$.

For the high density $(r_s < 1)$, the leading behavior of the high density expansion tying smoothly to the low density form gives following parametrization:

$$\varepsilon_c(\zeta) = A(\zeta) ln r_s + B(\zeta) + C(\zeta) r_s ln r_s + D(\zeta) r_s, \quad \text{(A. 19)}$$

$$v_c = A(\zeta) ln r_s + \{B(\zeta) - \frac{1}{3}A(\zeta)\} + \frac{2}{3}C(\zeta) r_s ln r_s + \frac{1}{3}\{2D(\zeta) - C(\zeta)\} r_s, \quad \text{(A. 20)}$$

by taking the values $A(0) = 0.0311$ and $B(0) = -0.048$ from the calculation of Gell-Mann and Brueckner,[109] fixing the values $A(1) = 0.01555$ and $B(1) = -0.0269$ from the random phase scaling relation by Hedin[18] and Misawa[110] and determining the values $C(0) = 0.0020$, $C(1) = 0.0007$, $D(0) = -0.0116$, $D(1) = -0.0048$ by matching the two limits at $r_s = 1$.

For intermediate values of ζ, the von Barth-Hedin interpolation[57] can be adopted. For the spin densities $\rho\uparrow(r)$ and $\rho\downarrow(r)$, the density is denoted to $\rho(r) = \rho\uparrow(r) + \rho\downarrow(r)$ and the polarization factor can be written by

$$\zeta(r) = \frac{1}{\rho(r)} [\rho\uparrow(r) - \rho\downarrow(r)]. \tag{A. 21}$$

The interpolation between the unpolarized paramagnetic ($\zeta = 0$) and the fully polarized ferromagnetic ($\zeta = \pm 1$) limits can be written by

$$\varepsilon_i(\zeta) = \varepsilon_i(\zeta = 0) + [\varepsilon_i(\zeta = 1) - \varepsilon_i(\zeta = 0)] f(\zeta(r)) \tag{A. 22}$$

for the exchange ($i = x$) and correlation ($i = c$) contributions to the energy per particle. The interpolation function

$$f(\zeta(r)) = \frac{(1+\zeta(r))^{4/3} + (1-\zeta(r))^{4/3} - 2}{2\left(2^{1/3} - 1\right)} \tag{A. 23}$$

is chosen to reproduce the ζ-dependence of the exchange and the correlation energies. In the para- and ferro-magnetic limits, the exchange term has the form

$$\varepsilon_x(\zeta = 0) = -\frac{3}{4}\left(\frac{3\rho}{\pi}\right)^{1/3} = -\frac{3}{4}\left(\frac{9\pi}{4}\right)^{1/3} r_s^{-1}, \tag{A. 24}$$

$$\varepsilon_x(\zeta = 1) = 2^{1/3}\varepsilon_x(\zeta = 0), \tag{A. 25}$$

and from the random phase scaling relation

$$\varepsilon_c(r_s, \zeta = 1) = \frac{1}{2}\varepsilon_c\left(r_s 2^{-4/3}, \zeta = 0\right). \tag{A. 26}$$

3. Electron-positron correlation energy

It is obvious that the electron can not see the positron through the exchange channel of the Feynman diagram because they are not identical particles. The positron correlation with the electron in an electron gas has been investigated by several authors.[26, 111, 112] However, the correlation is too difficult to analyze due to the complicated many-body interaction between electron and positron. There are several well-known approaches to this problem. Among them are the Bethe-Goldstone ladder approximation,[111] the non-linear two-component plasma theory and the resulting dielectric response function,[112] the interacting Sawada boson[78] approach as collective excitations of the random phase approximation(RPA),[26] and finally the Fermi hypernetted chain(FHNC) integral[27] with the Jastrow variational wavefunction.[79-82] The Sawada bosonic method gives better results for the annihilation rates than those of others and has been interpolated by Boronski and Nieminen[2] together with the results of the FHNC method. The interpolated form of the correlation energy in unit volume for $\rho_+ \le \rho_\sigma$ is written as

$$E_c^{ep}[\rho_\sigma, \rho_+] = \int d^3 r E_V^{ep}[\rho_\sigma, \rho_+], \tag{A. 27}$$

$$E_V^{ep}[\rho_\sigma, \rho_+] = \rho_<\left[a(\rho_>) + b(\rho_>)\rho_< + c(\rho_>)\rho_<^2\right], \tag{A. 28}$$

where $\rho_<(\rho_>)$ denotes the smaller (greater) of densities ρ_σ and ρ_+ at any position. The unknown coefficients are defined by

$$\frac{\delta}{\delta\rho_+} E_V^{ep}[\rho_\sigma, \rho_+]\Big|_{\rho_+ = \rho_\sigma = \rho} = \mu_0(\rho), \tag{A. 29}$$

$$\frac{\delta}{\delta\rho_+} E_V^{ep}[\rho_\sigma, \rho_+]\big|_{\rho \to 0} = \varepsilon_{AP}(\rho)\,, \tag{A. 30}$$

$$E_V^{ep}[\rho_\sigma, \rho_+]\big|_{\rho_+ = \rho_\sigma = \rho} = \rho\varepsilon_L(\rho)\,, \tag{A. 31}$$

and

$$a(\rho) = \varepsilon_{AP}(\rho)\,, \tag{A. 32}$$

$$b(\rho) = \frac{1}{\rho}[3\varepsilon_L(\rho) - 2\varepsilon_{AP}(\rho) - \mu_0(\rho)]\,, \tag{A. 33}$$

$$c(\rho) = \frac{1}{\rho^2}[\mu_0(\rho) + \varepsilon_{AP}(\rho) - 2\varepsilon_L(\rho)]\,, \tag{A. 34}$$

where interpolation formulas of the electron-positron correlation energy are based on the results of Arponen and Pajanne[26] which are taken as the limit of zero concentration corresponding to a single positron $\varepsilon_{AP}(\rho)$ in a homogeneous electron gas and Lantto's data[27] $\varepsilon_L(\rho)$ for equal densities between positrons and electrons.

The corresponding correlation potentials for the electron and the positron come from the functional derivatives of the electron-positron correlation energy. Without loss of generality, partial derivatives along the ρ_σ, ρ_+ directions on the surface of the energy density $E_V^{ep}[\rho_\sigma, \rho_+]$ may be equivalent with functional derivatives, which gives the following electron potential and positron correlation potential,

$$v_c^{ep-e} = \frac{\delta}{\delta\rho_\sigma} E_V^{ep}[\rho_\sigma, \rho_+] \tag{A. 35}$$

$$v_c^{ep-p} = \frac{\delta}{\delta\rho_+} E_V^{ep}[\rho_\sigma, \rho_+]\,. \tag{A. 36}$$

From Eq. (A.28) partial derivatives are as follows:

$$\frac{\partial E_V^{ep}}{\partial \rho_>} = \rho_< \left[\frac{\partial a(\rho_>)}{\partial \rho_>} + \frac{\partial b(\rho_>)}{\partial \rho_>}\rho_< + \frac{\partial c(\rho_>)}{\partial \rho_>}\rho_<^2\right] \tag{A. 37}$$

$$\frac{\partial E_V^{ep}}{\partial \rho_<} = a(\rho_>) + 2b(\rho_>)\rho_< + 3c(\rho_>)\rho_<^2, \tag{A. 38}$$

whereby using Eqs. (A.29-31) derivatives can be written as

$$\frac{\partial a(\rho_>)}{\partial \rho_>} = \frac{\partial \varepsilon_{AP}(\rho_>)}{\partial \rho_>}, \tag{A. 39}$$

$$\frac{\partial b(\rho_>)}{\partial \rho_>} = \frac{-1}{\rho_>^2}[3\varepsilon_L(\rho_>) - 2\varepsilon_{AP}(\rho_>) - \mu_0(\rho_>)]$$

$$+\frac{1}{\rho_>}\left[3\frac{\partial \varepsilon_L(\rho_>)}{\partial \rho_>} - 2\frac{\partial \varepsilon_{AP}(\rho_>)}{\partial \rho_>} - \frac{\partial \mu_0(\rho_>)}{\partial \rho_>}\right], \tag{A. 40}$$

$$\frac{\partial c(\rho_>)}{\partial \rho_>} = \frac{-2}{\rho_>^3}[\mu_0(\rho_>) + \varepsilon_{AP}(\rho_>) - 2\varepsilon_L(\rho_>)]$$

$$+\frac{1}{\rho_>^2}\left[\frac{\partial \mu_0(\rho_>)}{\partial \rho_>} + \frac{\partial \varepsilon_{AP}(\rho_>)}{\partial \rho_>} - 2\frac{\partial \varepsilon_L(\rho_>)}{\partial \rho_>}\right]. \tag{A. 41}$$

For the surface $E_V^{ep}[\rho_\sigma, \rho_+]$ which is symmetric with respect to ρ_+ and ρ_σ, the symmetric potential with the equal-density is defined as

$$\mu_0(\rho) = \mu(\rho_\sigma, \rho_+)\big|_{\rho_\sigma = \rho_+ = \rho} = \frac{1}{2}\frac{\partial}{\partial \rho}[\rho \varepsilon_L(\rho)], \tag{A. 42}$$

$$\mu_0(\rho_>) = \frac{1}{2}\varepsilon_L(\rho_>) + \frac{1}{2}\rho_>\frac{\partial \varepsilon_L(\rho_>)}{\partial \rho_>} \tag{A. 43}$$

$$\frac{\partial \mu_0(\rho_>)}{\partial \rho_>} = \frac{\partial \varepsilon_L(\rho_>)}{\partial \rho_>} + \frac{1}{2}\rho_>\frac{\partial^2}{\partial \rho_>^2}\varepsilon_L(\rho_>). \tag{A. 44}$$

Now interpolation formulas of the electron-positron correlation energy are based on the results of Arponen and Pajanne in the zero limiting concentration of a single positron $\varepsilon_{AP}(\rho)$ in a homogeneous electron gas and Lantto's data for equal densities between electrons and positrons $\varepsilon_L(\rho)$. The formula for the correlation energy functional and its derivatives are continuous in the whole range of r_s.

For one positron in homogeneous electron gas, the correlation energy and the corresponding potential derivatives with the Wigner-Seitz radius $r_s \le 0.302$ are

$$\varepsilon_{AP}[\rho_>(r_s)] = -0.78 r_s^{-1/2} + (0.0255 ln r_s - 0.0405) ln r_s + 0.572, \qquad \text{(A. 45)}$$

$$v_{AP} \equiv \frac{\partial \varepsilon_{AP}(\rho_>)}{\partial \rho_>} = \frac{\partial \varepsilon_{AP}}{\partial r_s}\frac{\partial r_s}{\partial \rho_>} = \frac{-1}{3} r_s \rho_> \frac{\partial \varepsilon_{AP}}{\partial r_s}$$

$$= \left(0.0135 - 0.13 r_s^{-1/2} - 0.017 ln r_s\right)\rho_>, \qquad \text{(A. 46)}$$

for $0.302 \le r_s \le 0.56$

$$\varepsilon_{AP}[\rho_>(r_s)] = -0.461525 - 0.027295 r_s^{-2}, \qquad \text{(A. 47)}$$

$$v_{AP} = -0.018196 r_s^{-2} \rho_>, \qquad \text{(A. 48)}$$

for $0.56 \le r_s \le 8.0$

$$\varepsilon_{AP}[\rho_>(r_s)] = -0.3149 + \frac{1.43275}{(r_s + 2.5)} - \frac{6.57555}{(r_s + 2.5)^2}, \qquad \text{(A. 49)}$$

$$v_{AP} = \frac{-3.189745 + 0.477583 r_s}{(r_s + 2.5)^3} r_s \rho_>, \qquad \text{(A. 50)}$$

for $8 \le r_s < \infty$

$$\varepsilon_{AP}[\rho_>(r_s)] = -0.262 + 22.25233 r_s^{-3} - 5125.2893 r_s^{-6}, \tag{A. 51}$$

$$v_{AP} = \left(22.25233 r_s^{-3} - 10250.57860 r_s^{-6}\right)\rho_>. \tag{A. 52}$$

For a fully compensated system ($\rho_+ = \rho$), the correlation energy and the first and the second derivatives are as follows:

for $0 \le r_s \le 0.8$

$$\varepsilon_L[\rho_>(r_s)] = -0.119155 + 0.039475 ln r_s, \tag{A. 53}$$

$$v_L = \frac{\partial \varepsilon_L}{\partial \rho_>} = \frac{\partial \varepsilon_L \partial r_s}{\partial r_s \partial \rho_>} = -\frac{1}{3} r_s \frac{\partial \varepsilon_L}{\partial r_s}\rho_> = -0.0131583\rho_>, \tag{A. 54}$$

$$\frac{\partial v_L}{\partial \rho_>} = \frac{\partial v_L \partial r_s}{\partial r_s \partial \rho_>} = \frac{\partial}{\partial r_s}\left(\frac{\partial \varepsilon_L \partial r_s}{\partial r_s \partial \rho_>}\right)\frac{\partial r_s}{\partial \rho_>}$$

$$= \frac{\partial^2 \varepsilon_L}{\partial r_s^2}\left(\frac{\partial r_s}{\partial \rho_>}\right)^2 + \frac{\partial \varepsilon_L}{\partial r_s}\frac{\partial}{\partial r_s}\left(\frac{\partial r_s}{\partial \rho_>}\right)\frac{\partial r_s}{\partial \rho_>} = 0.0131583\rho_>^2 \tag{A. 55}$$

for $0.8 \le r_s \le 6$

$$\varepsilon_L[\rho_>(r_s)] = -0.26274 + \frac{3.2233}{(r_s + 5.0)} - \frac{14.16125}{(r_s + 5.0)^2}, \tag{A. 56}$$

$$v_L = (-4.06868 + 1.07443 r_s)\frac{r_s \rho_>}{(r_s + 5.0)^3}, \tag{A. 57}$$

$$\frac{\partial v_L}{\partial \rho_>} = 0.33333\rho_> v_L - (5.85939 - 0.716288 r_s)\frac{\rho_>^2 r_s^2}{(r_s + 5.0)^4}, \tag{A. 58}$$

for $6 \le r_s \le 15.85$

$$\varepsilon_L[\rho_>(r_s)] = -0.1536325 - 0.074081\tanh[0.39145(r_s - 9.8)], \quad \text{(A. 59)}$$

$$v_L = 0.00966 r_s \rho_> \operatorname{sech}^2[0.39145(r_s - 9.8)], \quad \text{(A. 60)}$$

$$\frac{\partial v_L}{\partial \rho_>} = -1.3333\rho_> v_L\{1 - 0.195725 r_s \tanh[0.39145(r_s - 9.8)]\}, \quad \text{(A. 61)}$$

for $15.85 \le r_s < \infty$

$$\varepsilon_L[\rho_>(r_s)] = -0.253625 - 2\varepsilon_{PZ}, \quad \text{(A. 62)}$$

$$\varepsilon_{PZ} = \gamma(\zeta = 0)\left[1 + \beta_1(\zeta = 0) r_s^{1/2} + \beta_2(\zeta = 0) r_s\right]^{-1}, \quad \text{(A. 63)}$$

$$v_L = -\rho_>\left[\beta_1(\zeta = 0) r_s^{1/2} + 2\beta_2(\zeta = 0) r_s\right]\frac{\varepsilon_{PZ}^2}{3\gamma(\zeta = 0)}, \quad \text{(A. 64)}$$

$$\frac{\partial v_L}{\partial \rho_>} = -\rho_>\left[12 v_L + 2\rho_>\left(\frac{\varepsilon_{PZ}}{6\gamma(\zeta = 0)}\right)^2 A\right], \quad \text{(A. 65)}$$

$$A = 2\varepsilon_{PZ}\left[\beta_1(\zeta = 0) r_s^{-1/2} + 2\beta_2(\zeta = 0)\right]^2 + \beta_1(\zeta = 0)\gamma(\zeta = 0) r_s^{-3/2}, \quad \text{(A. 66)}$$

where $\varepsilon_{PZ}(r_s)$ is the result of Ceperley and Alder as interpolated by Perdew and Zunger.

APPENDIX B

FIRST-ORDER PERTURBATION THEORY OF POSITRONIUM IN THE MADELUNG POTENTIAL

The positron bound in an F-center can be modeled as a free positronium atom perturbed by the Madelung potential. From the viewpoint of first-order perturbation theory, the perturbed ground state wavefunction of positronium consists of the 1s wavefunction admixed with the 2s state of positronium by introduction of the crystal potential as the perturbation Hamiltonian. The Hamiltonian of this perturbation system gives the Schrödinger equation,

$$H_{F_c}\Psi(\boldsymbol{r}_+,\boldsymbol{r}_-) = E\Psi(\boldsymbol{r}_+,\boldsymbol{r}_-) \tag{B. 1}$$

and

$$H_{F_c} = H_{Ps} + H', \tag{B. 2}$$

$$H_{Ps} = -\frac{1}{2}\nabla_+^{\,2} - \frac{1}{2}\nabla_-^{\,2} - \frac{1}{|\boldsymbol{r}_+ - \boldsymbol{r}_-|}, \tag{B. 3}$$

$$H' = V(\boldsymbol{r}_+) - V(\boldsymbol{r}_-), \tag{B. 4}$$

where H_{Ps} is the Hamiltonian for free positronium and the crystal potential at the anion vacancy is defined as the perturbation, H'. The potential $V(\boldsymbol{r})$ is the effective potential of an anion vacancy of the host alkali halides.

The free positronium system can be reduced to the relative coordinate system between the electron and the positron. The reduced mass is $\mu = \frac{m}{2}$ and the Hamiltonian can be written as

$$H_{Ps} = -\nabla^2 - \frac{1}{r} \tag{B. 5}$$

with $\boldsymbol{r} = \boldsymbol{r}_+ - \boldsymbol{r}_-$. This gives the solution of the Schrödinger equation for free positronium, and the eigenfunctions are written as

$$\Psi_{1s}^{Ps}(r) = \left(\pi a'^{3}_{0}\right)^{-1/2} e^{-r/(a'_0)}, \tag{B. 6}$$

$$\Psi_{2s}^{Ps}(r) = \frac{1}{4}\left(2\pi a'^{3}_{0}\right)^{-1/2}\left(2-\frac{r}{a'_0}\right)e^{-r/(2a'_0)}. \qquad \text{(B. 7)}$$

The effective Bohr radius is changed from a_0 to $2a_0$ due to the reduced mass of the positronium;

$$a'_0 = 4\pi\varepsilon_0\frac{h^2}{\mu e^2} = 2\left(4\pi\varepsilon_0\frac{h^2}{me^2}\right) = 2a_0 = 2. \qquad \text{(B. 8)}$$

The free positronium ground state energy state is obtained as

$$E_{nl} = -\frac{\mu}{2h^2}\left(\frac{e^2}{4\pi\varepsilon_0}\right)^2\frac{1}{n^2} = -\frac{1}{2a'_0}\frac{e^2}{(4\pi\varepsilon_0)}\frac{1}{n^2} = -\frac{1}{4n^2}, \qquad \text{(B. 9)}$$

$$E_{10} = -\frac{1}{4}\ \text{a.u.} = -6.8\ \text{eV}, \qquad \text{(B. 10)}$$

and

$$E_{20} = -\frac{1}{16}\ \text{a.u.} = -1.7\ \text{eV}. \qquad \text{(B. 11)}$$

Simply speaking, the crystal potential as the perturbation Hamiltonian serves as a potential *well* for the electron and as a potential *barrier* for the positron. This is simply approximated as potential sphere for the Madelung potential $V_0 = 2\alpha/a$ with the Madelung constant of alkali halides $\alpha = 1.74755$ and the lattice constant a. This corresponding perturbation term for the positronium system can be written as

$$H' = V_0 \text{ for } 0 \le r \le L, \qquad \text{(B. 12)}$$

$$= 0 \quad \text{for } r > L,$$

where L is our model potential radius.

From first-order perturbation theory, the perturbed 1s state is given by

$$\Psi_{1s}^{F_c}(r) \cong \Psi_{1s}^{Ps}(r) + \frac{\langle \Psi_{1s}^{Ps} | H' | \Psi_{2s}^{Ps} \rangle}{E_{10}^{Ps} - E_{20}^{Ps}} \Psi_{2s}^{Ps}(r)$$

$$= \Psi_{1s}^{Ps}(r) - \frac{16}{3} C \Psi_{2s}^{Ps}(r) \quad , \tag{B. 13}$$

where the matrix element of the perturbation term can be derived from the integration on the anion vacancy with the width L,

$$C = \langle \Psi_{1s}^{Ps} | H' | \Psi_{2s}^{Ps} \rangle$$

$$= \left(\pi a'^{3}_{0} \right)^{-1/2} \frac{1}{4} \left(2\pi a'^{3}_{0} \right)^{-1/2} V_0 4\pi \int_0^L \left(2 - \frac{r}{a'_0} \right) r^2 e^{-3r/(2a'_0)} dr$$

$$= \frac{2V_0 L^3}{3\sqrt{2} a'^{3}_{0}} e^{-3L/(2a'_0)} . \tag{B. 14}$$

The annihilation rate of the positron is defined with the probability of the pair-annihilation per second of the electron density at the position of positron. The rate has the spin factor 4 for the annihilation process of the free positronium, that is,

$$\Gamma = \pi \alpha^3 \rho_{Ps}, \tag{B. 15}$$

$$\rho_{Ps} = 4 \langle \Psi_{1s}^{Ps}(r) | \delta(0) | \Psi_{1s}^{Ps}(r) \rangle$$

$$= 4 \left| \Psi_{1s}^{Ps}(0) \right|^2 = \frac{4}{\pi a'^{3}_{0}}, \tag{B. 16}$$

where α is the fine structure constant and $\pi\alpha^3 = 50.42$ GHz. This result gives the annihilation rate and the lifetime of the free positronium with the following values,

respectively,

$$\Gamma = 8.024 \text{ GHz} \tag{B. 17}$$

and

$$\tau = 0.125 \text{ nsec.} \tag{B. 18}$$

However, in the perturbed system such as condensed matter, the spin-freedom for the arbitrary permutation is no longer degenerate and the spin-averaged annihilation rate is useful.[101, 102, 113] The annihilation rate for the perturbed system at the F-center is written by

$$\Gamma = \pi\alpha^3 \rho_{F_c}, \tag{B. 19}$$

$$\rho_{F_c} = \left|\Psi_{1s}^{F_c}(0)\right|^2 = \frac{1}{\pi a_0'^3}\left[1 - \frac{16}{3\sqrt{2}}C + \frac{32}{9}C^2\right]. \tag{B. 20}$$

After inserting Eq. (B.14) into Eq. (B.20) and assuming widths of the potential well as the half of the lattice constants [7.6118 (LiF) , 8.7569 (NaF) , 9.7131 (LiCl) , 10.6580 (NaCl)], $L = a/2$, and the depth with the Madelung potential, the lifetimes has been obtained as shown in Table XV. The deeper Madelung potential [0.459 (LiF) , 0.399 (NaF) , 0.360 (LiCl) , 0.328 (NaCl)] with the smaller potential sphere radius gives a more perturbed positronium state and enhances the positron lifetime.

GRADUATE SCHOOL
UNIVERSITY OF ALABAMA AT BIRMINGHAM
DISSERTATION APPROVAL FORM

Name of Candidate Keunjoo Kim

Major Subject Physics

Title of Dissertation Density Functional Calculations of F-Center Related Positron Annihilation in Alkali Halides

Dissertation Committee:

Joseph Harrison , Chairman

David Shealy

H. T. Tohver

John Young

Ian Knowles

Koop Lammertsma

Director of Graduate Program

Dean, UAB Graduate School

Date 8/24/94